

**Syntheses of functional zeolites by interzeolite  
conversion method and its application**

(ゼオライト転換法による機能性ゼオライトの合成とその応用)

**Masaya Itakura**

Submitted to Hiroshima University

In partial fulfillment of the requirements for the degree of  
Philosophy of Doctor

**Supervisor: Professor Dr. Tsuneji Sano**

Department of Chemistry and Chemical Engineering, Graduate  
School of Engineering,  
Hiroshima University

**March 2013**

Referee in Chief: Professor Tsuneji Sano

Referees: Professor Takeshi Shiono

Professor Toshinori Tsuru

Associate Professor Masahiro Sadakane

Department of Chemistry and Chemical Engineering,  
Graduate School of Engineering,  
Hiroshima University

# Contents

## Chapter 1: Introduction

1.1 Introduction to zeolite.....	1
2. Zeolite synthesis.....	5
2.1 History of zeolite synthesis.....	5
2.2 Factors affecting zeolite synthesis.....	8
2.2.1 Mineralizing agent.....	9
2.2.2 Structure-directing agent.....	10
2.2.3 Solvent.....	15
2.3 Commercial production of zeolites.....	17
2.4 Layer structure as transients and precursors.....	18
2.5 Conversion of one zeolite into another.....	22
3. Zeolite Characterization.....	26
4. Application of zeolite.....	28
5. Overview of the thesis.....	31
References.....	33

## Chapter 2: Synthesis of LEV-type zeolite by interzeolite conversion method and its catalytic performance in ethanol to olefins reaction

1. Introduction.....	45
2. Experimental.....	48
2.1 Hydrothermal conversion.....	48
2.2 Characterization.....	49
2.3 Catalytic testing.....	50
3. Result and discussion.....	51
3.1 Synthesis and characterization of LEV-type zeolite.....	51
3.2 Ethanol to olefins reaction.....	57
4. Conclusions.....	59
References.....	60

## Chapter 3: FAU–LEV interzeolite conversion in fluoride media

1. Introduction.....	63
2. Experimental.....	65
2.1 Interzeolite conversion.....	65
2.2 Characterization.....	66
2.3 Thermal stability.....	67
3. Result and discussion.....	69
3.1 FAU–LEV interzeolite conversion using choline hydroxide as a SDA in the presence of fluoride anions.....	69
3.2 FAU–LEV interzeolite conversion using 1-adamantanamine as a SDA in the presence of fluoride anions.....	71
3.3 Thermal stability.....	77
3.4 Interzeolite conversion process.....	79
4. Conclusions.....	81
References.....	83

## Chapter 4: Synthesis of high-silica CHA-type zeolite from FAU-type zeolite and its catalytic application for ethanol to olefin reaction and membrane application for dehydration of acetic acid aqueous solution

1. Introduction.....	85
2. Experimental.....	87
2.1 Synthesis of high-silica CHA-type zeolite by interzeolite conversion of FAU-type.....	87

zeolite with BTMA <sup>+</sup>	
2.2 Synthesis of SSZ-13 using TMAda <sup>+</sup> .....	88
2.3 Synthesis of CHA-type zeolite with high Al content.....	88
2.4 Characterization.....	88
2.5 Catalytic testing.....	89
2.6 Acid stability (structure stability and composition stability).....	90
2.7 Fabrication of CHA-type zeolite membrane.....	90
2.8 Dehydration performance.....	91
3. Result and discussion.....	92
3.1 Synthesis and characterization of CHA-type zeolite.....	92
3.2 Ethanol to olefins reaction.....	100
3.3 Acid stability.....	102
3.4 Membrane performance.....	108
4. Conclusions.....	110
References.....	112
<b>Chapter 5: Synthesis of high-silica OFF-type zeolite by the interzeolite conversion method</b>	
1. Introduction.....	115
2. Experimental.....	117
2.1 Synthesis of OFF-type zeolite.....	117
2.2 Characterization.....	118
3. Result and discussion.....	119
4. Conclusions.....	126
References.....	128
<b>Chapter 6: Influence of starting zeolite on synthesis of RUT-type zeolite by interzeolite conversion method</b>	
1. Introduction.....	130
2. Experimental.....	132
2.1 Synthesis.....	132
2.2 Characterization.....	132
3. Result and discussion.....	134
4. Conclusions.....	142
References.....	143
<b>Chapter 7: Interzeolite conversion process of FAU-type zeolite</b>	
1. Introduction.....	145
2. Experimental.....	146
2.1 Interzeolite conversion.....	146
2.2 Characterization.....	147
3. Result and discussion.....	148
4. Conclusions.....	156
Acknowledgements.....	157
References.....	158
<b>Chapter 8: Summary</b>	160
<b>List of publications</b>	165
<b>Acknowledgements</b>	169

# Chapter 1

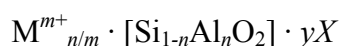
## Introduction

### 1. Introduction to zeolite

Many zeolites with different structures and compositions are commercially available. The zeolitic micropores are of molecular size, which give them adsorption, catalytic and ion exchange properties. These features are very important in both the chemical industrial field and the new applications related to process intensification, green chemistry, hybrid materials, medicine, cosmetic, animal food uses, optical and electrical materials, reaction and sensing microsystems, and nanotechnology. There have been considerable academic and industrial research efforts carried out in the field of zeolite so far.

Strictly defined, zeolites are crystalline aluminosilicates having microporous ( $2.0 \text{ nm} \geq d_p$ ) with tetrahedrally-connected framework structure based on corner-sharing  $\text{TO}_4$  tetrahedra ( $T = \text{Si}, \text{Al}$ ). For a completely siliceous structure, combination of  $\text{TO}_4$  units in this fashion leads to silica ( $\text{SiO}_2$ ), which is an uncharged solid. To substitute  $\text{Si}^{4+}$  to  $\text{Al}^{3+}$  in the pure silica frameworks gives an overall negative charge to the framework. This is balanced by the presence of extra-framework charge-balancing cations located within the pore space, coordinated to framework O atoms, which is also able to take in neutral atoms and molecules small enough to enter via the pore windows.

A simplified empirical formula for an aluminosilicate zeolite is



where  $n$  can vary from 0–0.5 and M represents extraframework inorganic or organic cations. In the as-made zeolites they are typically alkali or alkali earth metal cations or alkylammonium cations. The extraframework cations are ion exchangeable and give rise to the rich ion-exchange chemistry of these materials. X represents neutral guest molecules or included species such as H<sub>2</sub>O. The novelty of zeolites arises from their microporosity and is a result of the topology of the framework.

The primary building blocks of the framework are the tetrahedral. Typically, Al-O and Si-O bond distances are 1.73 and 1.61 Å, respectively, with OTO angles close to the tetrahedral angle, 109.4°. There is more variation in the SiOSi bond angles between tetrahedral, where the average angle is 154° with a range of 135-180° and a mode of 148° [1]. Variation of TOT angles enables a wide diversity of frameworks to exist.

The amount of Al within the framework can vary over a wide range, with Si/Al = 1 to ∞, the completely siliceous form being polymorphs of SiO<sub>2</sub>. Löwenstein proposed that the lower limit of Si/Al = 1 of a zeolite framework arises i.e. Al-O-Al linkages are not observed in hydrothermally-synthesized zeolite, because the negative charge associated with aluminate tetrahedra interact unfavorably, an observation expressed as Löwenstein's rule. The framework composition depends on the synthesis conditions. Post-synthesis modifications that insert/remove Si or Al into the framework have also been searched well. By increasing the Si/Al ratio of the framework, the hydrophobicity and the hydrothermal stability rise.

Typically, in as-synthesized zeolites, water molecules are present in the internal voids of zeolite. The sorbed phase and organic non-framework cations can be removed by thermal treatment/oxidation, making the intracrystalline space available. The crystalline nature of the framework ensures that the pore openings are uniform throughout the

crystal and can readily discriminate against molecules with dimensional differences less than 1 Å, giving rise to the name molecular sieves.

Although aluminosilicate zeolites are by far the best studied and most widely applied materials that have tetrahedrally-coordinated porous frameworks, many compositional variants (including pure silica forms) have been prepared, and some 20 elements have been reported to be included via substitution into framework cation sites. These can be aliovalent, with a different valency from silicon or isovalent. The inclusion of some elements has stronger effects on chemical characteristics than on structural features whereas the inclusion of high levels of elements such as Ga or Ge can result in the crystallization of frameworks with distinctly different structural features. In their ease of substitution, stability in the tetrahedral site and structure directing properties depend on cationic radius and electron negatively.

Since the first description of hydrothermal synthesis of zeolites achieved in the laboratory by Barrer in 1940s, the scientific and industrial interest in the field increased [2]. A large number (206) of different structures for tetrahedral frameworks of all compositions have been discovered since 1940s [3]. The Structure Commission of the International Zeolite Association identifies each framework with a three-letter mnemonic code (e.g. LTA for Linde zeolite A, MFI for ZSM-5, etc.) [3]. Fig. 1-1 shows the framework projections for commonly studied zeolites.

Fig. 1-2 shows how the sodalite unit can be assembled to form common zeolitic frameworks: zeolites X/Y (FAU), ZSM-12 (MTW), ZSM-5 (MFI), and Theta-1 (TON). In these commonly used representations, the T-atoms are located at the vertices, and the lines connecting them stand for T–O–T bonds. For example, if 24 tetrahedra are linked together as shown in the top line of Fig. 1-2, the cubo-octahedron, also referred to as a

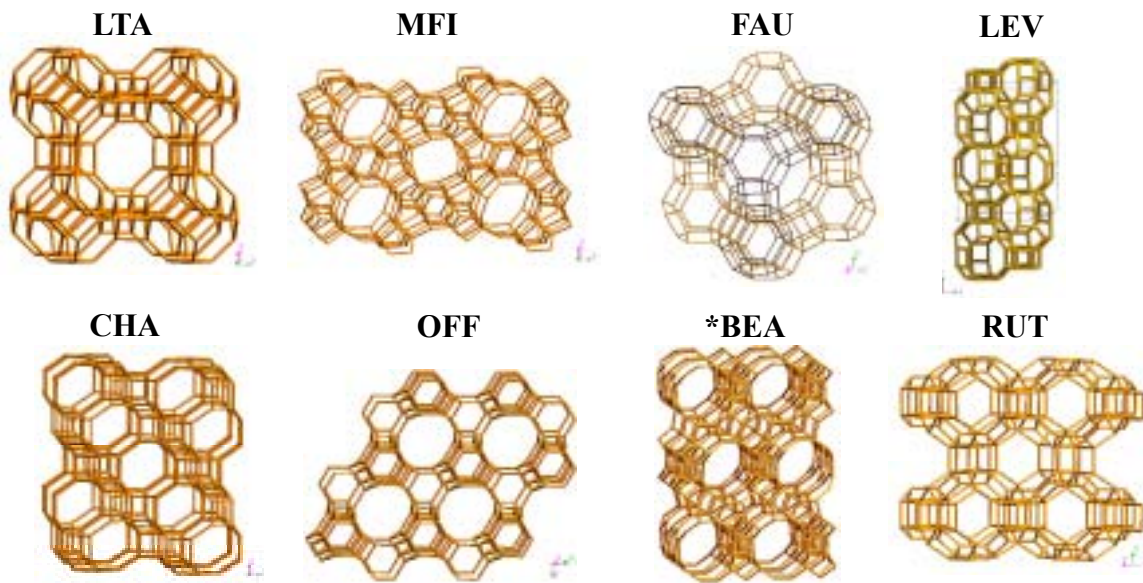


Fig. 1-1 Various framework structures of the zeolites.

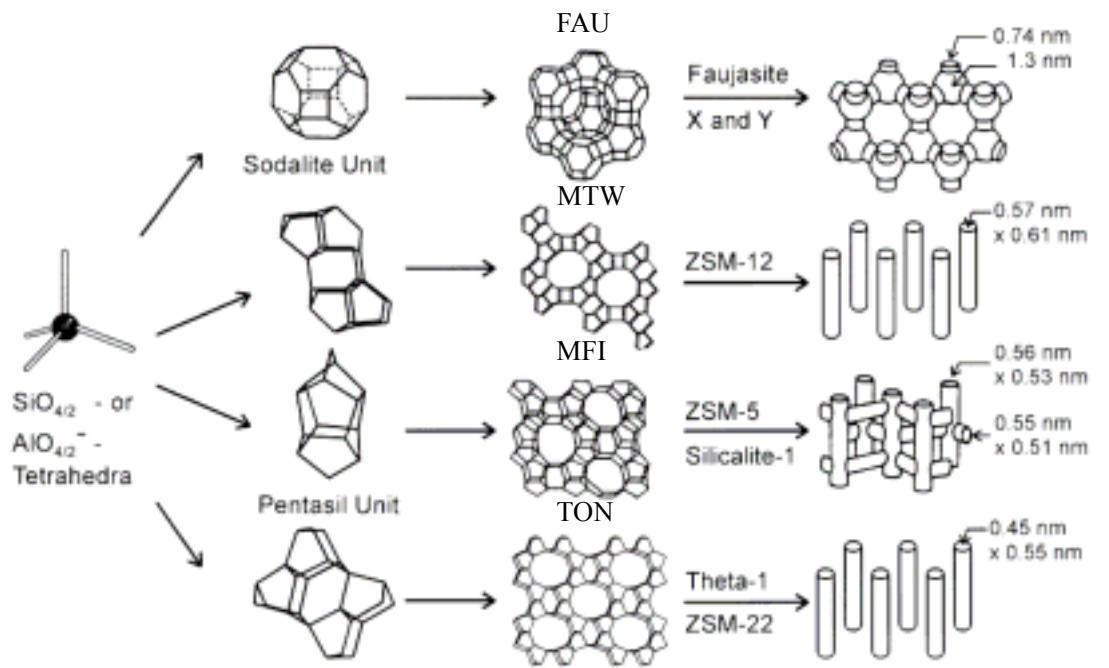


Fig. 1-2 Structures of four selected zeolites from top to bottom: faujasite or zeolites X, Y (FAU); ZSM-12 (MTW); ZSM-5 or sicalite-1 (MFI); Theta-1 or ZSM-22 (TON) and their micropore systems and dimensions [4]. In a less cluttered representation, the oxygen atoms are omitted and straight lines are drawn connecting the T atoms.

sodalite unit or  $\beta$ -cage, results. It is important secondary building unit (SBU) derives various zeolite structures.

As shown in Figure 1-3, the structure of the mineral sodalite consists of  $\beta$ -cages face sharing six-membered rings (6MRs). Instead, if they linked through their 4MRs via

double four-membered ring (D4R) units, the zeolite A framework results (topology type LTA). Sodalite cage can also be linked through D6Rs on their 6MR faces. Whereas there is only one way of arranging the cages for sodalite and zeolite A, there are different ways of linking layers of sodalite cages through D6Rs. The two end member variants are cubic zeolites with the faujasite (FAU) structure type, where FAU refers to the mineral form of this material, faujasite, and its hexagonal polytype EMC-2 (structure type EMT).

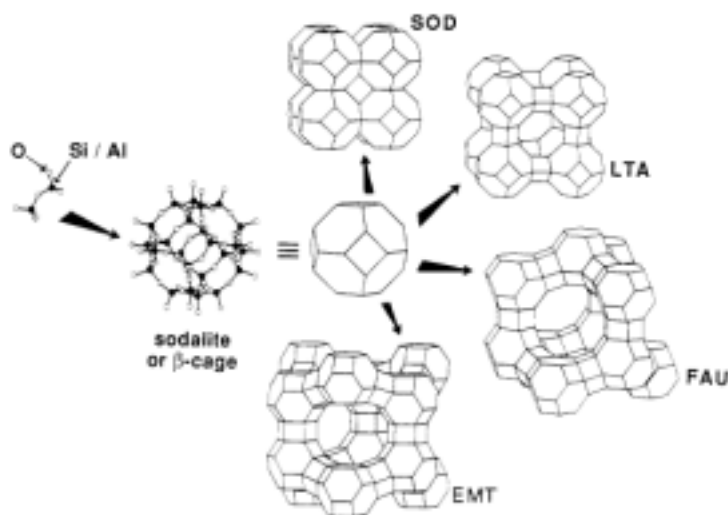


Fig. 1-3 The construction of four different zeolite frameworks with sodalite or  $\beta$  cages. A pair of TO<sub>4</sub> tetrahedra is linked to a single sodalite cage by T–O–T bonds. The sodalite cage unit is found in SOD, LTA, FAU, and EMT frameworks [5].

There is no doubt of the great importance of zeolites in the general subject of materials science. Zeolites, and in a broader sense zeolitic materials, are today studied and applied in many different ways and fields, even through some of their essential features are not wholly understood, and many challenges remain for the now and future.

## 2. Zeolite synthesis

### 2.1 History of zeolite synthesis

The history of man-made zeolites can be traced back to the claimed laboratory preparation of levynite by St Claire Deville in 1862 [6]. However, zeolite synthesis as we know it today had its origins in the work of Barrer, commencing in 1940s [2]. Barrer began his work by investigating the conversion of known mineral phases under the action of strong salt solutions at fairly high temperatures (170–270 °C). Obtained KFI-type zeolite displayed unique characteristics and represented the first synthetic zeolite [7-10] determined subsequently for zeolite ZK-5 [11,12]. Milton pioneered the use of more reactive starting materials (freshly precipitated aluminosilicate gels), enabling reactions to be carried out under milder conditions and leading to the discovery of zeolite A [13] and X [14]. By 1953, Milton and his colleagues had synthesized 20 zeolites, including 14 unknown as natural minerals [15]. These zeolites, prepared using inorganic cations, tend then to have relatively high Al contents, because their pore space contains many exchangeable cations.

Above-mentioned syntheses were conducted only in the presence of inorganic cations. Using organic cations such as quaternary ammonium cations to obtain new structure types became common following pioneering work in 1961 by Barrer et al. [16-18]. The introduction of organic constituents was to have a major impact upon zeolite synthesis. Among the most important new structure types prepared with tetraethyl- and tetrapropylammonium cations were Beta and ZSM-5, respectively. [19,20]. More recently, these organic constituents have been called organic structure-directing agents (OSDA). They can be bulky, so fewer can be included in the zeolite pores than would be the case for inorganic cations. This necessitates a lower density of framework negative charge and consequently a lower Al content.

There has subsequently been a large rise in the number of known synthetic zeolite and

also the discovery of new families of zeolite-like or zeolite-related materials [21].

The discovery of aluminophosphate (AlPO) zeotype by UOP in 1982 heralded a major expansion of the compositional range of this type of microporous solid [22]. They can be thought of as derived from pure silica zeolites by the ordered substitution Al and P to 2Si, is that their framework composition is  $\text{AlPO}_4$  and Al and P show strict alternation in tetrahedral framework sites. There are strong similarities between AlPO zeotypes and zeolites in their structure and a more importantly, in chemistry. The most obvious structure difference is that the strict alternation of Al and P in framework sites rules out the presence of odd numbered rings in AlPO structure. VPI-5 is the 18MR AlPO, this framework structure observed in only AlPO structure [23]. Silicoaluminophosphates (SAPOs) are derived from AlPOs by two mechanisms. In the first, P is replaced by Si, leaving a net negative charge on the framework that is charge-balanced by a proton after template removal ( $\text{H}_x\text{AlP}_{1-x}\text{Si}_x\text{O}_4$ ). This bridging hydroxyl Si-OH-Al is usually less strongly acidic than those found in the  $\text{H}^+$  form of aluminosilicate zeolites. The second mechanism of substitution involves the coupled replacement of Al and P by two Si atoms. This cannot happen in isolation, due to the unfavorability of Si surrounded by nearest neighbor P atoms, but can be considered to occur when direct Si-P substitution has resulted in the formation of Si-O-P linkage. This second type of substitution results in the formation of aluminosilicate islands.

These isovalent substitutions are of importance in zeotypic silicates of  $\text{Ti}^{4+}$  and  $\text{Ge}^{4+}$ . The titanosilicates is primarily of significance for their catalytic properties whereas germanosilicates are remarkable for the novel topologies they exhibit. Titanium-containing high silica zeotypes such as TS-1 [24] contain a few mole percent of Ti in framework cation sites. Although the Ti is tetrahedral in the template-free,

dehydrated form, it readily acts as a Lewis acid to expand its coordination sphere in the presence of water, with important application in selective oxidation, peroxide species. Other zeotypic titanosilicates have been reported including the large pore Ti- $\beta$  [25] and Ti-Y [26]. The inclusion of germanium in silicates has resulted in the crystallization of remarkable zeotypic structures including ITQ-17, IM-12, and ITQ-33 [27–29]. The fully tetrahedral frameworks of these structures are characterized by D4R units, 3MRs and even D3Rs, giving rise to framework with low tetrahedral site densities and large pores. The tendency for the inclusion of germanium in tetrahedral sites to favor the formation of small ring SBUs is attributed to the larger non-bonding radius of Ge vs. Si and consequently the ability to form smaller OTO angles that stabilize 3MRs and 4MRs.

Investigative work aimed at gaining an understanding of the synthesis mysterious process has its origins in the 1960s. These studies have continued up to the present day, spurred on at various points by discoveries of new materials, advances in synthetic techniques, innovations in theoretical modeling methods and, especially, by the development of new techniques for the investigation of reaction mechanisms and characterization of products.

## **2.2 Factors affecting zeolite synthesis**

Principally, zeolites can be synthesized in aqueous media under hydrothermal conditions (temperatures between 100 °C and 200 °C) in the presence of organic and/or inorganic cations and a mobilizing agent. A large number of variables influences the hydrothermal crystallization of molecular sieves, and determines the kinetics and the final crystalline phases formed. Despite the important efforts to rationalize the

preparation of zeolites, connection between the structure formed and the initial synthesis variables is not fully understood due to the complexity of the synthesis mechanism and the metastable nature of zeolites.

### **2.2.1 Mineralizing agent**

The mineralizing agent is the chemical species that allows increasing the solubility of the silicate or aluminosilicate species, among others, in the synthesis gel by means of dissolution and precipitation. The mineralizing agent acts as a catalyst in those processes, which is consumed during the dissolution of species, and recovered after the zeolite crystallization. The most extended mineralizing agent is the  $\text{OH}^-$ . The hydroxyl anion increases the solubility of silicon and aluminum sources, directing the formation of soluble silicate and aluminate anions. Typically the  $\text{OH}^-$  source is an alkali-metal hydroxide and large amount of positive charges are introduced in the final crystalline solid by those extra-framework small inorganic cations. They must be balanced by the presence of large number of aluminum atoms in the framework. In contrast, when an OSDA, such as amine or quaternary ammonium salt, is introduced in the synthesis gel, the Si/Al ratio is increased. High-silica zeolites can be achieved because the organic molecules are filling the zeolite void volume, inserting less positive charges in the final solid, and therefore, less aluminum atoms in the framework are required [16].

The introduction of fluoride anions as mineralizing agents was a breakthrough in zeolite synthesis. It was first described by Flanigen and Patton in 1978 [30]. In this case, some fluoro complexes species ( $\text{TF}_6$ , where T is Si, Al...) are formed in the synthesis gel. One advantage of fluoride route synthesis versus the traditional alkaline one is that the former can be performed at near neutral (or slight alkaline) pH, increasing the

stability of the organic molecules used as OSDA, because their degradation by the Hoffman mechanism is avoided [31]. In general, high-silica zeolites synthesized at high pH have a large amount of connectivity defects, due to the requirements for balancing the positive charges of the OSDA molecules precluded in the zeolite pores and cavities [32]. However, high-silica zeolites prepared in  $F^-$  media present less number of defects than the materials synthesized in  $OH^-$  media. This is because fluoride anions directs the formation of small cages (such as D4R), remaining inside of these cages in the final solid and balancing the positive charges of the OSDA. Moreover, the synthesis of zeolites in  $F^-$  media tends to form larger crystals than alkaline-mediated preparation. As consequence, the preparation of more perfect crystals in fluoride media (large crystals and less defects-containing) will affect their hydrophobicity/hydrophilicity properties, and then their adsorption and catalytic properties [33]. Since fluoride media route was reported, several new zeolitic structures have been synthesized [34-37].

### **2.2.2 Structure-directing agent**

As described above, the first zeolites were synthesized in alkaline media. They crystallized as aluminum-rich zeolites ( $Si/Al =$  close to 1) due to the presence of large amount of extra-framework alkali-metal cations. Nevertheless, in 1961, the OSDA is introduced for the first time in zeolite synthesis by Barrer et al. [16]. The use of tetraalkylammonium cations allowed increasing the framework  $Si/Al$  ratio, determined by the OSDA incorporated into the zeolite. As it can be seen in Fig. 1-4 [5], less positive charges are introduced by the organic molecule than by the small inorganic cations in the SOD cage, requiring less anionic charges in the zeolite framework. Therefore, the organic molecule can determine the amount of trivalent elements in the

zeolite framework, but also the structural characteristics, such as pore dimensions and cavities, depending in shape, size, hydrophobicity, and number of charges of the OSDA molecule.

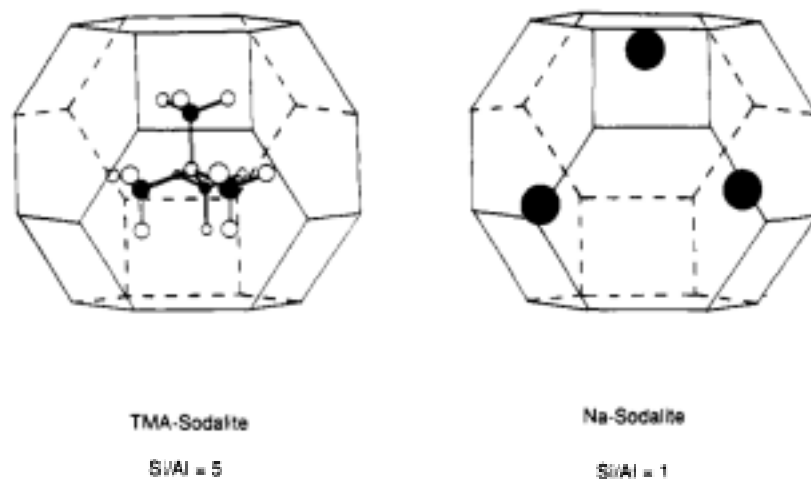


Fig. 1-4 Scheme of tetramethylammonium cation (left) or sodium cations (right) into the sodalite cage [5].

Amines and quaternary ammonium ions are the most frequently used OSDA in zeolite synthesis. The OSDA increases the thermodynamic stability in the organic-inorganic system during the nucleation step, by means of interactions with the zeolitic framework. There are no covalent bonds between organic and inorganic in this composite, but the assembly process occurs by weak interactions such as van der Waals forces, showing the structural directing effect [38]. The ideal correlation between the shape and size of the OSDA and the framework cavity is known as “template” effect. Two excellent examples of template structure-direction are the synthesis of ZSM-18 using tris(quaternary ammonium) cation as OSDA [39], and MCM-61 synthesis using the 18-Crown-6 molecule [40]. The relationship between OSDA properties and the characteristics of cages and pores of formed zeolites have been studied [41]. Gies and Marler found that sixty-one molecules can be used to control the structure of the

clathrasils. They showed that large molecules direct the formation of clathrasils with large cages, while small molecules direct the crystallization of clathrasils with small cages [42]. Moreover, Nakagawa and Zones increased the size of the structure-directing agent, showing that when the size of the OSDA is increased, the product selectivity changes from a clathrasil to a microporous, large-pore zeolite. Furthermore, if the geometry is changed from cyclic to linear molecules, there is a transition from clathrasils to microporous molecular sieve with 10-ring pores, and the evolution from linear to branched organic molecule allows getting three-dimensional 10-ring (MFI) instead of one-dimensional 10-ring (ZSM-48) [41,43]. In general, the selectivity of the OSDA towards a zeolite is correlated with the size of molecule. If the number of carbon and nitrogen atoms in the structure-directing molecule increases, the quantity of structures obtained is reduced [41], therefore, the specificity as “template” increases when it evolves from small and flexible to large and rigid molecules. The synthesis of extra-large pore zeolites (pores with more than 12 T atoms) is highly desired in catalysis for their potential application in the reactivity of large molecules. The use of relatively large and rigid OSDAs was thought to be the adequate strategy to synthesize extra-large pore zeolites. Following this methodology, some extra-large pore zeolites with 14 MR openings were synthesized, UTD-1, CIT-5, SSZ-53, and SSZ-59 [44–47]. However, as it will be shown in the section 2.1, the main achievements in the synthesis of extra-large pore molecular sieves have been accomplished with the introduction of Ge in the synthesis gel.

A new molecular sieve, ITQ-37, has been described in 2009 showing a chiral extra-large framework [48]. For the preparation of this zeolite, an organic molecule with four chiral centers has been used (Fig. 1-5). However, in this case, the enormous helical

channels are achieved by the presence of connectivity defects in the structure, and therefore the “true organic-template effect” cannot be claimed. There is an example in the investigation towards the design of chiral molecular sieve. The scientists have to increase the efforts in the preparation of this type of solids by their enormous potential impact fields, as chemistry, pharmacy, and biology.

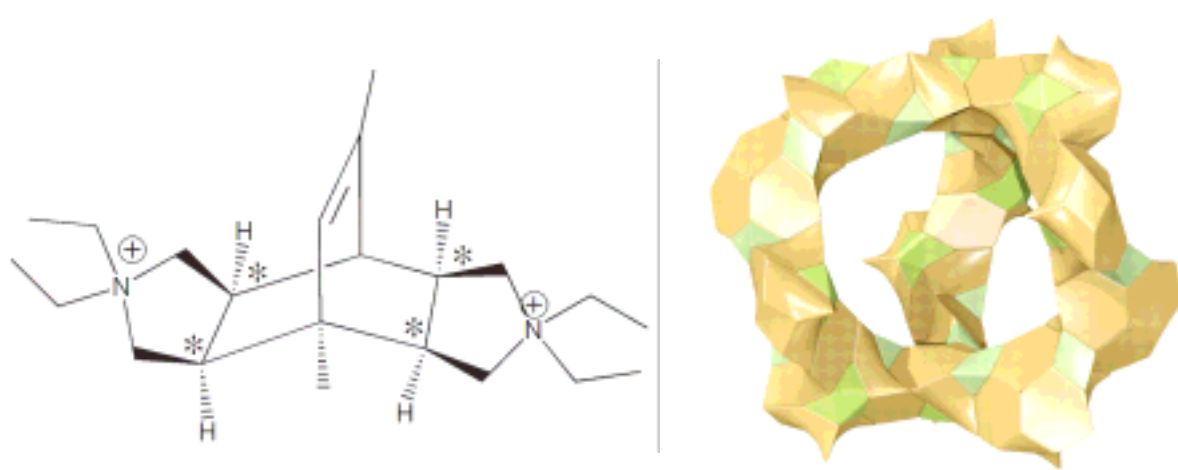


Fig. 1-5 (Left) OSDA used for the ITQ-37 zeolite showing four chiral centers (asterisks), (right) chiral structure of the ITQ-37 [48].

As it was mentioned, the synthesis of large pore zeolites requires the use of bulky OSDAs. Sometimes, the crystallization process cannot be energetically favorable because during the nucleation, the OSDA requires to assemble large number of  $TO_4$ . In this sense, the rational design of zeolites by using a combination of small organic molecules with bulkier OSDAs would allow creating cooperative structure-directing effects, where each type of organic molecule will show a precise task. The small cation (tetramethylammonium cation; TMA) could direct the small cage formation, and the bulk OSDA (1-benzyl-1-methylpyrrolidinium; bmp) could assemble that final structure (Fig. 1-6). Following this technology, the synthesis of the FER-type zeolite has been reported by Perez-Pariante et al. in a very nice series of papers [49–51]. Interestingly, they have shown that depending on the combination of organic molecules,

the distribution of the acid site in the structure can be populated between the ferrierite cage accessible through 8-ring windows and the 10-ring channel [52,53]. A very good correlation between the accessibility and catalytic activity has been achieved in the isomerization reaction of *m*-xylene and conversion of n-butene [52]. The same interesting correlation has been observed for the low-temperature carbonylation of dimethyl ether with carbon monoxide [54].

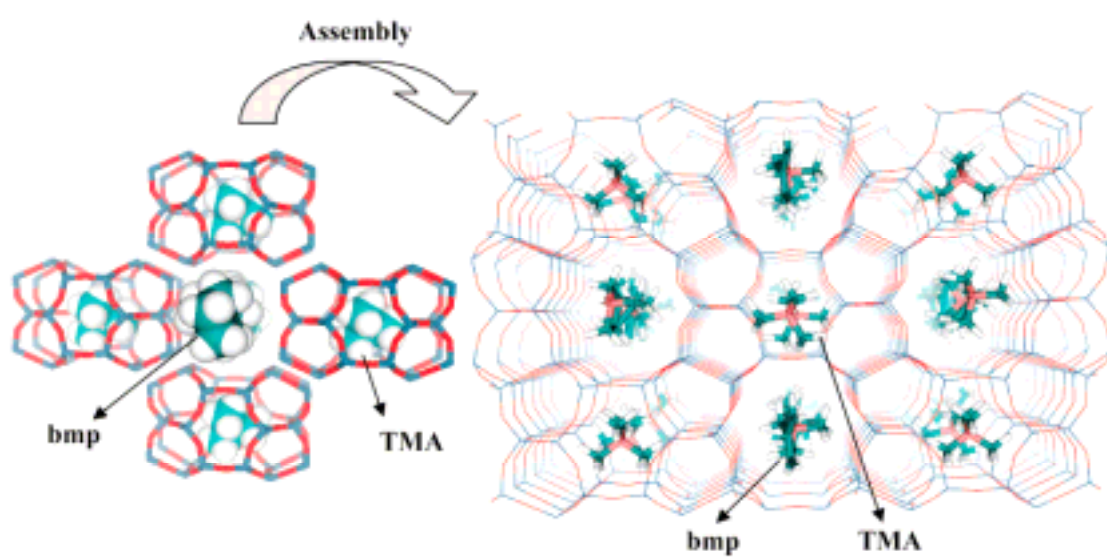


Fig. 1-6 Scheme of the ferrierite containing two different OSDA [49].

Large variety of quaternary ammonium salts has been used as OSDA [41,55]. However, those molecules can suffer the Hoffman degradation reaction at high pH and temperature. As a new concept, the use of tetraalkylphosphonium cations has been introduced in the zeolite synthesis [56,57]. Those compounds are more thermally stable than tetraalkylammonium molecules, and allow their use in severe preparation conditions. As a consequence, three new zeolite structure have been discovered by using phosphonium cations, ITQ-27, 34, and 40 [58–60]. Another interesting advantage in the OSDA design has been introduced by the use of phosphazene-derivatives. They can be synthesized by block similar to Legos, with a large variety of substituents, creating

nearly unlimited synthesis options. Moreover, phosphazenes can mobilize silica, and also have the adequate polarity and stability. Their enormous basicities allow to the phosphazene reacting with water, forming the corresponding hydroxides. Boggsite zeolite has been synthesized for the first time by using this methodology [61]. This material shows the appropriated structure for aromatic alkylation reactions, thanks to the combination of 12 and 10MR channels.

### **2.2.3 Solvent**

The most used solvent in zeolite synthesis is water. The main characteristics of water are the non-toxicity, low-cost, good thermal stability and conductivity. Also, water helps the mineralizing agent in the dissolution of species needed for the crystallization, and can act as template in association with other templating species. Despite the large benefits of using as solvent, some examples can be found in the literature in non-aqueous systems. In a nice communication, Bibby and Dale hypothesized that silica can complex with many organic molecules, such as hydroxyl- and amine-compounds [62]. Therefore, many organic solvents would be available for the synthesis of silicates in non-aqueous systems. Following this hypothesis, they synthesized the silica-sodalite structure from non-aqueous systems with ethylene glycol and propanol [62]. Expanding this initial work, other related sodalite structures have been synthesized in presence of ethanolamine or ethylenediamine [63,64].

The introduction of ionic liquids in zeolite synthesis by Morris et al. as a new preparation method instead of using water as solvent has been a very attractive discovery in 2004 [65]. Ionic liquids act as both solvent and OSDA. They are very good solvents because they are ionic and, present enough polarity to dissolve many types of

inorganic salts required in zeolite synthesis [66]. Moreover, ionic liquids (imidazolium) are chemically very similar to the usual quaternary ammonium cations used as OSDA in the traditional zeolite synthesis. However, the most exciting property of ionic liquids is the very low vapor pressure. Then, at elevated temperature, the ionic liquid produces no autogeneous pressure [67], permitting the manufacture of zeolites at ambient pressure [68]. Moreover, the ionic liquid can be recovered and recycled after the synthesis procedure for a further use. Following this novel methodology, several new type materials have been discovered (Fig. 1-7) [69–71].

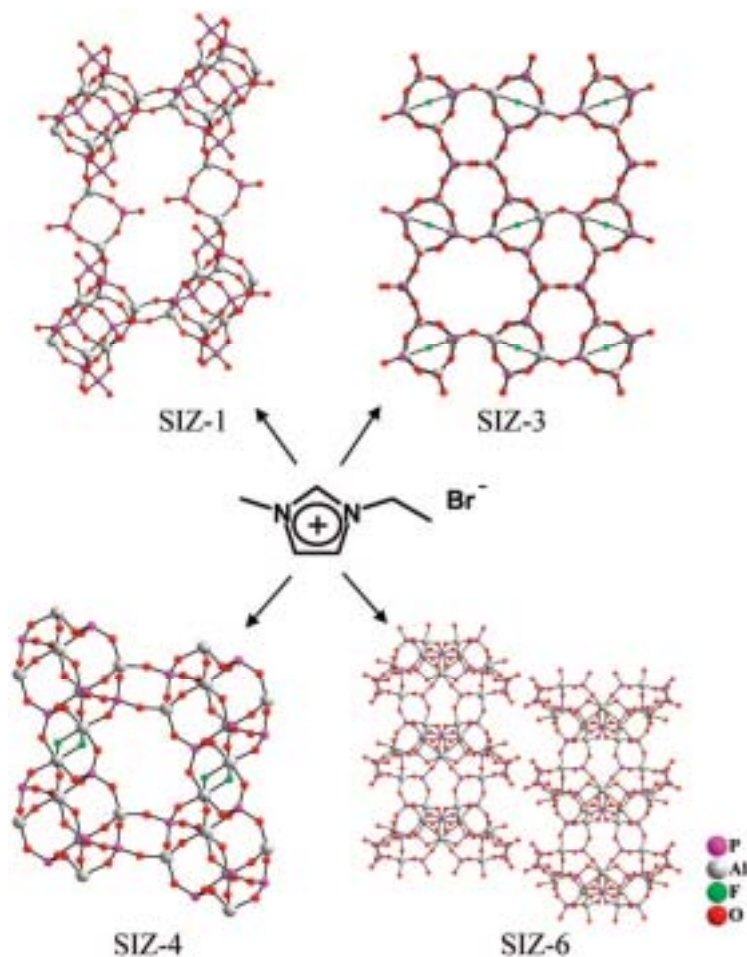


Fig. 1-7 Some examples of zeotypes synthesized by using ionic liquids [71].

### 2.3 Commercial production of zeolites

Despite the large number of zeolite structures discovered (more than 200), only 10% of them are in commercial production. The most part of chemical processes that require a zeolitic catalyst are covered by the use of only five zeolites: FAU, \*BEA, MFI, MOR, and FER [72]. This can be explained because the preparation of those materials does not require high costs (expensive OSDAs are not used), and they show a broad spectrum of framework topologies and physical-chemical properties (small, medium, or large pores; large cavities; different acidities...) that allow their application in different type of catalytic processes. Some of new structures that have been recently reported in the literature show better activities or selectivities than the commercial zeolites, but in the scale-up of their manufacture it is mandatory to study their commercial viability. In this way, costs are not only introduced by the use of expensive raw materials (complex OSDA, or expensive elements such as Ge), but also synthesis time, filtration (waste management), synthesis yield, environmental permissions, and safety considerations [72]. Moreover, scientific and industrial collaborations between zeolite manufacturers and application developers are required in order to improve the technology required to introduce a new material in commercial applications [72,73].

During the last sixty years, scientists have performed many efforts in order to rationalize the synthesis of zeolites, as it has been shown along above section. It has been possible to synthesize different type of structure modulating their physicochemical properties, by rationalizing the synthesis variables, such as OSDA, inorganic cations, mineralizing agents, other heteroatoms, solvents... Now, the reduction of manufacture costs in the design and synthesis of new or known structures is compulsory for their industrial application. Some examples of new approaches have been reported. Recently,

some zeolites have been synthesized in OSDA-free media: Beta [74], ZSM-12 [75], ZSM-34 [76,77], and RUB-13 [78]. The removal of the OSDA from the synthesis media will reduce the economical costs of manufacture. Also, some examples of OSDA recyclability have been introduced, as the free combustion methodology [79–81] and the use of ionic liquids as solvent and OSDA. The recyclability of the OSDA will allow the reuse of these expensive organic molecules during several synthesis cycles, reducing the total economical costs. Finally, the replacement of most of the OSDA in the synthesis gel by less-expensive pore filler (more than 80% of the original OSDA can be replaced by an inexpensive quaternary ammonium salt) will permit large economical savings in a possible zeolite commercial production [82]. Then, new chemical concepts must be introduced in zeolite synthesis, in order to boost the design of “low-cost” zeolites with very interesting and novel properties.

Zeolites and zeolite-related porous materials synthesis has recently focused on the creation of functional materials tailored to specific processes through directed assembly strategies.

#### **2.4 Layer structure as transients and precursors**

Zeolites are three-dimensional (3-D) crystalline materials containing tetrahedral framework atoms, while clays are two-dimensional (2-D) materials containing both tetrahedral and octahedral atoms. The 2-D building units can be regarded as layers that are aligned the third dimension by ionic or hydrogen bonds. About four decade ago, researchers found that the interlayer inorganic cations of smectite clays are converted to oxide pillars such as alumina, titania and zirconia, which keep the layers separated from each other to build 3-D interlayer microporous network structures.

There have been several different instances of the appearance of lamellar materials during the course of zeolite syntheses. Materials with layer structure such as the silicates kanemite, magadiite or ilerite (sodium “*octasilicate*”) have been used as starting materials [83]. A number of such syntheses fall into the category of apparent “*solid state transformations*”. In some cases, amorphous micro-precipitates have been observed in the form of lamellae, upon which the zeolite product appeared to nucleate [84]. In other situations, crystalline intermediates having layer structures have been observed before zeolite crystallization and have been regarded as precursors to the subsequent three-dimensional microporous networks [85-87]. In the crystallization of TEA-beta, a similar observation led Lohse et al. to conclude that the zeolite was formed via a direct transformation of a layered aluminosilicate [88]. In none of these cases is there proof of the suggested 2D → 3D transformation. Some possible structural relationships between layered alkali metal silicates and the mordenite and pentasil-group zeolites have been discussed by Garcés et al. [89].

Tuel has made a detailed study of the synthesis of zeolites ZSM-48 and beta with hexamethonium and tetraethylammonium cations, respectively [90]. In both cases, high crystalline layered organo-silicates or organo-aluminosilicates were formed at short synthesis times but gradually decomposed to amorphous materials. The zeolite products started to form only after the complete degradation of the layered structures. The two layered compounds, although from different reaction systems seemed to possess very similar structures, whereas there were no elements common to the XRD patterns of the final zeolite products. It was concluded that the layered materials dissolved in the reaction medium, providing nutrients which were reused in the crystallization of the zeolites, the structure of which depended only on the nature of the quaternary

ammonium OSDA cation present in the liquid phase.

A very different situation exists with a family of materials which do not convert to zeolite phases hydrothermally but which do so upon isolation and high-temperature calcination. In general, the initial structure is that of a two-dimensional, layered complex which, on removal of the organic “*spacers*”, becomes converted into a three-dimensional framework by the condensation of silanol groups. The first example of a zeolite formed by calcination of a layer-structured precursor appears to be that of NU-6 [91]. Later examples include the silica polymorph EU-20 [92] and the borosilicate ERB-1 [93]. Most detail is available in the case of “*PREFER*”, where the transformation of this two-dimensional aluminosilicate into the zeolite ferrierite on calcination at 550 °C has been carefully studied [94]. The XRD pattern of *PREFER* contains diffraction lines similar to those of the derived zeolite, reflecting the structural conformity between the two materials. The precursor appears to consist of ferrierite-type sheets in the *bc* plane, separated by molecules of the bulky OSDA (4-amino-2,2,6,6-tetramethylpiperidine). On burning out the occluded organic molecule, the ferrierite layers progressively link together in the  $\alpha$ -direction as new T–O–T linkages are formed by condensation reactions. However, it is also possible to modify this process. *PREFER* and related materials can be delaminated and reassembled in a number of ways to give a series of high surface area derivatives with catalytically active sites accessible to bulky reactants. Examples from the Valencia school are ITQ-2 [94], ITQ-6 and ITQ-36 [95]. Similar relationships characterize the noble MCM-22 family [96,97] which already form the basis for a new and commercially operating process for the manufacture of ethyl benzene [98]. The synthesis of MCM-22 was claimed to occur through a lamellar zeolitic precursor, MWW (P), formed by individual sheets (thickness of 2.5 nm), which

are ordered perpendicularly to axis c and separated one to each other by the OSDA. After calcination, the layers condense, and the tridimensional structure of MWW is obtained. This is composed of two independent pore systems: one formed by 12MR cages connected by 10MR apertures, and the other is defined by a well differentiated 10MR circular channel (Fig. 1-8) [99-103].

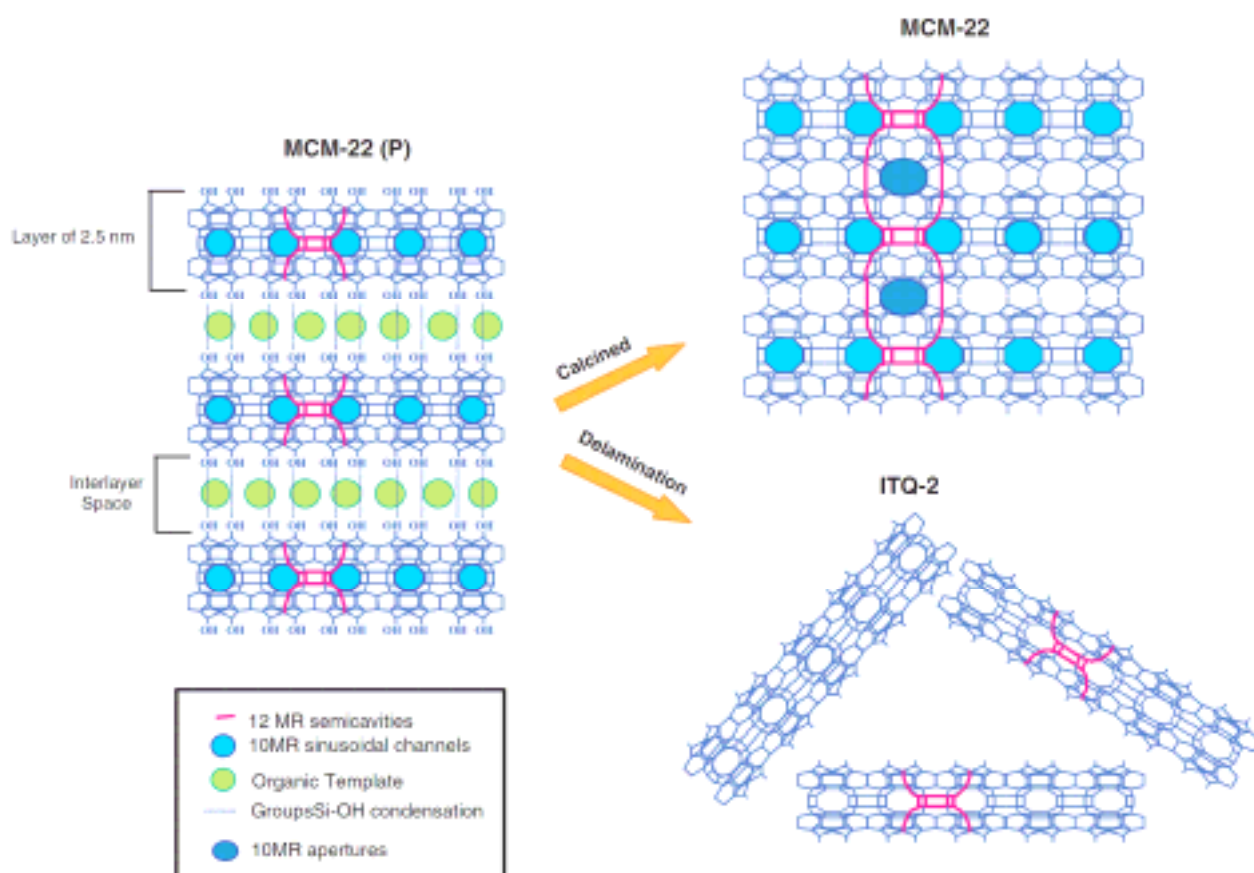


Fig. 1-8 Scheme for the preparation of various materials from the MWW-type zeolite precursor MCM-22 (P) and ITQ-2 [103].

Tatsumi et al. have applied a similar strategy to layered zeolite precursors to obtain crystalline microporous materials, which were named interlayer expanded zeolites (IEZ) [104]. Treatment of the zeolitic layered precursor of Al-MWW (MCM-22(P)) with diethoxydimethylsilane (DEDMS) in acid media gave an aluminosilicate-type

interlayer-expanded zeolite MWW (Al-IEZ-MWW) with expanded 12MR micropores (Fig. 1-9). By the interlayer-silylation of Al-MWW (P), the micropore diameter of interlayer with 12MR supercages enlarged from ca. 7.0 to 8.0 Å, verifying the formation of the interlayer-expanded structure. Thus prepared Al-IEZ-MWW serves as a useful acid catalyst for large molecules, e.g. the Friedel-Crafts acylation of anisole with acetic anhydride [105], and the Bechmann rearrangement of cyclohexanone oxime [104], being superior to Al-MWW with only 10MR micropores. This novel methodology for preparing IEZ materials can be widely applied to various layered zeolitic precursors such as Ti- and Ga-MWW(P), PREFER, PLS-1, and MCM47 in addition to Al-MWW(P) [104].

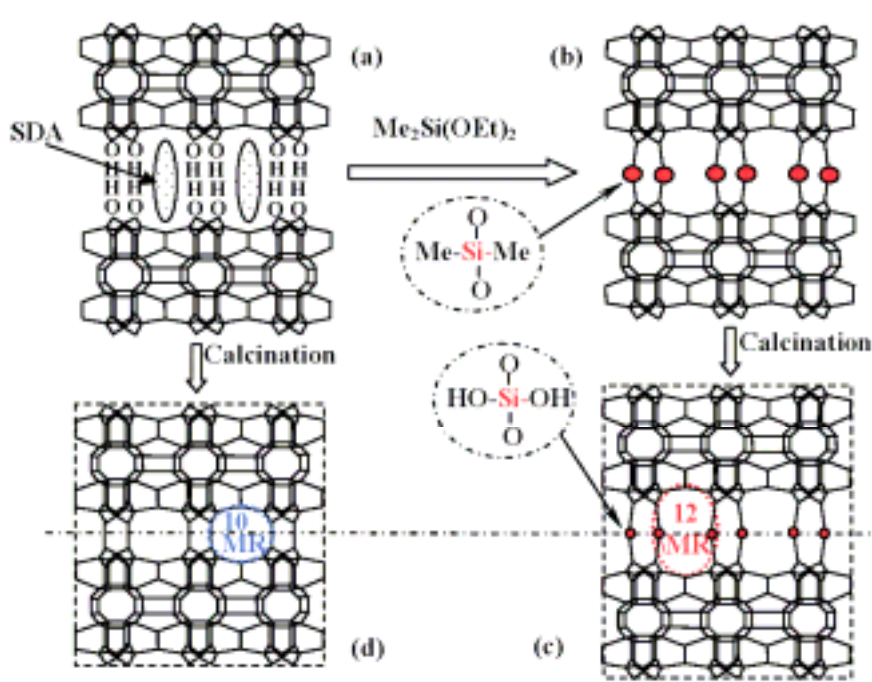


Fig.1-10 Formation of interlayer-expanded zeolite (IEZ) of Al-MWW as an example.

## 2.5 Conversion of one zeolite into another

Just as lamellar phases are sometimes transiently observed during the course of

zeolite preparations, the formation of one zeolite phase may be preceded by another. In early work on the synthesis of ZSM-5, Erdem and Sand observed the intermediate appearance of mordenite and analcime during the synthesis of Na, TPA-ZSM-5 as the TPA/Na ratio was lowered [106]. For the TPA, K system, metastable harmotome was observed. However, zeolite metastability is most commonly encountered in the phenomenon of reaction over-run, in which the zeolite product decomposes under the reaction conditions to afford a more dense phase. In this way, aluminous zeolites transform into dense silica phases, usually quartz or cristobalite. Intermediate cases maintain the materials balance by undergoing a type of disproportionation, so that aluminous ZSM-5 products decompose to quartz and a more aluminous zeolite such as mordenite or (for high-Al samples) analcime. These latter cases provide examples of the conversion of one zeolite into another. Whilst these instances are more likely to be troublesome than helpful, there are cases in which zeolite interconversions can be of practical use, or interesting from a mechanistic point of view.

One of the earliest successful zeolite syntheses –and the first synthesis of a zeolite not found in nature– was the conversion of analcime into two KFI-type phases by Barrer in 1948 [7–9]. This synthesis was not of the  $\text{OH}^-$ -mediated type but involved heating the starting phase in strong solutions of barium salts at 170-270 °C. The same generic procedure was the subject of a more recent detailed study of the hydrothermal conversion of zeolite LTA into zeolite Li-A(BW) using aqueous LiCl at temperature of 180-260 °C [107]. The crystallisation was followed by in-situ time resolved synchrotron XRPD combined with ex-situ SEM of partially converted samples. These combined techniques clearly showed that the inter-zeolite conversion was a solution-mediated process, the Li-A(BW) product growing radially from nucleation sites on the parent

LTA crystals.

A complex and interesting system of transformations surrounds the synthesis of zeolite omega, the synthetic analogue of the mineral zeolite mazzite and also isostructural with the synthetic phase ZSM-4. Many syntheses of zeolite Na-Y will over-run to give zeolite Na-P. However, in the presence of tetramethylammonium (TMA) ions, this transition does not occur, the faujasite decomposing instead to zeolite ZSM-4. In the study by Dwyer and Chu [108], no ZSM-4 was formed until the faujasite crystallisation was complete and there was no evidence for any amorphous or crystalline intermediate, the ZSM-4 appearing to nucleate on the surface of the dissolving faujasite crystals. Broadly similar results were reported for zeolite omega [109]. A more recent investigation found that faujasite appeared as an intermediate in Na, TMA-omega synthesis at 100 °C but was not observed at 135 °C. Depending upon the choice of reagents and the reaction conditions, sodalite, analcime, mordenite and cristbalite were also observed as co-products [110]. Other transformations which have been reported include pseudomorphic transformation of zeolite Na-A into nepheline by the action of water vapor at 600 °C [111].

Two research groups have made particular studies of zeolite-zeolite transformation. Subotić and coworkers carried out a detailed investigation of the conversion of zeolite A into hydroxyl sodalite which occurs in concentrated (>10%) sodium hydroxide solutions [112,113]. Working in the temperature range 70-85 °C, they monitored the reaction mixture and particle populations present in the reaction mixture and measured the concentrations of silica and alumina in solution. From a detailed analysis of the reaction kinetics, they concluded that the reaction was a solution-mediated process in which the zeolite A dissolved and the sodalite product nucleated heterogeneously. The growth of

the sodalite crystals (by surface addition of monomeric silicate and aluminate ions) was the rate-limiting step of the conversion. No intermediate phases were detected and the transformation rate increased strongly with increasing NaOH concentration. Similar conclusions were reached in parallel study of the conversion of zeolite A into zeolite P which occurs under comparable conditions but at lower base concentrations [114].

The other team to investigate zeolite-zeolite transformations in detail is that of Zones et al. The work initially set out along the lines of the faujasite  $\rightarrow$  omega conversion, exploiting the unusual organo-cations which were to become such a characteristic feature of this group's work. In this way, cubic zeolite P (Na-P<sub>C</sub>) was transformed into zeolite SSZ-13 (a high-silica chabazite) by the action of the *N,N,N*-trimethylammonium-1-adamantane cation, although the presence of further silica was necessary to satisfy the mass balance [115]. By using Na-P<sub>C</sub> as starting material, other templates gave sodalite (from TMA) and (from quaternaries containing cyclic units) the zeolite SSZ-16, SSZ-17 (NU-3) and SSZ-19 [116]. In all cases, the organocations were incorporated into the crystalline products. With the extension of this work to faujasites as starting reagents [117], an interesting synthetic method began to develop, since it was found that the reactivity of the system could be modified by treating the primary zeolites in different ways, for example by steaming, calcination or ion exchange. The synthetic utility of inter-zeolite conversions was subsequently well demonstrated by the versatility discovered for boron-beta zeolite, which gave enhanced nucleation, increased reaction rates, greater flexibility in choice of template and new possibilities for lattice substitution. In later studies, it was also found that, for a given template, product selectivities could be altered by changing the initial B/SiO<sub>2</sub> ratio, for example by adding extra borate to the reaction mixture [118].

These new synthesis strategies for zeolite to zeolite transformations have subsequently been adopted by other workers [119]. Their utility stems from the additional degree of control attainable in these crystalline products. In addition, a crystalline precursor may have unusual surface reactivity, e.g. for the generation of heterogeneous nucleation sites.

Sano et al. have also investigated the synthesis of zeolites using another zeolite. They termed this methodology the “interzeolite conversion method” and have succeeded in the syntheses of \*BEA- [120], RUT- [121], and MTN-type zeolites [122] from FAU-type zeolite. Moreover, they reported that interzeolite conversion of FAU-\*BEA [123] and LEV [124] under the OSDA-free condition. Although these zeolites were obtained from amorphous materials under the same condition, the use of FAU-type zeolite as the starting material resulted in a crystallization rate superior to that achieved with conventional zeolite synthesis, in which amorphous aluminosilicate gel is used as the starting material. The enhanced crystallization rate was due to the decomposition/dissolution of the starting zeolite species, which generated locally ordered aluminosilicate species (nanoparts), which in turn assembled and transformed into a different type of zeolite [125].

As mentioned above, the interzeolite conversion method affords the design synthesis of a zeolite, which cannot be obtained via a conventional hydrothermal technique from amorphous materials, and explaining the formation mechanism of zeolite structure.

### **3. Zeolite Characterization**

Over the last decade advancement in the area of characterization of nanoporous

materials has taken place employing a variety of techniques. Characterization of microporous materials is essential in understanding their physical properties, their structure-application relationships, why certain structures favor specific reactions, and for a greater knowledge into the design of new materials. The most valuable and obvious information that can be gained from diffraction experiments, is the automatically resolved crystal structure, its geometry, i.e. the framework structure, the pore opening and volume, the connectivity of channels, and its composition including the distribution of active centers in the framework. X-ray diffraction is the most widely used technique for structure elucidation using single crystal X-ray diffraction and powder diffraction data for the analysis. In that regard, the book *Collection of Simulated XRD powder patterns of zeolites* is most valuable and also provides information about the space group and unit cell parameters [127].

Field emission scanning electron microscopy (FE-SEM) is the method of choice for determining the size and morphology of zeolite crystallites. High-resolution transmission electron microscopy has been extensively used to study intergrowth fault planes and stacking faults and recently for structural analysis [128,129]. Moreover, the advent of atomic force microscopy (AFM), a very powerful technique for imaging nonconducting solid surfaces, now enables the imaging of surface growth features of zeolites [130].

Common spectroscopic methods for analyzing zeolite structure include magic angle spinning (MAS)  $^{29}\text{Si}$  and  $^{27}\text{Al}$  nuclear magnetic resonance (NMR) spectroscopy [131,132]. Information regarding the coordination environment around Si and Al and the framework Si/Al ratio can be obtained. Infrared spectroscopy via the frequencies of structure-sensitive bands provides information regarding framework properties,

including Si/Al ratios and nature of acidity by the –OH stretching vibration [133,134]. Other techniques used include Raman spectroscopy, which provides information complementary to infrared, X-ray fluorescence spectroscopy and inductively coupled plasma for elemental analysis, and X-ray photoelectron spectroscopy for surface analysis [135-140].

High-energy XRD (HEXRD) is a diffraction technique carried out at short wavelength, which can be used to determine various atom-atom correlations present in a system. This technique does not depend on the symmetry present in the solid and can be used to determine the structure of ordered and disordered materials. Depending on the available data range, it is possible to extract near neighbor information of up to ca. 10 Å [141]. In addition, computational chemistry is now aiding structure analysis, modeling of synthetic pathway, and chemical reactivity [142].

#### **4. Application of zeolite**

Zeolites are important industrial materials that have a broad range of applications. Many zeolites with different structures and compositions are commercially available and used in refining and chemical processing. In addition, natural zeolites because of their lower cost are used in bulk mineral applications.

In Table 1-1, a summary of the typical commercial zeolite adsorbent product is presented, together with short descriptors of the chemical composition and example applications. A brief study of the information in Table 1-1 will quickly draw attention to the fact that majority of the key adsorbents for the industrial gas business are essentially low silica zeolites, in general processing  $\text{SiO}_2/\text{Al}_2\text{O}_3$  ratios  $< 5$ . The higher  $\text{SiO}_2/\text{Al}_2\text{O}_3$

ratio zeolites, which are commonplace amongst industrial zeolite catalysts, have found niche applications in adsorption processes, with the focus being in hydrocarbon and/or desulfurization applications. In commercially available low silica zeolite family, those belonging to the A and X types have the greatest number of currently available products. The primary differentiator between these different products is the type of extra-framework cation, and for the zeolite X family, the  $\text{SiO}_2/\text{Al}_2\text{O}_3$  ratio. The use of ion-exchange techniques to alter the adsorption properties of these A and X, and to a lesser extent zeolite Y adsorbents, has proven to be the most successful method of adsorbent modification, in current commercial use [143].

<sup>a</sup>. PSA: pressure swing adsorption, VPSA: vacuum pressure swing adsorption, HC: hydrocarbon  
 Table 1-1 Important industrial adsorbents and example applications<sup>a</sup>.

Framework code	Commercial products	$\text{SiO}_2/\text{Al}_2\text{O}_3$	Cations	Application Examples
LTA	3A	2	K > 70%	EtOH dehydration, Drying
	4A	2	Na > 99%	Desiccant, Medical O <sub>2</sub> , other PSA, Natural gas processing
	5A	2	Ca > 70%	H <sub>2</sub> PSA, Medical O <sub>2</sub> , VPSA O <sub>2</sub> , Natural gas processing
FAU (Zeolite X)	13X	2-2.5	> 99% Na	Air prepurification
	LiX	2-2.5	> 88% Li	VPSA O <sub>2</sub> , Medical O <sub>2</sub>
	AgX	2-2.5	> 80% Ag	CO, H <sub>2</sub> adsorbent
	BaX		Ba, K	<i>p</i> -xylene recovery
	CaX	2-2.5	> 70% Ca	H <sub>2</sub> PSA, N <sub>2</sub> O removal, VPSA
FAU (Zeolite Y)	NaY	3-5	> 99% Na	Desulfurization, HC separation
	HY	20-1000	H <sup>+</sup>	Desulfurization, HC separation
MOR	Small/Large Port	5	Na	Desulfurization, HC separation
HEU	TSM-140/CS400	6	Mixed (Na, K, Ca, Mg)	N <sub>2</sub> O removal

hydrocarbon

Catalysis is one of the most important fields of application of zeolites. In 1999, Tanabe and Holderich have published an interesting survey of the industrial processes based on the use of solid acid-base catalysts, highlighting the primary role played by zeolites. They found that a total of 127 industrial processes employ 180 solid catalysts, of which

74 include at least a zeolite phase. A more detailed view of the survey results indicated that only a few framework types are effectively used, being MFI, FAU, MOR, and \*BEA the most extensively employed [144]. Oil refining and petrochemistry are important industrial sectors where zeolites find a widespread use as heterogeneous acid catalysts and molecular sieves. The role and the increasing importance of zeolite catalysts is examined through the Fluid Catalytic Cracking (FCC), one of the most important process in the modern refinery, and the synthesis of cumene, the intermediate in the production of phenol. Advantages of zeolites that are being exploited include heterogenization of catalysts for easy separation framework, doping with metals for selective oxidation chemistry, and ease of regeneration of catalysts. Among the most important properties of zeolites with respect to their use as catalyst is their surface acidity. Both Brønsted and Lewis acid sites occur in zeolites. To describe the acidity of zeolites in an adequate manner, it is mandatory to clearly distinguish between (i) the nature of acid sites (i.e. Brønsted vs. Lewis acidity), (ii) the density or concentration of these sites, (iii) their strength of strength distribution and, last but not least, (iv) the precise location of the acid sites.

By their negatively charged porous framework and the small and mobile cations sitting in the pores, zeolites are typical ion exchangers. In fact, zeolites are widely used as builders in laundry detergents where their role is to take up calcium and magnesium ions in exchange for sodium ions, thereby softening the washing water. Obviously, an as high as possible cation exchange capacity and, hence the highest possible aluminum content in the framework ( $\text{Si/Al ratio} = 1$ ) are desired for this application. This is the domain of zeolite A, and as a whole, the use of zeolites as ion-exchangers in detergents represents their largest market in terms of tonnage with a worldwide production rate

close to 1 million t/year [4].

Over the past twenty years the development of zeolite-based membrane has attracted considerable research efforts [145,146]. The great expectations related with zeolites as separation media are based on their selectivity that could be used to separate molecules with difference in size below 1 Å [147]. Besides the unraveled selectivity, the particular properties of zeolite membranes that attracted the attention of academic and application scientists are: (i) long-term stability at high temperature, (ii) resistance to harsh environments, (iii) resistance to high pressure drop, (iv) inertness of microbiological degradation, (v) easy cleanability and catalytic activation. The interest in zeolite membrane is also related with the nowadays requirements for the minimization of energy consumption and cleaner technologies [148,149].

Other niche applications include sensor, photochemical organic transformations, and conversion of solar energy. Bulk applications for zeolite powders have emerged for odor removal and as plastic additives.

## **5. Overview of the thesis**

As described the previous sections, zeolites are attractive due to unique properties. They have been already applied in many industrial areas widely. Even today, however, the design synthesis of zeolites with desirable structure and composition is very difficult. To expand the versatility of interzeolite conversion, in this thesis, I focused on following four research areas in interzeolite conversion method.

1. Effect of SDA (Chapter 2, 3)
2. Effect of synthesis conditions (Chapter 4, 5)

3. Effect of starting materials (Chapter 6)

4. Interzeolite conversion process (Chapter 7)

Through my study, it was clarified that the interzeolite conversion method has the high potential for alternative zeolite synthesis.

## References

- [1] D.S. Wragg, R.E. Morris, A. W. Burton, *Chem. Mater.* 20 (2008) 1561.
- [2] R.M. Barrer, *J. Chem. Soc.* (1948) 127.
- [3] Database of Zeolite Structures, Structure Commission of the International Zeolite Association, <http://www.izastructure.org/databases/>
- [4] J. Weitkamp, *Solid State Ionics.* 131 (2000) 175.
- [5] M.E. Davis, R.F. Lobo, *Chem. Mater.* 4 (1992) 756.
- [6] H. de St Claire Deville, *Compt. Rend. Séances Acad. Sci.* 54 (1862) 324.
- [7] R.M. Barrer, *J. Chem. Soc.* (1948) 127.
- [8] R.M. Barrer, L. Hinds, E.A. White, *J. Chem. Soc.* (1953) 1466.
- [9] R.M. Barrer, C. Marcilly, *J. Chem. Soc. (A)* (1970) 2735.
- [10] Ch. Baerlocher, W.M. Meier, D.H. Olson, *Atlas of Zeolite Structure Types*, fifth ed., Elsevier, Amsterdam, (2001).
- [11] G.T. Kerr, *Science* 140 (1963) 1412.
- [12] G.T. Kerr, *Inorg. Chem.* 5 (1966) 1539.
- [13] R.M. Milton, US Patent 2,882,243 (1959).
- [14] R.M. Milton, US Patent 2,882,244 (1959).
- [15] R.M. Milton, M.L. Occelli, H.E. Robson (Eds.), *Zeolite Synthesis*, ACS Symp. Ser.

398 (1989) 1.

[16] R.M. Barrer, P.J. Denny, *J. Chem. Soc.* (1961) 971.

[17] G.T. Kerr, G.T. Kokotailo, *J. Am. Chem. Soc.* 83 (1961) 4675.

[18] G.T. Kerr, *Inorg. Chem.* 5 (1966) 1537.

[19] R.L. Wadlinger, G.T. Kerr, E.J. Rosinski, US Patent 3,308,069 (1967).

[20] R.J. Argauer, G.R. Landolt, US Patent 3,702,886 (1972).

[21] R. Szostak, *Molecular Sieves—Principles of Synthesis and Identification*, Van Nostrand Reinhold, New York, 1989, second ed., Blackie, London, (1998).

[22] S.T. Wilson, B.M. Lok, C.A. Messina, T.R. Cannan, E.M. Flanigen, *J. Am. Chem. Soc.* 104 (1982) 1146.

[23] M.E. Davis, C. Saldarriaga, C. Monte, J. Garces, C. Crowder, *Nature* 331 (1988) 698.

[24] S.M. Kuznicki, US Patents 4,853,202 (1989), 4,938,939 (1990).

[25] T. Blasco, M.A. Camblor, A. Corma, P. Esteve, A. Martinez, C. Prieto, S. Valencia, *Chem. Commun.* (1996) 2367.

[26] Y. Oumi, T. Manabe, H. Sasaki, T. Inuzuka, T. Sano, *Appl. Catal. A* 388 (2010) 256.

[27] A. Corma, M.T. Navarro, F. Rey, J. Rius, S. Valencia, *Angew. Chem. Int. Ed.* 40 (2001) 2277.

- [28] J.-L. Paillaud, B. Harbuzaru, J. Patarin, and N. Bats, *Science* 304 (2004) 990.
- [29] A. Corma, M.J. Diaz-Cabanas, J.L. Jorda, C. Martinez, M. Moliner, *Nature* 443 (2006) 842.
- [30] E. Flanigen, R.L. Patton, US Patent 4,073,865 (1978).
- [31] P. A. Barrett, M.A. Camblor, A. Corma, R.H. Jones, L.A. Villaescusa, *J. Phys. Chem. B* 102 (1998) 4147.
- [32] H. Koller, R.F. Lobo, S.L. Burkett, M.E. Davis, *J. Phys. Chem.* 99 (1995) 12588
- [33] T. Blasco, M.A. Camblor, A. Corma, P. Esteve, J.M. Guil, A. Martinez, J.A. Perdigon-Melon, S. Valencia, *J. Phys. Chem. B* 102 (1998) 75.
- [34] H. Kessler, J. Patarin, C. Schott-Daric, *Stud. Surf. Sci. Catal.* 85 (1994) 75.
- [35] M. Estermann, L.B. McCusker, C. Baerlocher, A. Merrouche, H. Kessler, *Nature* 352 (1991) 320.
- [36] M.A. Camblor, A. Corma, P. Lightfoot, L.A. Villaescusa, P.A. Wright, *Angew. Chem. Int. Ed.* 36 (1997) 2659.
- [37] L.A. Villaescusa, P.A. Barrett, M.A. Camblor, *Angew. Chem. Int. Ed.* 38 (1999) 1997.
- [38] S. L. Burkett, M. E. Davis, *Chem. Mater.* 7 (1995) 920.
- [39] J. Ciric, US Patent 3,950,496 (1976).

- [40] D.F. Shantz, A. Burton, R.F. Lobo, *Micropor. Mesopor. Mater.* 31 (1999) 61
- [41] R. Lobo, S. I. Zones, M. E. Davis, *J. Inclus. Phenom. Mol. Rec. Chem.* 21 (1995) 47.
- [42] H. Gies, B. Marler, *Zeolites*, 12 (1992) 42.
- [43] A. Moini, K.D. Schmitt, R.F. Polomski, *Zeolites*, 18 (1997) 2.
- [44] C.C. Freyhardt, M. Tsapatsis, R.F. Lobo, K.J. Bulkus, M.E. Davis, *Nature* 295 (1996) 381.
- [45] P. Wagner, M. Yoshikawa, M. Lovallo, K. Tsuji, M. Taspatsis, M.E. Davis, *Chem. Commun.*, (1997) 2179.
- [46] S.A. Elomari, S.I. Zones, *Stud. Surf. Sci. Catal.* 135 (2001) 479.
- [47] A. Burton, S. Elomari, C.-Y. Chen, R.C. Medrud, I.Y. Chan, L.M. Bull, C. Kibby, T.V. Harris, S. I. Zones, E.S. Vittoratos, *Chem. Eur. J.* 9 (2003) 5737.
- [48] J. Sun, C. Bonneau, Angel Cantin, A. Corma, M.J. Diaz-Cabanas, M. Moliner, D. Zhang, M. Li, X. Zou, *Nature* 458 (2009) 1154.
- [49] A.B. Pinar, L. Gomez-Hortiguera, J. Perez-Pariente, *J. Phys. Chem. C* 115 (2011) 1096.
- [50] R. García, L. Gómez-Hortiguera, I. Díaz, E. Sastre, J. Pérez-Pariente, *Chem. Mater.* 20 (2008) 1099.

- [51] C. Marquez-Alvarez, A.B. Pinar, R. Garcia M. Grande-Casas, J. Perez-Pariente, *Top. Catal.* 52 (2009) 1281.
- [52] A.B. Pinar, C. Márquez-Álvarez, M. Grande-Casas, J. Pérez-Pariente, *J. Catal.* 263 (2009) 258.
- [53] L. Gomez-Hortiguela, A.B. Pinar, F. Cora, J. Perez-Pariente, *Chem. Commun.*, 46 (2010) 2073.
- [54] Y. Roman-Leshkov, M. Moliner, M.E. Davis, *J. Phys. Chem. C* 115 (2011) 1096.
- [55] A. Jackowski, S.I. Zones, S.-J. Hwang, A.W. Burton, *J. Am. Chem. Soc.* 131 (2009) 1092.
- [56] A. Tuel, Y.B. Taarit, *Zeolites*, 13 (1993) 357.
- [57] A. Tuel, Y.B. Taarit, *Zeolites*, 14 (1994) 272.
- [58] D.L. Dorset, G.J. Kennedy, K.G. Strohmaier, M.J. Diaz-Cabanas, F. Rey, A. Corma, *J. Am. Chem. Soc.* 126 (2006) 8862.
- [59] A. Corma, M.J. Diaz-Cabanas, J.L. Jorda, F. Rey, G. Sastre, K.G. Strohmaier, *J. Am. Chem. Soc.* 130 (2008) 16482.
- [60] A. Corma, M.J. Díaz-Cabañas, J. Jiang, M. Afeworki, D.L. Dorset, S.L. Soled, K.G. Strohmaier, *Proc. Natl. Acad. Sci. U.S.A.* 107 (2010) 11935.
- [61] R. Simancas, D. Dari, N. Velamazán, M.T. Navarro, A. Cantín, J.L. Jordá, G. Sastre,

- A. Corma, F. Rey, *Science* 330 (2010) 1219.
- [62] D.M. Bibby, M.P. Dale, *Nature* 317 (1985) 157.
- [63] C.M. Braunbarth, P. Behrens, J. Felsche, G. van de Goor, G. Wildermuth, G. Engelhardt, *Zeolites* 16 (1996) 207.
- [64] C.M. Braunbarth, P. Behrens, J. Felsche, G. van de Goor, *Solid State Ionics* 101-103 (1997) 1273.
- [65] E.R. Cooper, C.D. Andrews, P.S. Wheatley, P.B. Webb, P. Wormald, R.E. Morris, *Nature* 430 (2004) 1012.
- [66] M. Antonietti, D. Kuang, B. Smarsly, Y. Zhou, *Angew. Chem. Int. Ed.* 43 (2004) 4988.
- [67] R. Ludwig, U. Kragl, *Angew. Chem. Int. Ed.* 46 (2007) 6582.
- [68] R.E. Morris, *Angew. Chem. Int. Ed.* 47 (2008) 442.
- [69] E.R. Parnham, R.E. Morris, *J. Mater. Chem.* 16 (2006) 3682.
- [70] E.R. Parnham, R.E. Morris, *J. Am. Chem. Soc.* 128 (2006) 2204.
- [71] E.R. Parnham, R.E. Morris, *Acc. Chem. Res.* 40 (2007) 1005.
- [72] S.I. Zones, *Micropor. Mesopor. Mater.* 144 (2011) 1.
- [73] F. Schmidt, *Appl. Catal. A: Gen.* 221 (2001) 15.
- [74] B. Xie, J. Song, L. Ren, Y. Ji, F.-S. Xiao, *Chem. Mater.*, 20 (2008) 4533.

- [75] K. Iyoki, Y. Kamimura, K. Itabashi, A. Shimojima, T. Okubo, *Chem. Lett.* 39 (2010) 730.
- [76] L. Zhang, C. Yang, X. Meng, B. Xie, L. Wang, L. Ren, S. Ma, F.-S. Xiao, *Chem. Mater.* 22 (2010) 3099.
- [77] Z. Wu, J. Song, Y. Ji, L. Ren, F.-S. Xiao, *Chem. Mater.*, 20 (2008) 357.
- [78] T. Yokoi, M. Yoshioka, H. Imai, T. Tatsumi, *Angew. Chem. Int. Ed.* 48 (2009) 9884.
- [79] H. Lee, S.I. Zones, M.E. Davis, *Nature*, 458 (2003) 1154.
- [80] H. Lee, S.I. Zones, M.E. Davis, *J. Phys. Chem. B* 109 (2005) 2187.
- [81] H. Lee, S.I. Zones, M.E. Davis, *Micropor. Mesopor. Mater.* 88 (2006) 266.
- [82] S.I. Zones, U.S. Patent 20080075656 (2008).
- [83] F. Feng, K.J. Balkus Jr., *Micropor. Mesopor. Mater.* 69 (2004) 85.
- [84] C.S. Cundy, B.M. Lowe, D.M. Sinclair, *J. Cryst. Growth* 100 (1990) 189.
- [85] U. Oberhagemann, P. Bayat, B. Marler, H. Gies, J. Rius, *Angew. Chem. Int. Ed.* 35 (1996) 2869.
- [86] S. Vortmann, J. Rius, S. Siegmann, H. Gies, *J. Phys. Chem. B* 101 (1997) 1292.
- [87] S. Vortmann, J. Rius, B. Marler, H. Gies, *Eur. J. Mineral.* 11 (1999) 125.
- [88] U. Lohse, B. Altrichter, R. Fricke, W. Pilz, E. Schreier, Ch. Garkisch, K. Jancke, *J. Chem. Soc. Faraday Trans.* 93 (1997) 505.

- [89] J.M. Garcés, S.C. Rocke, C.E. Crowder, D.L. Hasha, *Clays Clay Miner.* 36 (1988) 409.
- [90] A. Tuel, *Chem. Mater.* 11 (1999) 1865.
- [91] T.V. Whittam, *Eur. Patent* 0054364 (1982).
- [92] A.J. Blale, K.R. Franklin, B.M. Lowe, *J. Chem. Soc. Dalton Trans.* (1988) 2513.
- [93] R. Millini, G. Perego, W.O. Parker, Jr., G. Bellussi, L. Carluccio, *Micropor. Mater.* 4 (1995) 221.
- [94] L. Schreyeck, P. Caullet, J.-C. Mougénel, J.-L. Guth, B. Marler, *Micropor. Mater.* 6 (1996) 259.
- [95] A. Corma, V. Fornes, S.B. Pergher, Th.L.M. Maesen, J.G. Buglass, *Nature* 396 (1998) 353.
- [96] A. Corma, U. Diaz, M.E. Domine, V. Fornes, *J. Am. Chem. Soc.* 122 (2000) 2804.
- [97] M.K. Rubin, P. Chu, *US Patent* 4, 954, 325 (1990).
- [98] S.L. Lawton, A.S. Fung, G.J. Kennedy, L.B. Alemany, C.D. Chang, G.H. Hatzikos, D.N. Lissy, M.K. Rubin, H.-K.C. Timken, S. Steuernagel, D.E. Woessner, *J. Phys. Chem.* 100(1996) 3788.
- [99] L. Puppe, J. Weisser, *US Patent* 4,439,409 (1984).
- [100] M.K. Rubin, P. Chu, *US Patent* 4,954,325 (1990).

- [101] S.I. Zones, Eur. Patent 231860 (1987).
- [102] R. Millini, G. Perego, W.O. Parker, G. Bellussi, L. Carluccio, *Microporous Mater.* 4 (1995) 221.
- [103] U. Diaz, V. Fornés, A. Corma, *Micropor. Mesopor. Mater.* 90 (2006) 73.
- [104] P. Wu, J. Ruan, L. Wang, L. Wu, Y. Wang, Y. Liu, W. Fan, M. He, O. Terasaki, T. Tatsumi, *J. Am. Chem. Soc.* 130 (2008) 8178.
- [105] S. Inagaki, H. Imai, S. Tsujiuchi, H. Yakushiji, T. Yokoi, T. Tatsumi, *Micropor. Mesopor. Mater.* 142 (2011) 354.
- [106] A. Erdem, L.B. Sand, *J. Catal.* 60 (1979) 241.
- [107] P. Norby, *J. Am. Chem. Soc.* 119 (1997) 5215.
- [108] F.G. Dwyer, P. Chu, *J. Catal.* 59 (1979) 263.
- [109] A.J. Perrotta, C. Kibby, B.R. Mitchell, E.R. Tucci, *J. Catal.* 55 (1978) 240.
- [110] F. Fajula, M. Vera-Pacheco, F. Figueras, *Zeolites* 7 (1987) 203.
- [111] J. Richter-Mendau, W. Lutz, A. Grossmann, *Cryst. Res. Technol.* 23 (1988) 1245.
- [112] B. Subotić, D. Škrtić, I. Šmit, L. Sekanović, *J. Cryst. Growth* 50 (1980) 498.
- [113] B. Subotić, L. Sekanović, *J. Cryst. Growth* 75 (1986) 561.
- [114] B. Subotić, I. Šmit, O. Madžija, L. Sekanović, *Zeolites* 2 (1982) 135.
- [115] S.I. Zones, R.A. Van Nordstand, *Zeolites* 8 (1988) 166.

- [116] S.I. Zones, R.A. Van Nordstand, *Zeolites* 8 (1988) 409.
- [117] S.I. Zones, *J. Chem. Soc. Faraday Trans.* 87 (1991) 3709.
- [118] S.I. Zones, Y. Nakagawa, *Micropor. Mater.* 2 (1994) 557.
- [119] R.K. Ahedi, Y. Kubota, Y. Sugi, *J. Mater. Chem.* 11 (2001) 2922.
- [120] H. Jon, K. Nakahata, B. Lu, Y. Oumi, T. Sano, *Micropor. Mesopor. Mater.* 96 (2006) 72.
- [121] H. Jon, S. Takahashi, H. Sasaki, Y. Oumi, T. Sano, *Micropor. Mesopor. Mater.* 113 (2008) 56.
- [122] H. Sasaki, H. Jon, M. Itakura, T. Inoue, T. Ikeda, Y. Oumi, T. Sano, *J. Porous Mater.* 16 (2009) 465.
- [123] K. Honda, A. Yashiki, M. Itakura, Y. Ide, M. Sadakane, T. Sano, *Micropor. Mesopor. Mater.* 142 (2011) 161.
- [124] A. Yashiki, K. Honda, A. Fujimoto, S. Shibata, Y. Ide, M. Sadakane, T. Sano, *J. Cryst. Growth* 325 (2011) 96 .
- [125] H. Jon, N. Ikawa, Y. Oumi, T. Sano, *Chem. Mater.*, 20 (2008), 4135.
- [126] G.T. kokotailo, C.A. Fyfe, Y. Feng, H. Grondey, H. Gies, B. Marler, D.E. Cox, *Stud. Surf. Sci. Catal.* 94 (1995) 78.
- [127] M.M.J. Treacy, J.B. Higgins, *Collection of Simulated XRD Powder Patterns for*

Zeolites (2007) 484.

[128] J.M. Thomas, O. Terasaki, P.L. Gai, W. Zhou, J. Gonzales-Calbet, *Acc. Chem. Res.* 34 (2001) 583.

[129] O. Terasaki, T. Ohsuna, *Top. Catal.* 24 (2003) 13.

[130] J.R. Agger, N. Pervaiz, A.K. Cheetham, M.W. Anderson, *J. Am. Chem. Soc.* 120 (1998) 10754.

[131] D.F. Shantz, R.F. Lobo, *Top. Catal.* 9 (1999) 1.

[132] C.A. Fyfe, Y. Feng, H. Grondy, G.T. Kokotailo, H. Gies, *Chem. Rev.* 91 (1991) 1525.

[133] C. Arean, *Inorg. Chem.* 22 (2000) 241.

[134] H.G. Karge, *Micropor. Mesopor. Mater.* 22 (1998) 547.

[135] P.-P. Knops-Girrits, D.E. De Vos, E.J.P. Feijen, P.A. Jacobs, *Micropor. Mater.* 9 (1997) 3.

[136] N. Ortins, T. Kruger, P.K. Dutta, In: M. Pelletier, ed. *Analytical Application of Raman Spectroscopy*. Oxford: Blackwell, (1999) 328.

[137] D. Biglino, H. Li, R. Erckson, A. Lund, H. Yahiro, M. Shiotani, *Phys. Chem., Chem. Phys.*, 1 (1999) 2887.

[138] M. Stocker, *Microporous Mater.* 6 (1996) 235.

- [139] D.A. Peru, R.J. Collins, *Fresenius J. Anal. Chem.* 346 (1993) 909.
- [140] A.E. Pillay, M. Peisach, *J. Radioanal. Nucl. Chem.* 153 (1991) 75.
- [141] T. Wakihara, S. Kohara, G. Sankar, S. Saito, M. Sanchez-Sanchez, A.R. Overweg, W. Fan, M. Ogura, T. Okubo, *Phys. Chem. Chem. Phys.* 8 (2006) 224.
- [142] R. Catlow, R. Bell, F. Cora, B. Slater, *Stud. Surf. Sci. Catal.* 168 (2007) 659.
- [143] C. Martinez, J. Perez-Pariente eds., *Zeolites and Ordered Porous Solids: Fundamentals and Applications* (2011).
- [144] K. Tanabea, W.F. Holderich, *Appl. Catal. A*, 181 (1999) 399.
- [145] R.D. Noble, J.L. Falconer, *Catal. Today* 25 ( 1995) 209.
- [146] T. Bein, *Chem. Mater.* 8 (1996) 1636.
- [147] M. Matsukata, E. Kikuchi, *Bull. Chem. Soc. Jpn.* 70 (1997) 2341.
- [148] E.E. McLeary, J.C. Jansen, F. Kapteijn, *Micropor. Mesopor. Mater.* 90 (2006) 198.
- [149] J. Caro, M. Noack, *Micropor. Mesopor. Mater.* 115 (2008) 215.

## **Chapter 2**

# **Synthesis of LEV-type zeolite by interzeolite conversion method and its catalytic performance in ethanol to olefins reaction**

### **1. Introduction**

It is well known that zeolites are industrially important microporous materials due to their numerous properties such as ion-exchange, adsorption, and catalytic properties. In fact, zeolites are greatly used in petrochemical industries, oil refineries and fine chemicals industries [1-3]. Recently, the application of zeolites in the production of biofuels from various biomass derived feedstock as a solid acid catalyst has been investigated [4]. Although bio-ethanol obtained by fermentation of biomass is well known as a gasoline additive, bio-ethanol also has great potential to be a candidate for the source of light olefins such as ethylene and propylene. Production of biofuels and light olefins from biomass is an example of the carbon neutral process, However, there are only a few reports concerning ethanol conversion to light olefins [5-8]. The ethanol conversion to hydrocarbons is assumed to proceed in a similar mechanism to the methanol conversion. According to the literature, zeolites with a 8-membered ring (8-MR) pore system are excellent for the catalyst of methanol to light olefins (MTO) reaction [9]. One of them, CHA-type

zeolite group, has been known to have a high selectivity to light olefins [10-12].

In general, a zeolite is synthesized under a hydrothermal condition using an amorphous aluminosilicate gel as a starting material. However, at times the formation of a zeolite phase may be preceded with another phase during the course of zeolite crystallization. This phenomenon, therefore, can be considered to be an alternative synthesis strategy for the hydrothermal conversion of one zeolite into another, i.e., interzeolite conversion [13]. This method is of attractive research area, since it may provide information about the crystallization mechanism and also is an outstanding route to obtain a new zeolite which cannot be crystallized by a conventional method. However, there are only a few studies concerning this route, in which a particular zeolite is used as a crystalline aluminosilicate source instead of an amorphous aluminosilicate gel. The detailed studies on the hydrothermal conversion of A zeolite into sodalite (SOD) [14,15] and P zeolite (GIS) [16] were carried out by Subotić et al. Moreover, Zones et al. investigated the conversion of various zeolites, for instance Y zeolite (FAU) to SSZ-13 [17]; B-\*BEA to B-SSZ-24, B-SSZ-31, and B-SSZ-33; Al-\*BEA to Al-SSZ-24 and Al-SSZ-31 in presence of adamantammonium cation and its derivatives [18,19]. Kubota and Sugi et al. succeeded in the direct synthesis of Al-SSZ-31 from Al-\*BEA and Ti-SSZ-24 from Ti-\*BEA [20,21].

Sano et al. have also investigated the potential of the interzeolite conversion method. The highly crystalline and pure \*BEA- [22], RUT- [23], and MTN- [24] type zeolites were obtained from FAU-type zeolite in the presence of tetraethylammonium hydroxide (TEAOH), tetramethylammonium hydroxide (TMAOH), and benzyltrimethylammonium hydroxide (BTMAOH), respectively.

Moreover, it was found that when the zeolite was used as the starting material, the crystallization rate of the obtained zeolite was remarkably fast. In the recent result, locally ordered aluminosilicate species (nanoparts) coming from the decomposition and/or dissolution of FAU-type zeolite during the hydrothermal conversion of FAU-type zeolite into \*BEA-type zeolite were present in the mesoporous materials synthesized in the presence of surfactant [25]. Their assembly under a specific structure-directing agent (SDA) gave rise to the fast crystallization rate. This phenomenon indicates an possibility that when FAU-type zeolite is dissolved at lower temperatures, more locally ordered aluminosilicate species having the building unit of FAU-type zeolite are generated.

LEV-type (levyne) zeolite belonging to CHA-type zeolite group was discovered in 1825 [26]. The structure is composed of a sequence of single six-membered rings (S6-MR) and the dimensions of the 8-MR pores are  $4.8 \times 3.6 \text{ \AA}$ , suggesting the high potential of a specific shape selectivity for conversion of ethanol to light olefins. The general chemical composition of natural levyne is given by  $\text{Ca}_3(\text{Al}_{18}\text{Si}_{36}\text{O}_{108}) \cdot 50\text{H}_2\text{O}$ . In 1969 the synthetic LEV-type zeolite named ZK-20 was first synthesized from an aluminosilicate gel containing expensive 1-methyl 1-azonia 4-azabicyclo[2,2,2]octane (Me-DABCO) [27]. In the presence of methylquinuclidine the zeolites which have a LEV structure called Nu-3 [28] and LZ-132 [29] were obtained. Moreover, ZSM-45, which is also isotypic with LEV-type zeolite, was obtained with the help of inexpensive choline chloride [30]. Dimethyldiethylammonium cation [31] and *N,N'*-bis-trimethylpentane-diyldiammonium cation [32] can also be used to synthesize LEV-type zeolite. However, in the case of using choline cation, the crystallization time was more than

100 days and an impurity was present when the synthesis temperature was high. Therefore, a lot of efforts have been paid to the efficient synthesis of LEV-type zeolite using inexpensive SDAs.

From such viewpoints, I focused on the synthesis of LEV-type zeolite by the hydrothermal conversion of FAU-type zeolite in the presence of choline hydroxide in the present work. There is high structural similarity between FAU and LEV structures. LEV-type zeolite was obtained to degrade FAU-type zeolite under the mild hydrothermal condition. The catalytic performance of the obtained LEV-type zeolite for ethanol to light olefins (ETO) reaction was also evaluated.

## **2. Experimental**

### **2.1. Hydrothermal conversion**

FAU-type zeolites with various Si/Al ratios used in this work were prepared from NH<sub>4</sub>-Y zeolite (Si/Al = 2.8, Tosoh Co., Japan) through dealumination treatment involving a combination of steaming at 700 °C and H<sub>2</sub>SO<sub>4</sub> (0.47 – 0.71 M) treatment at 75 °C for 4 h. The XRD pattern of the dealuminated zeolite showed no peaks other than those corresponding to FAU structure and then the intensities of the peaks observed were almost the same as those of the parent zeolite, indicating no structural degradation (See XRD pattern in Fig. 2-1(a)). The particle size of dealuminated FAU-type zeolite was 0.4 – 0.8 μm (See SEM image in Fig. 2-2(a)).

The hydrothermal conversion was performed as follows. The dealuminated FAU-type zeolite was mixed well with an aqueous solution containing choline hydroxide ( $((\text{CH}_3)_3\text{NC}_2\text{H}_4\text{OH})^+\text{OH}^-$ ) 50 wt% in water (Tokyo Chemical Ind. Co.

Ltd., Japan) and NaCl (Kanto Chemical Co. Inc., Japan) and then the mixture was placed into a 30 cm<sup>3</sup> Teflon-lined stainless steel autoclave. The chemical compositions of the starting mixtures were SiO<sub>2</sub> : Al<sub>2</sub>O<sub>3</sub> : Choline hydroxide : NaCl : H<sub>2</sub>O = 1 : 0.011-0.042 : 0.5 : 0.2 : 5. The hydrothermal conversion was conducted at 125 °C for 2 h – 21 days in a convection oven. The solid product was collected by centrifugation and washed thoroughly with deionized water until pH = 7 and then dried overnight at 70 °C. For comparison, the starting gels from amorphous silica powder produced by wet process (SiO<sub>2</sub> = 88 wt%, Al<sub>2</sub>O<sub>3</sub> = 0.27 wt%, Nipsil, Nippon Silica Ind. Japan) and Al(OH)<sub>3</sub> (Wako Pure Chemical Ind. Ltd., Japan) or  $\gamma$ -Al<sub>2</sub>O<sub>3</sub> (JGC Catalysts & Chemicals Ltd., Japan) as other Si and Al sources respectively were also prepared.

## 2.2. Characterization

The X-ray diffraction (XRD) patterns of the solid products were collected using a powder X-ray diffractometer (Bruker, D8 Avance) with graphite monochromatized Cu K $\alpha$  radiation at 40 kV and 30 mA. Si/Al ratios were determined by X-ray fluorescence (XRF, Philips PW 2400). 0.5 g of a sample was fused with 5 g of dilithium tetraborate (Li<sub>2</sub>B<sub>4</sub>O<sub>7</sub>) at 1100 °C. The crystal morphology was observed by scanning electron microscopy (SEM, JEOL JSM-6320FS). The thermal analysis was carried out using a TG/DTA apparatus (SSC/5200 Seiko Instruments). The sample ca. 7 mg was heated in a flow of air (50 mL min<sup>-1</sup>) at 10 °C min<sup>-1</sup> from room temperature to 800 °C. <sup>13</sup>C CP/MAS NMR, <sup>27</sup>Al MAS NMR, and <sup>29</sup>Si MAS NMR spectra were recorded using a 7 mm diameter zirconia rotor on Bruker Avance DRX-400 at 100.6 MHz, 104.3 MHz, and 79.5 MHz, respectively. The rotor was

span at 6 kHz for  $^{13}\text{C}$  CP/MAS NMR, 9 kHz for  $^{27}\text{Al}$  MAS NMR, and 4 kHz for  $^{29}\text{Si}$  MAS NMR. The spectra were accumulated with 6.0  $\mu\text{s}$  pulses, 25 s recycle delay and 1000 scans for  $^{13}\text{C}$  CP/MAS NMR, 2.3  $\mu\text{s}$ , 1 s and 4000 scans for  $^{27}\text{Al}$  MAS NMR, and 5  $\mu\text{s}$ , 20 s and 1000 scans for  $^{29}\text{Si}$  MAS NMR. Glycine ( $\text{H}_2\text{NCH}_2\text{COOH}$ ),  $\text{Al}(\text{NO}_3)_3 \cdot 9\text{H}_2\text{O}$ , and  $\text{Si}(\text{CH}_3)_4$  were used as chemical shift references for  $^{13}\text{C}$  CP/MAS NMR,  $^{27}\text{Al}$  MAS NMR, and  $^{29}\text{Si}$  MAS NMR, respectively. Prior to  $^{27}\text{Al}$  MAS NMR measurement, the sample was moisture-equilibrated over a saturated solution of  $\text{NH}_4\text{Cl}$  for 24 h. Micropore volume and surface area were determined by nitrogen physisorption using the t-plot and Brunauer–Emmett–Teller (BET) methods, respectively. Nitrogen adsorption isotherms at  $-196\text{ }^\circ\text{C}$  were performed using a conventional volumetric apparatus (Bel Japan, BELSORP 28SA). Prior to adsorption measurements, the calcined samples (ca. 0.1 g) were evacuated at  $400\text{ }^\circ\text{C}$  for 10 h. The IR spectra were recorded on a FT-IR spectrometer (JEOL JIR-7000) with a resolution of  $4\text{ cm}^{-1}$  at room temperature. For OH groups stretching region measurements, the sample was pressed into a self-supporting thin wafer (ca.  $6.4\text{ mg cm}^{-2}$ ) and placed into a quartz IR cell equipped with  $\text{CaF}_2$  windows. Prior to measurement, each sample was dehydrated under vacuum at  $400\text{ }^\circ\text{C}$  for 2 h. For acidity measurements, self-supporting thin wafer samples were previously degassed at  $400\text{ }^\circ\text{C}$  for 2 h under vacuum and recorded at room temperature as background spectra. Ammonia adsorption was admitted at  $100\text{ }^\circ\text{C}$  for 1 h in order to reach adsorption equilibrium and degassed at  $100\text{ }^\circ\text{C}$  for 1 h, and then the IR spectrum was measured.

### 2.3. Catalytic testing

The catalytic performance of the protonated LEV-type zeolite (H-LEV) for the ethanol conversion reaction was tested using a quartz fixed-bed reactor at 400 °C and atmospheric pressure. The protonated form was prepared by an ion-exchange method with a 1 M  $\text{NH}_4\text{NO}_3$  solution, followed by calcination at 400 °C for 10 h. The reaction gas, EtOH/ $\text{N}_2$  (50/50 vol%), was fed at a W/F (g (H-LEV)/mL (EtOH/ $\text{N}_2$ ) per min) of 0.005-0.05  $\text{g min mL}^{-1}$ . The gaseous products were analyzed by on-time GC on Shincarbon ST (Shinwa Chem. Ind. Lds., Japan) for  $\text{N}_2$ ,  $\text{H}_2$ , and  $\text{CO}_2$ , on Gaskropack54 (GL Sciences, Japan) for ethanol and on RT-alumina PLOT (Restek USA) for  $\text{C}_1$ - $\text{C}_4$  hydrocarbons. The product yields were calculated using  $\text{N}_2$  as an internal standard.

### 3. Results and discussion

#### 3.1. Synthesis and characterization of LEV-type zeolite

Fig. 2-1 shows the hydrothermal conversion process monitored by XRD. XRD data were taken after 1, 2, 3, 4, and 7 days of hydrothermal treatment. The typical diffraction peaks corresponding to FAU-type zeolite remarkably disappeared after 1 day of hydrothermal treatment (Fig. 2-1(b)). The XRD pattern showed an amorphous halo centered at  $2\theta = 22^\circ$  and a broad peak centered at  $2\theta = 26^\circ$ . After 3 days of hydrothermal treatment the diffraction peaks corresponding to LEV-type zeolite were initially observed, implying that the nucleation of LEV-type zeolite occurred during the first 3 days of treatment. The highly crystalline LEV-type zeolite with no impurity (see SEM image in Fig. 2-2 (b)) was obtained after 7 days of hydrothermal treatment (Fig. 2-1 (f), Table 2-1 sample no. 3). The yield of LEV-type zeolite was

Table 2-1 Hydrothermal conversion of FAU-type zeolite into LEV-type zeolite.

Sample no.	Synthesis conditions <sup>a</sup>				Product (by-product)			
	Si & Al source	Si/Al ratio	Temp /°C	Time/days	Phase <sup>b</sup>	Bulk Si/Al ratio	BET surface area/m <sup>2</sup> g <sup>-1</sup>	Micropore volume/cm <sup>3</sup> g <sup>-1</sup>
1	FAU	12	125	7	LZ-133(LEV)	-	-	-
2	FAU	16	125	7	LEV	8.8	700	0.27
3	FAU	22	125	7	LEV	12	660	0.27
4	FAU	30	125	21	Am.(LEV)	-	-	-
5	FAU	45	125	7	LZ-133(LEV)	-	-	-
6	FAU	22	135	7	Am.(LEV)	-	-	-
7	FAU	22	170	7	RUT	-	-	-
8	SiO <sub>2</sub> , γ-Al <sub>2</sub> O <sub>3</sub>	22	125	7	Am.	-	-	-
9	SiO <sub>2</sub> , Al(OH) <sub>3</sub>	22	125	7	SOD(Am.)	-	-	-

<sup>a</sup> Choline hydroxide/SiO<sub>2</sub> = 0.5, H<sub>2</sub>O/SiO<sub>2</sub> = 5, NaCl/SiO<sub>2</sub> = 0.2

<sup>b</sup> Am.: amorphous

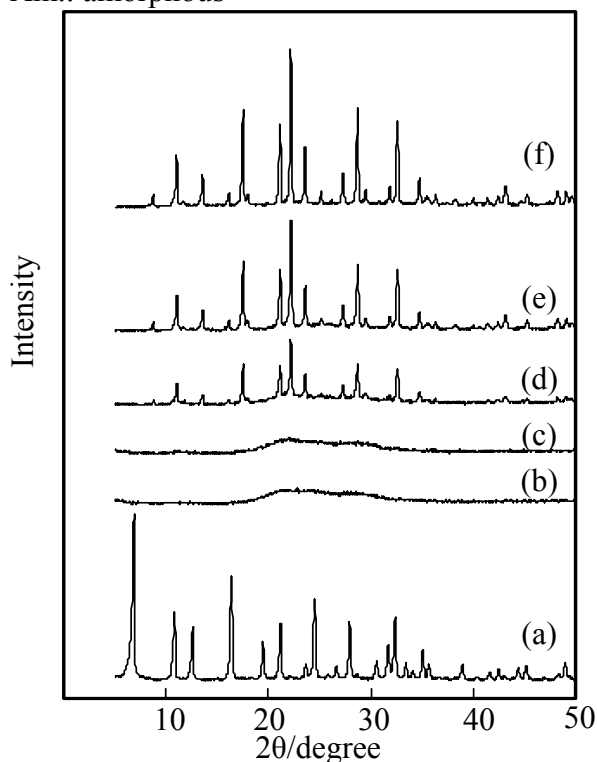


Fig. 2-1 XRD patterns of the products obtained from FAU-type zeolite at various crystallization times: (a) LEV-type zeolite (Sample dealuminated FAU-type zeolite (Si/Al=22), (b) 1 d, (c) 2 d, (d) 3 d, (e) 4 d, and (f) 7 d.

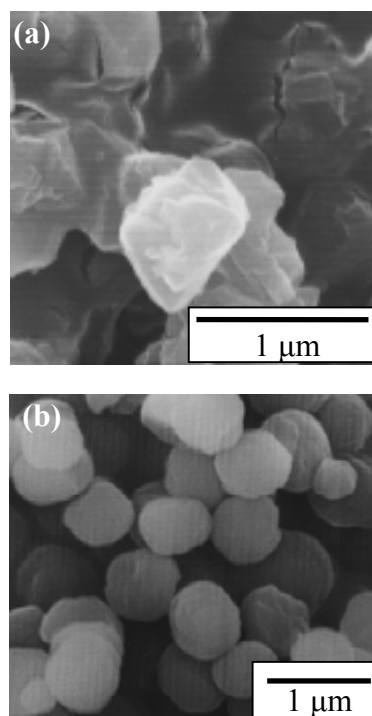


Fig. 2-2 SEM images of (a) FAU-type zeolite and (b)

60-70% based on the weight of FAU-type zeolite. These results suggest that FAU-type zeolite was not directly transformed into LEV-type zeolite. It seems that the interzeolite conversion took place via a liquid-phase-mediated mechanism. At

first FAU-type zeolite crystals decomposed and/or dissolved in alkaline media of choline hydroxide and then locally ordered aluminosilicate species coming from FAU-type zeolite assembled into LEV-type zeolite framework. To clarify the advantage of using FAU-type zeolite for the synthesis of LEV-type zeolite, I attempted to synthesize LEV-type zeolite from amorphous  $\text{SiO}_2/\text{Al}_2\text{O}_3$  (Table 2-1 sample no. 8) and amorphous  $\text{SiO}_2/\text{Al}(\text{OH})_3$  (sample no. 9). However, LEV-type zeolite was not obtained, indicating the advantage and uniqueness of the hydrothermal conversion of FAU-type zeolite.

In previous results concerning the hydrothermal conversion showed that the conversion was strongly dependent on the Si/Al ratio of the starting FAU-type zeolite [24,25]. In order to study the influence of the Si/Al ratio of the starting FAU-type zeolite on LEV-type zeolite synthesis, FAU-type zeolites with various Si/Al ratios (Si/Al = 12-45) were prepared by the dealumination treatment and subjected to the hydrothermal treatment. The hydrothermal conversion conditions are listed in detail in Table 2-1. It is obvious that only FAU-type zeolites with Si/Al ratios of 16-22 could be converted into pure LEV-type zeolites, indicating a very narrow synthesis region. There was no difference in the crystallinity between samples 2 and 3. In the case of FAU-type zeolite with Si/Al ratio of 30, an amorphous phase still remained even after heating for 21 days. FAU-type zeolites with Si/Al ratios of 12 and 45 were converted to LZ-133 zeolite as a major phase together with a small amount of LEV-type zeolite. LZ-133 zeolite is often obtained from LEV-type zeolite synthesis condition, especially when the Si/Al ratio of the starting gel is high [33]. Although LZ-133 zeolite was classified as a LEV-type zeolite in the original patent, its XRD pattern is quite different from that of LEV-type

zeolite [34]. Fig. 2-2 (b) shows the SEM image of LEV-type zeolite obtained from FAU-type zeolite (Si/Al=22) after 7 days of hydrothermal treatment. After thorough observation, I did not find any crystals of the starting FAU and impurities. Only crystals of LEV-type zeolite with spherical shape were observed. The average diameter of the crystals was 0.7  $\mu\text{m}$ . The nitrogen adsorption isotherm of the calcined LEV-type zeolite showed I type. The BET surface area and micropore volume calculated were  $700 \text{ m}^2\text{g}^{-1}$  and  $0.27 \text{ cm}^3\text{g}^{-1}$ , respectively. The high surface area indicates that the obtained LEV-type zeolite has the potential to be a solid acid catalyst.

Fig. 2-3 depicts the  $^{13}\text{C}$  CP/MAS NMR spectrum of sample no. 3, which was previously washed with ethanol and acetone before recording to remove physically adsorbed organics on outer surfaces of zeolite crystals. The spectrum revealed the presence of 3 resonances which centered at 56, 57, and 69 ppm. The resonance at 56

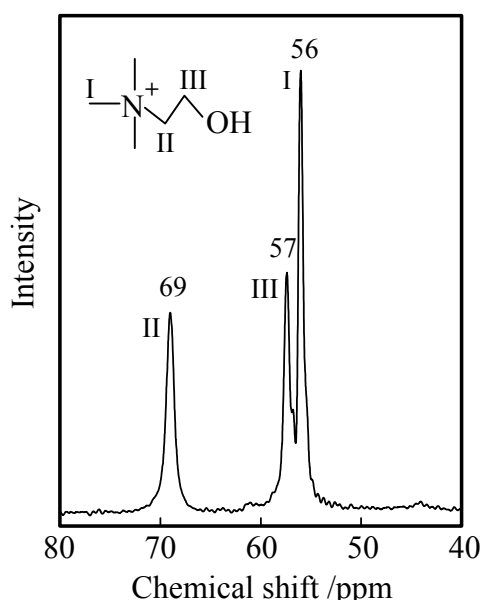


Fig. 2-3  $^{13}\text{C}$  CP/MAS NMR spectrum of LEV-type zeolite (sample no.3).

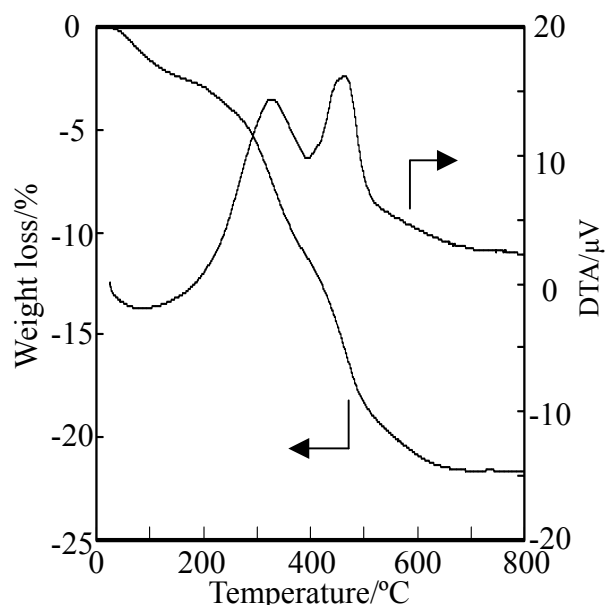


Fig. 2-4 TG/DTA curves of LEV-type zeolite obtained from FAU-type zeolite (sample no.3).

ppm indicates methyl groups attached to N, namely  $-\text{CH}_3$  of  $\text{N-CH}_3$ , while the resonance at 69 and 57 ppm correspond to methylene groups of  $\text{N-CH}_2-$  and  $-\text{CH}_2-\text{OH}$ , respectively. Therefore, choline cation was the only organic species existing in LEV-type zeolite pores. Moreover, based on my observation, it seems that choline easily decomposed into  $\text{TMA}^+$  cation at the temperature of above 135 °C, resulting in formation of RUT-type zeolite (Table 2-1 sample no. 7). Actually, the presence of  $\text{TMA}^+$  cation in the obtained RUT-type zeolite was confirmed by the  $^{13}\text{C}$  CP/MAS NMR spectrum [23].

The TG/DTA curves of sample no. 3 are presented in Fig. 2-4. From the DTA curve, the thermal profiles were categorized into three zones: (I) 25-200 °C, (II) 200-370 °C, and (III) 370-600 °C. The first zone with endothermic profile corresponds to the desorption of adsorbed water. The second zone with exothermic profile centered at 330 °C is probably attributed to the decomposition and the oxidation of either choline hydroxide occluded in pores or choline cation interacting with silanol groups of crystal defects. The third zone with exothermic profile centered at 465 °C is assigned to the decomposition and the oxidation of choline cation balancing the negative charge of the framework generated by framework aluminum species [35, 36]. Based on the thermal profiles described above, the weight loss between 200 and 600 °C, which corresponds to the total decomposition of organic moieties, was about 18 wt%, implying the presence of ca. 7 molecules of choline/u.c.

The chemical state of aluminum in the obtained LEV-type zeolite was investigated by  $^{27}\text{Al}$  MAS NMR spectroscopy. The  $^{27}\text{Al}$  MAS NMR spectrum of the as-made LEV-type zeolite is shown in Fig. 2-5(a). It is clear that only one resonance centered at 55.5 ppm was observed, while no resonance corresponding to

octahedrally coordinated aluminum species, namely extraframework aluminum species, around 0 ppm was observed. This means that all of aluminum species which are present in LEV-type zeolite obtained from the hydrothermal conversion of FAU-type zeolite exist within the zeolitic framework. The  $^{29}\text{Si}$  MAS NMR spectrum of the as-made LEV-type zeolite is also shown in Fig. 2-5(b). As the LEV structure contains two crystallographically different tetrahedral sites, 36  $T_1$  and 18  $T_2$  sites, great care has to be taken in interpreting the NMR spectrum. The NMR resonance at  $-115$  ppm is assigned to  $\text{Si}(0\text{Al})$  configuration of the  $T_2$  sites. The other NMR resonances are tentatively interpreted as follows:  $-98$  ppm ( $\text{Si}(\text{OM})_2 + \text{Si}(2\text{Al})_{T1} + \text{Si}(3\text{Al})_{T2}$ ),  $-103$  ppm ( $\text{SiOM} + \text{Si}(1\text{Al})_{T1} + \text{Si}(2\text{Al})_{T2}$ ), and  $-108$  ppm ( $\text{Si}(0\text{Al})_{T1} + \text{Si}(1\text{Al})_{T2}$ ) ( $M = \text{Choline, Na, H}$ ). These results are similar with the previous report [37].

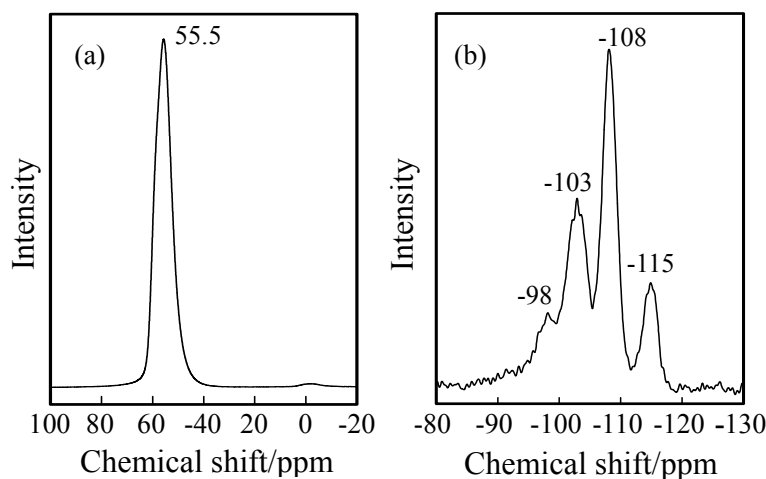


Fig. 2-5 (a)  $^{27}\text{Al}$  and (b)  $^{29}\text{Si}$  MAS NMR spectra of LEV-type zeolite (sample no.3).

Fig. 2-6 shows FT-IR spectra in the hydroxyl groups region of the protonated LEV-type (H-LEV-type) zeolite before and after  $\text{NH}_3$  adsorption. Before  $\text{NH}_3$  adsorption (Fig. 2-6 (a)), four peaks attributed to hydroxyl groups at 3743, 3620, 3604 and  $3564\text{ cm}^{-1}$  were observed. The peak at  $3743\text{ cm}^{-1}$  can be assigned to

isolated silanol group. Due to a few data, however, I cannot assign other three peaks in the present work. Fig. 2-6 (b) shows the FT-IR spectrum after  $\text{NH}_3$  adsorption. After the adsorption of  $\text{NH}_3$ , the three peaks observed before the adsorption clearly disappeared, implying the peaks of the acidic OH groups. Moreover, the peak of N-H stretching of  $\text{NH}_4^+$  was also observed at  $3228\text{ cm}^{-1}$  [38].

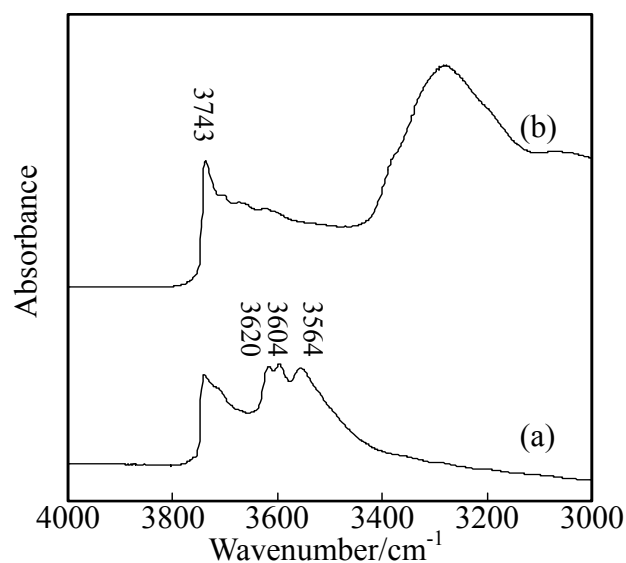


Fig. 2-6 FT-IR spectra in OH group region of H-LEV-type zeolites (sample no.3) (a) before and (b) after  $\text{NH}_3$  adsorption.

### 3.2. Ethanol to olefins reaction

The catalytic performance of H-LEV-type zeolites (Si/Al ratios of 8.8 and 12) for ethanol conversion to light olefins (ETO) reaction was evaluated using a fixed-bed reactor at atmospheric pressure. The obtained results are shown in Fig. 2-7. For both H-LEV-type zeolites, the ethanol conversion was still 100% even after 5 h time on stream. As expected, ethanol completely converted to hydrocarbons, especially light olefins with a high selectivity. The distribution of products was dependent on the Si/Al ratio of the H-LEV-type zeolite. At 0.5 h time on stream  $\text{C}_2\text{H}_4$  and  $\text{C}_3\text{H}_6$  yields

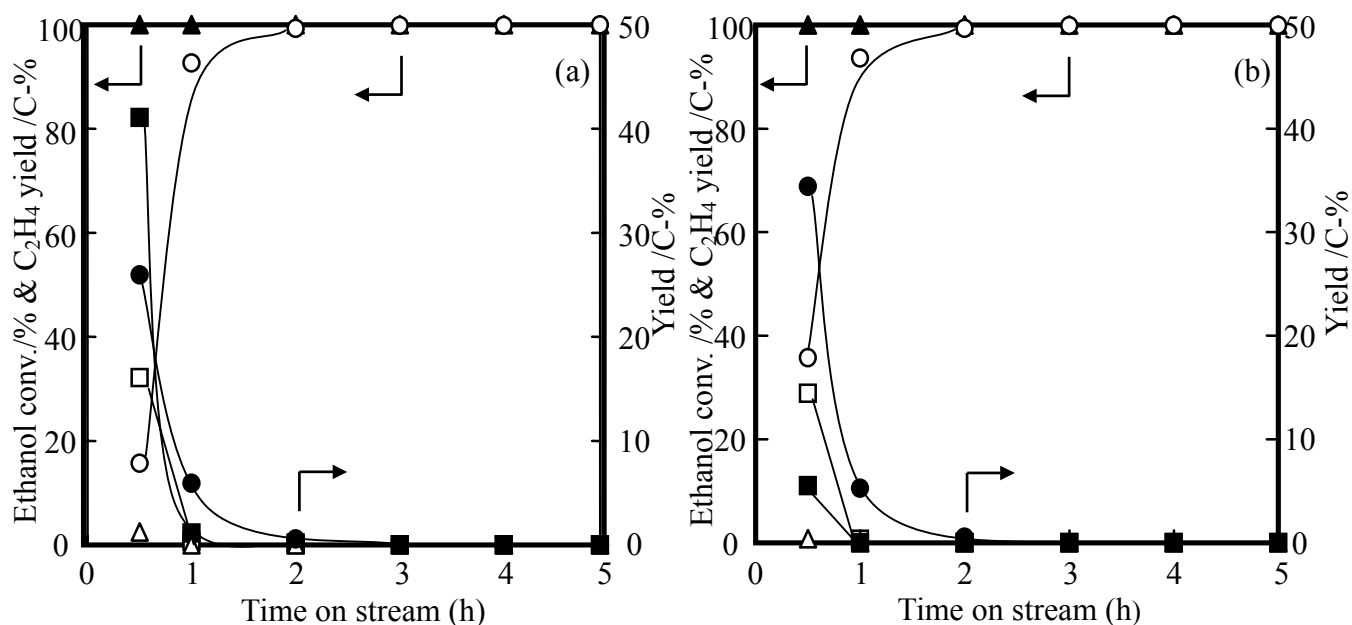


Fig. 2-7 Ethanol conversion over H-LEV-type zeolites with Si/Al ratios of (a) 8.8 (Sample no.2) and (b) 12 (Sample no. 3). Reaction conditions: Temp. = 400°C, W/F = 0.0125 g min mL<sup>-1</sup>, EtOH/N<sub>2</sub> = 50/50 vol%. (○) C<sub>2</sub>H<sub>4</sub>; (□) C<sub>3</sub>H<sub>6</sub>; (△) C<sub>4</sub>H<sub>8</sub>; (●) C<sub>1</sub>-C<sub>4</sub> paraffins; (○) others; (●) Ethanol conversion.

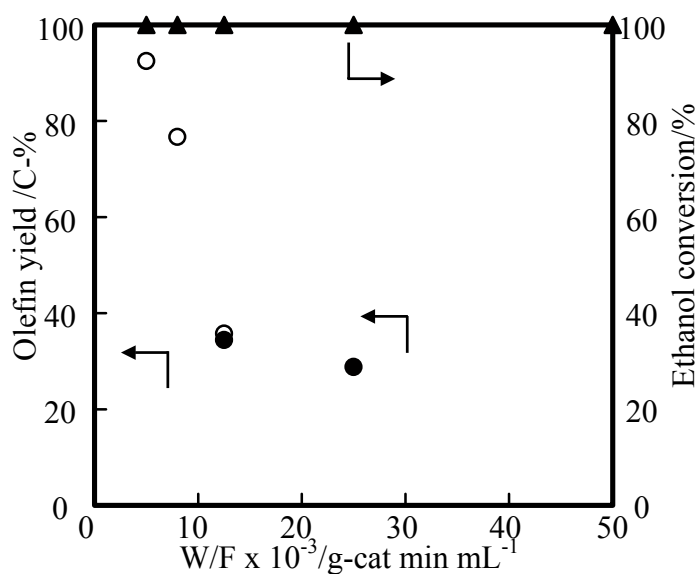


Fig. 2-8 Influence of W/F on olefin yield over H-LEV-type zeolite (Sample no. 3). (○) C<sub>2</sub>H<sub>4</sub>; (□) C<sub>3</sub>H<sub>6</sub>; (△) C<sub>4</sub>H<sub>8</sub>; (●) Ethanol conversion.

(C-%) for the Si/Al ratio of 8.8 were lower than those for the Si/Al ratio of 12, while yield of other hydrocarbons including BTX for Si/Al ratio of 8.8 were higher than that for the Si/Al ratio of 12. However, both of catalysts produced almost no C<sub>3</sub>H<sub>6</sub>

after 2 h time on stream. The rapid change in the product distribution is probably due to coke deposition. The amount of coke measured by TG analysis was 15-16 wt%. Fig. 2-8 shows the effect of W/F value on the ETO reaction over H-LEV-type zeolite with the Si/Al ratio of 12. With an increase in the W/F value, C<sub>2</sub>H<sub>4</sub> yield rapidly decreased and C<sub>4</sub>H<sub>8</sub> yield increased. Moreover, C<sub>3</sub>H<sub>6</sub> yield reached the maximum value (34.4 C-%) when the W/F value was 0.0125 g min mL<sup>-1</sup>.

#### 4. Conclusions

Here I reported that first time synthesis of pure LEV-type zeolite from the hydrothermal conversion of FAU-type zeolite only 7 days. As LEV-type zeolite was not obtained from both amorphous SiO<sub>2</sub>/Al<sub>2</sub>O<sub>3</sub> and amorphous SiO<sub>2</sub>/Al(OH)<sub>3</sub>, the advantage and uniqueness of the hydrothermal conversion of FAU-type zeolite was proven. The obtained LEV-type zeolites were pure and highly crystalline, as confirmed by XRD patterns and SEM images. Based on the results of <sup>27</sup>Al MAS NMR and FT-IR spectra, the obtained LEV-type zeolites have a significant acidic property, indicating that they are potential solid acid catalysts. The catalytic test showed that H-LEV-type zeolites are effective catalysts for ethanol to light olefins (ETO) reaction. From these findings, it was confirmed again that the hydrothermal conversion route is an alternative strategy for zeolite synthesis.

**References**

- [1] T. Maeson, *Stud. Surf. Sci. Catal.* 168 (2007) 1.
- [2] M. Stöcker, *Micropor. Mesopor. Mater.* 82 (2005) 257.
- [3] J.A. Rabo, M.W. Schoonover, *Appl. Catal. A* 222 (2001) 261.
- [4] G.W. Huber, A. Corma, *Angew. Chem. Int. Ed.* 46 (2007) 7184.
- [5] K. Murata, M. Inda, I. Takahara, *J. Jpn. Petrol. Inst.* 51 (2008) 234.
- [6] H. Oikawa, Y. Shibata, K. Inazu, Y. Iwase, K. Murai, S. Hyodo, G. Kobayashi, T. Baba, *Appl. Catal. A* 312 (2006) 181.
- [7] A.T. Aguayo, A.G. Gayubo, A.M. Tarno, A. Atutxa, J. Bibao, *J. Chem. Technol. Biotech.* 77 (2002) 211.
- [8] A.K. Talukdar, K.G. Bhattacharyya, S. Silvasanker, *Appl. Catal. A* 148 (1997) 357.
- [9] J.W. Park, J.Y. Lee, K.S. Kim, S.B. Hong, G. Seo, *Appl. Catal. A* 339 (2008) 36.
- [10] M. Stöcker, *Micropor. Mesopor. Mater.* 29 (1999) 3.
- [11] J.Q. Chen, A. Bozzano, B. Glover, T. Fuglerud, S. Kvisle, *Catal. Today* 106 (2005) 103.
- [12] Q. Zhu, J.N. Kondo, T. Tatsumi, S. Inagaki, R. Ohnuma, Y. Kubota, Y. Shimodaira, H. Kobayashi, K. Domen, *J. Phys. Chem. C* 111 (2007) 5409.
- [13] C.S. Cundy, P. A. Cox, *Micropor. Mesopor. Mater.* 82 (2005) 1.
- [14] B. Subotić, D. Škrtić, I. Šmit, L. Sekovanić, *J. Cryst. Growth* 50 (1980) 498.
- [15] B. Subotić, L. Sekovanić, *J. Cryst. Growth* 75 (1986) 561.
- [16] B. Subotić, I. Šmit, O. Madžija, L. Sekovanić, *Zeolites* 2 (1982) 135.
- [17] S.I. Zones, *J. Chem. Soc., Faraday Trans.* 87 (1991) 3709.

- [18] S.I. Zones, L.T. Yuen, Y. Nakagawa, R.A. van Nordstrand, D.D. Toto, in R. von Ballmoos, J. B. Higgins, M. M. J. Treacy (Eds.), Proceedings of the 9<sup>th</sup> International Zeolite Conference, Butterworth-Heinemann, Boston, 1993, p. 163
- [19] S.I. Zones, Y. Nakagawa, *Micropor. Mesopor. Mater.* 2 (1994) 557.
- [20] Y. Kubota, H. Maekawa, S. Miyata, T. Tatsumi, Y. Sugi, *Micropor. Mesopor. Mater.* 101 (2007) 115.
- [21] R.K. Ahedi, Y. Kubota, Y. Sugi, *J. Mater. Chem.* 11 (2001) 2922.
- [22] H. Jon, K. Nakahata, B. Lu, Y. Oumi, T. Sano, *Micropor. Mesopor. Mater.* 96 (2006) 72.
- [23] H. Jon, S. Takahashi, H. Sasaki, Y. Oumi, T. Sano, *Micropor. Mesopor. Mater.* 113 (2008) 56.
- [24] H. Sasaki, H. Jon, M. Itakura, T. Inoue, T. Ikeda, Y. Oumi, T. Sano, *J. Porous Mater.* 16 (2009) 465.
- [25] H. Jon, N. Ikawa, Y. Oumi, T. Sano, *Chem. Mater.* 20 (2008) 4135.
- [26] G. Gottardi, E. Galli, *Natural Zeolites*, Springer, Berlin, 1825, p. 192.
- [27] G.T. Kerr, US Pat. 3 459 676, 1969.
- [28] G.D. Shorte, T.V. Whittam, E.P. 0040016, 1981.
- [29] T.R. Cannon, M.T. Brent, E.M. Flanigen, E.P. 0091048A1, 1983.
- [30] E.J. Rosinski, M.K. Rubin, E.P. 0107370A1, 1983.
- [31] G.H. Kuehi, US Pat. 4 495 303, 1985.
- [32] B. Han, S. Lee, C. Lee, C. Shin, P.A. Cox, S.B. Hong, *Chem. Mater.* 17 (2005) 477.
- [33] C.V. Tuoto, A. Regina, J.B. Nagy, A. Nastro, *Micropor. Mesopor. Mater.* 20 (1998) 247.

- [34] M. Breant, US Pat. 4 842 836, 1989.
- [35] E. Bourgeat-Lami, F. Di Renzo, F. Fajula, P.H. Mutin, T.D. Courieres, J. Phys. Chem. 96 (1992) 3807.
- [36] M.A. Cambor, A. Corma, S. Valencia, J. Mater. Chem. 8 (1998) 2137.
- [37] P. Lentz, J. B. Nagy, L. Delevoye, Y. Dumazy, C. Fernandez, J.-P. Amoureux, C.V. Tuoto, A. Nastro, Colloid Surface A 158 (1999) 13.
- [38] C.T-W. Chu, C.D. Chang, J. Phys. Chem. 89 (1985) 1569.

## Chapter 3

### FAU–LEV interzeolite conversion in fluoride media

#### 1. Introduction

LEV-type (levyne) zeolite belonging to CHA-type zeolite group was discovered in 1825 [1]. The structure is composed of a sequence of single six-membered rings (S6-MR) and the dimensions of the 8-MR pores are  $4.8 \times 3.6 \text{ \AA}$ , suggesting the high potential of a specific shape selectivity for conversion of ethanol to light olefins. The general chemical composition of natural levyne is given by  $\text{Ca}_3(\text{Al}_{18}\text{Si}_{36}\text{O}_{108}) \cdot 50\text{H}_2\text{O}$ . In 1969 the synthetic LEV-type zeolite named ZK-20 was first synthesized from an aluminosilicate gel containing expensive 1-methyl 1-azonia 4-azabicyclo[2,2,2]octane (Me-DABCO) [2]. In the presence of methylquinuclidine the zeolites which have a LEV structure called Nu-3 [3] and LZ-132 [4] were obtained. Moreover, ZSM-45, which is also isotypic with LEV-type zeolite, was obtained with the help of inexpensive choline chloride [5]. Dimethyldiethylammonium cation [6] and *N,N'*-bis-trimethylpentane-diyldiammonium cation [7] can also be used to synthesize LEV-type zeolite. However, in the case of using choline cation, the crystallization time was more than 100 days and an impurity was present when the synthesis temperature was high.

Typical zeolite synthesis is performed using amorphous aluminosilicate gel as a starting material in the presence of an organic or inorganic structure-directing agent (SDA). Most zeolite syntheses usually result in the direct conversion of amorphous

phase to a given type of zeolite. However, the formation of a given zeolite proceeds through a gradual transformation in the following sequence: amorphous phase → less stable zeolite → most stable zeolite [8,9]. This phenomenon indicates an alternative synthesis strategy for the hydrothermal conversion of one zeolite into another, i.e., interzeolite conversion. This alternative method has attracted much attention.

In chapter 2, I presented that the highly crystalline LEV-type zeolite with no impurity was obtained after only seven days of hydrothermal treatment at low temperature (125 °C) in the presence of choline hydroxide. In the case of conventional hydrothermal synthesis using aluminosilicate gel and choline cation as a SDA, the crystallization time was more than 100 days, and an impurity was present when the synthesis temperature was high. Because LEV-type zeolite has building units that are similar to those of FAU-type zeolite, the enhanced rate of crystallization of LEV-type zeolite from FAU-type zeolite seems to be because of the fact that the more locally ordered aluminosilicate species contain the building units of FAU-type zeolite. However, synthesis of LEV-type zeolite was required large amount of SDA ( $\text{SDA}/\text{SiO}_2 = 0.5$ ). Thus, Si/Al ratio of obtained LEV-type zeolite was relatively low due to high alkalinity condition [10].

In the hydrothermal synthesis of zeolite, hydroxide anions are commonly used as a mineralizer. However, since the work of Flanigen and Patton in which a pure silica MFI (silicalite-1) was synthesized in media containing fluoride anions [11], fluoride anions have been widely used in the synthesis of zeolite [12,13]. The zeolite synthesized using fluoride anions display a low density of Si–OH groups (connectivity defects) and thus has a high degree of thermal stability [14–16].

Considering the abovementioned research, in this work, in order to gain further

insight into methods used for interzeolite conversion, FAU–LEV interzeolite conversion was carried out in the presence of fluoride anions and the characteristics of the obtained LEV-type zeolite were investigated in detail.

## 2. Experimental

### 2.1. Interzeolite conversion

The FAU-type zeolites with various Si/Al ratios that were used in this work were prepared from NH<sub>4</sub>-Y zeolite (Si/Al = 2.8, Tosoh Co., Japan) through a dealumination treatment that involved a combination of steaming at 700 °C and H<sub>2</sub>SO<sub>4</sub> (0.42–0.86 M) treatment at 75 °C for 4 h. The XRD pattern of the dealuminated zeolite showed no peaks other than those corresponding to the FAU structure, and the intensities of the peaks observed were almost the same as those of the parent zeolite, which indicate no structural degradation. The particle size of the dealuminated FAU-type zeolite was 0.4–0.8 μm (see the SEM image in Fig. 3-1(a)).

The reagents used in this work were a 50 wt% aqueous solution of choline hydroxide ( $((\text{CH}_3)_3\text{NC}_2\text{H}_4\text{OH})^+\text{OH}^-$ , Aldrich, USA), sodium chloride (Kanto Chemical Co. Inc., Japan), sodium fluoride (Wako Pure Chemical Ind. Ltd., Japan), ammonium fluoride (Wako Pure Chemical Ind. Ltd., Japan) and 1-adamantanamine hydrochloride (Tokyo Chemical Ind. Co. Ltd., Japan). The 1-adamantanamine was prepared by adding an equimolar amount of NaOH to an aqueous solution of the hydrochloride, and it was extracted with diethylether.

The FAU–LEV interzeolite conversion was performed as follows. The dealuminated FAU-type zeolite was mixed with an aqueous solution containing choline hydroxide or

1-adamantanamine as a SDA, and an additive (NaCl, NaF, or  $\text{NH}_4\text{F}$ ) was added and homogenized thoroughly. The mixture was then placed into a 30 cm<sup>3</sup> Teflon-lined stainless steel autoclave. The hydrothermal conversion was conducted at 125 or 150 °C for 2–14 days in a convection oven. After crystallization, the solid product was collected by centrifugation and washed thoroughly with deionized water until it was nearly neutral, and then dried overnight at 70 °C. For comparison, starting gels from amorphous silica powder produced by a wet process ( $\text{SiO}_2 = 88 \text{ wt}\%$ ,  $\text{Al}_2\text{O}_3 = 0.27 \text{ wt}\%$ , Nipsil, Nippon Silica Ind. Japan), and  $\gamma\text{-Al}_2\text{O}_3$  (JGC Catalysts and Chemicals Ltd. Japan) or  $\text{Al}(\text{OH})_3$  (Wako Pure Chemical Ind., Ltd. Japan) as other Si and Al sources, respectively, were also prepared. Detailed conditions of the interzeolite conversion are listed in Tables 3-1 and 2.

## 2.2. Characterization

The powder X-ray diffraction (XRD) patterns of the solid products were obtained using a powder X-ray diffractometer (Rigaku, Mini Flex) with graphite monochromatized Cu K $\alpha$  radiation at 30 kV and 15 mA. The Si/Al ratios were determined by X-ray fluorescence (XRF, Philips PW 2400). 0.5 g of sample was fused with 5 g of dilithium tetraborate ( $\text{Li}_2\text{B}_4\text{O}_7$ ) at 1100 °C. The Si/Al ratio was calculated from the Si and Al concentrations as determined by the corresponding calibration curves. The crystal morphology was observed with a scanning electron microscope (SEM, Hitachi S-4800). Micropore volume and surface area were determined by nitrogen physisorption using the t-plot and Brunauer–Emmett–Teller (BET) methods, respectively. Nitrogen adsorption isotherms at -196 °C were performed using a conventional volumetric apparatus (Bel Japan, BELSORP 28SA). Prior to adsorption

measurements, the calcined samples (ca. 0.1 g) were evacuated at 400 °C for 10 h.  $^{13}\text{C}$  CP/MAS NMR,  $^{27}\text{Al}$  MAS NMR, and  $^{29}\text{Si}$  MAS NMR spectra were recorded using a 7 mm diameter zirconia rotor on a Bruker Avance DRX-400 at 100.6 MHz, 104.3 MHz, and 79.5 MHz, respectively. The rotor was spun at 4 kHz for  $^{29}\text{Si}$  and  $^{13}\text{C}$  CP/MAS NMR, and at 6 kHz for  $^{27}\text{Al}$  MAS NMR. The spectra were accumulated with 6.0  $\mu\text{s}$  pulses, a 25 s recycle delay, and 1000 scans for  $^{13}\text{C}$  CP/MAS NMR, 2.3  $\mu\text{s}$ , 1 s, and 1000 scans for  $^{27}\text{Al}$  MAS NMR, and 5  $\mu\text{s}$ , 20 s and 2000 scans for  $^{29}\text{Si}$  MAS NMR.  $\text{Al}(\text{NO}_3)_3 \cdot 9\text{H}_2\text{O}$  was used as a chemical shift reference for  $^{27}\text{Al}$  MAS NMR, and  $\text{Si}(\text{CH}_3)_4$  was used as a chemical shift reference for  $^{13}\text{C}$  CP/MAS NMR and  $^{29}\text{Si}$  MAS NMR. Prior to  $^{27}\text{Al}$  MAS NMR measurement, the sample was moisture-equilibrated over a saturated solution of  $\text{NH}_4\text{Cl}$  for 24 h. The thermal analysis was carried out using a TG/DTA apparatus (SSC/5200 Seiko Instruments). Beginning at room temperature the sample of ca. 7 mg was heated to 800 °C in a flow of air ( $50 \text{ mL min}^{-1}$ ) at a heating rate of  $5 \text{ }^\circ\text{C min}^{-1}$ .

### 2.3. Thermal stability

The thermal stability of the obtained LEV-type zeolites was evaluated by XRD analysis by comparing the change in the intensities of the peaks at  $2\theta = 11.1, 13.5, 17.5, 21.2, 22.2, 28.8$  and  $32.6$  of samples before and after calcination at 700–1050 °C for 1 h. Prior to calcination, the as-made sample was calcined to remove any organic SDA in the zeolitic pores. Although choline cations in zeolitic pores were removed by calcination at 450 °C for 48 h, 1-adamantanamine cations could not be completely removed at the temperature. Therefore, the as-made LEV-type zeolites synthesized using 1-adamantanamine were calcined at 550 °C for 24 h. The relative crystallinity was

determined as follows:

$$\text{Relative crystallinity (\%)} = \frac{\text{Sum of intensities of the peaks at } 2\theta = 11.2, 13.7, 17.7, 21.4, 22.4, 29.0, \text{ and } 32.8 \text{ after calcination at various temperatures for 1 hour}}{\text{Sum of intensities of the peaks at } 2\theta = 11.2, 13.7, 17.7, 21.4, 22.4, 29.0 \text{ and } 32.8 \text{ after calcination to remove organic species}} \times 100$$

Table 3-1 Interzeolite conversion of FAU-type zeolite into LEV-type zeolite using choline hydroxide as an SDA<sup>a</sup>.

Sample No.	Synthesis conditions			Product			
	Si & Al source	NaCl/SiO <sub>2</sub>	F <sup>-</sup> /SiO <sub>2</sub> (fluoride source)	Phase	Bulk Si/Al ratio	BET surface area (m <sup>2</sup> g <sup>-1</sup> )	Micropore volume (cm <sup>3</sup> g <sup>-1</sup> )
1	FAU (22)		0.2 (NaF)	LEV	10.7	620	0.27
2	FAU (22)		0.2 (NH <sub>4</sub> F)	no product			
3	FAU (22)	0.2	0.05 (NH <sub>4</sub> F)	LEV	11.5	630	0.28
4	FAU (22)	0.2		LEV	12.0	660	0.27

<sup>a</sup> Choline hydroxide/SiO<sub>2</sub> = 0.5, H<sub>2</sub>O/SiO<sub>2</sub> = 5, Temp.: 125 °C, Time: 7 days.

Table 3-2 Interzeolite conversion of FAU-type zeolite into LEV-type zeolite using 1-adamantanamine as SDA in the presence of fluoride anions<sup>a</sup>.

Sample No.	Synthesis conditions				Product			
	Si & Al source	Si/Al ratio	NH <sub>4</sub> F/SiO <sub>2</sub>	Time (days)	Phase <sup>b</sup>	Bulk Si/Al ratio	BET surface area (m <sup>2</sup> g <sup>-1</sup> )	Micropore volume (cm <sup>3</sup> g <sup>-1</sup> )
5	FAU	10	0.05	7	FAU,LEV			
6	FAU	13	0.05	7	LEV	12.8	590	0.24
7	FAU	22	0.05	7	LEV	21.3		
8	FAU	29	0.05	10	LEV	28.6	520	0.22
9	FAU	42	0.05	14	LEV,DDR			
10	FAU	70	0.05	14	DDR	75.0	340	0.14
11	FAU	22		14	FAU			
12	FAU	22	0.5	14	DDR			
13	FAU	22	0.05 (NaF)	14	LEV	21.6	560	0.23
14	SiO <sub>2</sub> /Al(OH) <sub>3</sub>	22	0.05	14	Am.,LEV			
15	SiO <sub>2</sub> /γ-Al <sub>2</sub> O <sub>3</sub>	22	0.05	14	Am.,Un.			

<sup>a</sup> 1-adamantanamine/SiO<sub>2</sub> = 0.3, H<sub>2</sub>O/SiO<sub>2</sub> = 10, Temp.: 150 °C.

<sup>b</sup> Am.: amorphous, Un.: unknown.

### 3. Results and discussion

#### 3.1. FAU-LEV interzeolite conversion using choline hydroxide as a SDA in the presence of fluoride anions

First, I investigated the influence of the addition of fluoride anions on FAU-LEV interzeolite conversion using choline hydroxide as a SDA. The conditions for interzeolite conversion are listed in Table 3-1. In the case of in which NaF was used as a fluoride source, highly crystalline LEV-type zeolite was obtained (sample no. 1). When  $\text{NH}_4\text{F}$  was used, on the other hand, no product was obtained (sample no. 2). With a combination of NaCl and  $\text{NH}_4\text{F}$ , however, highly crystalline LEV-type zeolite was obtained (sample no. 3). Taking into account the result of synthesis of LEV-type zeolite with NaCl (sample no. 4), I attribute this to the fact that a sodium cation is essential for

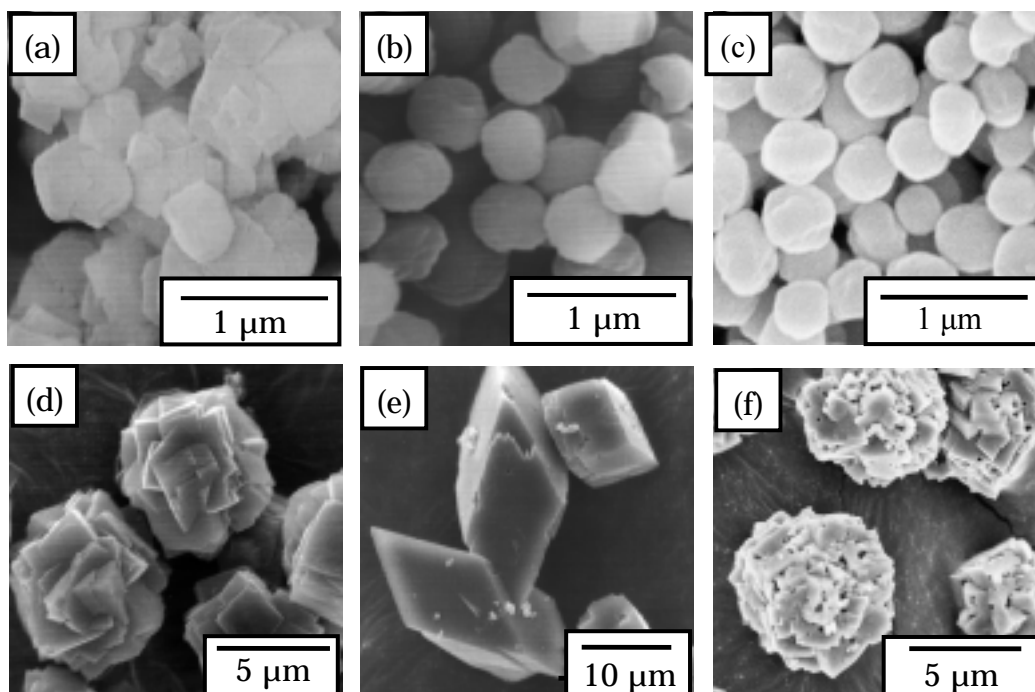


Fig. 3-1 SEM images of (a) starting FAU, (b) LEV (sample no. 3), (c) LEV (sample no. 4), (d) LEV (sample no. 6), (e) DDR (sample no. 10), and (f) LEV (sample no. 13).

an interzeolite conversion method that synthesizes LEV-type zeolite using choline hydroxide as a SDA. As can be seen in Fig. 3-1(b) and (c), the crystal morphology of LEV-type zeolite prepared with a combination of NaCl and NH<sub>4</sub>F was similar to that obtained with NaCl (sample no. 4). There was also no difference in the BET surface area and micropore volume. The Si/Al ratios of the obtained LEV-type zeolites were smaller than that of the starting FAU-type zeolite, probably due to the high alkalinity of the aqueous solution ( $\text{OH}^-/\text{SiO}_2 = 0.5$ ).

The chemical states of the silicon in the obtained LEV-type zeolites were investigated by <sup>29</sup>Si MAS NMR both with and without <sup>1</sup>H-<sup>29</sup>Si cross polarization (CP). The <sup>29</sup>Si MAS NMR spectrum of the as-made LEV-type zeolite is shown in Fig. 3-2(A). Because the structure contains two crystallographically different tetrahedral sites, 36 T<sub>1</sub> and 18 T<sub>2</sub> sites, great care must be taken in interpreting the NMR spectrum. The NMR resonance at -115 ppm is assigned to the Si(0Al) configuration of the T<sub>2</sub> sites. The other NMR resonances are tentatively interpreted as follows: -98 ppm (Si(OM)<sub>2</sub> + Si(2Al)<sub>T1</sub> + Si(3Al)<sub>T2</sub>), -103 ppm (SiOM + Si(1Al)<sub>T1</sub> + Si(2Al)<sub>T2</sub>), -108 ppm (Si(0Al)<sub>T1</sub> + Si(1Al)<sub>T2</sub>) (M = choline, Na, H). These results are similar to those in a previous report [17]. The <sup>29</sup>Si MAS NMR spectra of calcined LEV-type zeolites are shown in Fig. 3-2(B). The intensities of the peaks at -99 and -104 ppm decreased after calcination at 450 °C. In generally, zeolites synthesized in the presence of fluoride anions show a low density of Si-OH groups (connectivity defects) [13]. There was no difference, however, between the peak intensities of the as-made and calcined zeolites (Fig. 3-2(A) and (B)). In addition, in the CP spectra of both as-made LEV-type zeolites (Fig. 3-2(C)), the peak intensities at -99 and -104 ppm were considerably enhanced. Taking into account the fact that no difference in their thermal stability was observed either, as described later

(Fig. 9), the above results strongly indicate that as compared with conventional zeolite synthesis in the presence of fluoride anions, there is no pronounced influence of fluoride anions in interzeolite conversion with choline hydroxide. This is probably due to the stronger mineralizing ability of hydroxide anions as compared to fluoride anions. Therefore, in successive experiments I investigated the influence of the addition of fluoride on FAU–LEV interzeolite conversion in the absence of hydroxide anions.

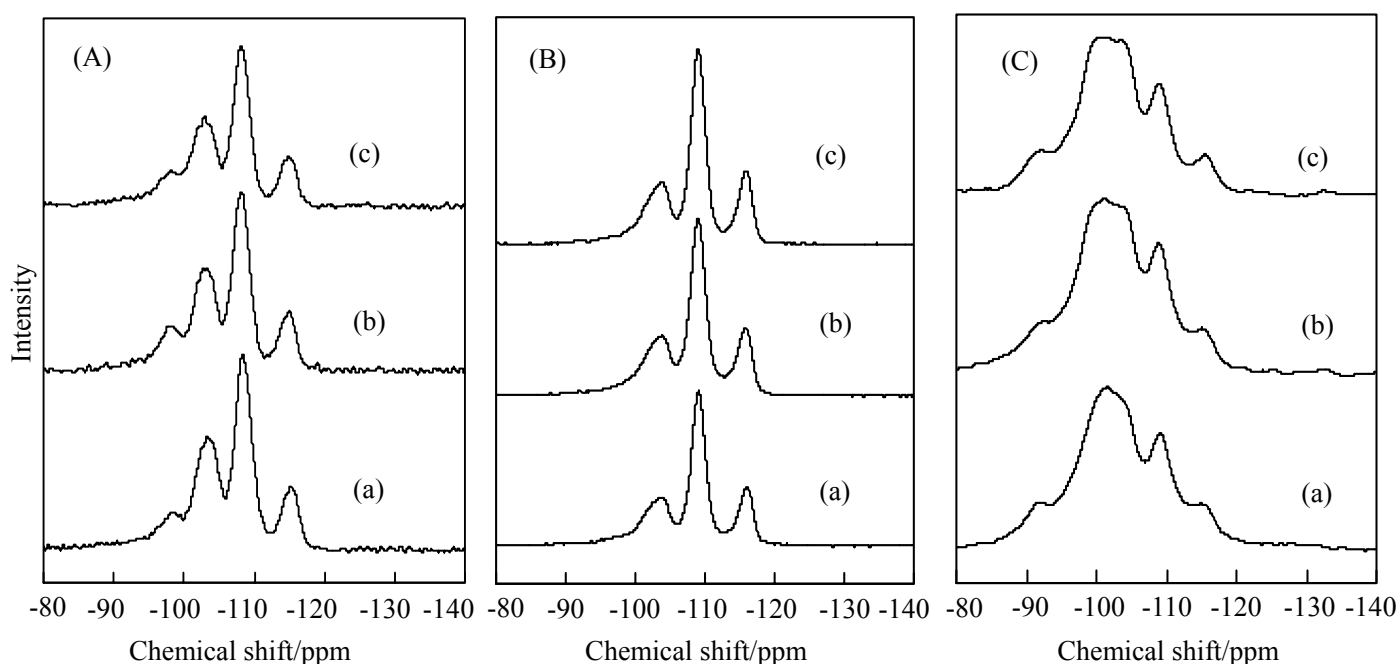


Fig. 3-2  $^{29}\text{Si}$  MAS NMR spectra measured without and with CP for LEV-type zeolites obtained using choline hydroxide as SDA. (A) As-made sample measured without CP, (B) calcined sample measured without CP, and (C) calcined sample measured with CP. sample nos.: (a) 1, (b) 3, and (c) 4.

### 3.2. FAU–LEV interzeolite conversion using 1-adamantanamine as a SDA in the presence of fluoride anions

The hydrothermal treatment of FAU-type zeolite was preliminarily carried out with various amine compounds. Complete FAU–LEV interzeolite conversion did not occur in the absence of fluoride anions. However, in the presence of  $\text{NH}_4\text{F}$  when 1-adamantanamine was used as a SDA which is known to be one of the SDAs for the

synthesis of LEV-type zeolite, the interzeolite conversion proceeded easily [19]. Detailed investigation of the influence of fluoride anions was carried out using 1-adamantanamine as a SDA. The interzeolite conversion conditions are listed in Table 3-2.

Our previous results concerning the interzeolite conversion showed that the conversion was strongly dependent on the Si/Al ratio of the starting FAU-type zeolite [10]. In order to study the influence of the Si/Al ratio of the starting FAU-type zeolite on LEV-type zeolite synthesis, FAU-type zeolites with various Si/Al ratios (Si/Al = 10–70) were prepared by dealumination treatment and subjected to hydrothermal treatment. Fig. 3-3 shows the XRD patterns of the as-made products from FAU-type zeolites with various Si/Al ratios. It is obvious that FAU-type zeolites with Si/Al ratios of 13–29 could be converted into pure LEV-type zeolites after a synthesis time of 7–10 days in the presence of  $\text{NH}_4\text{F}$  (sample nos. 6–8). The XRD patterns of the as-made samples were consistent with that of Nu-3 zeolite with a LEV structure, which is slightly different from that of Levyne [18]. After calcination at 550 °C for 24 h to remove organic species in the zeolitic pores, however, the XRD pattern was consistent with that of Levyne. In the case of FAU-type zeolite with a Si/Al ratio of 10, the starting FAU-type zeolite still remained (sample no. 5). In the case of FAU-type zeolite with a Si/Al ratio of 42, it was converted to LEV-type zeolite as a major phase together with a small amount of DDR zeolite (sample no. 9). FAU-type zeolite with a high Si/Al ratio (70) was completely converted into pure DDR-type zeolite (sample no. 10). 1-Adamantanamine is recognized as being effective for the synthesis of DDR-type zeolite [20,21]. Fig. 3-1(d) and (e) show SEM images of the as-made LEV- and DDR-type zeolites obtained. After thorough observation, I did not find any impurities or

any crystals of the starting FAU-type zeolite. Only aggregate crystals of LEV-type zeolites were observed, whose morphology was considerably different from that of the zeolites synthesized with choline hydroxide. The average diameter of the aggregate was ca. 5  $\mu\text{m}$ . The crystal of the DDR-type zeolite was lozenge-shaped and was ca. 10–20  $\mu\text{m}$  in size. The Si/Al ratios (13–29) of LEV-type zeolite obtained were relatively high values that were almost consistent with that of the starting FAU-type zeolite, which indicates the complete transfer of aluminosilicate species from the former zeolite (FAU) into the new zeolite (LEV). The yield of LEV-type zeolite was 70–80% based on the weight of FAU-type zeolite. The Si/Al ratios of LEV-type zeolites synthesized using quinuclidine as a SDA in the presence of fluoride anions were only 8–11 [20]. Fig. 3-4 shows a nitrogen adsorption isotherm of the calcined LEV-type zeolite (sample no. 6). It was a type I isotherm, and the BET surface area and micropore volume were calculated

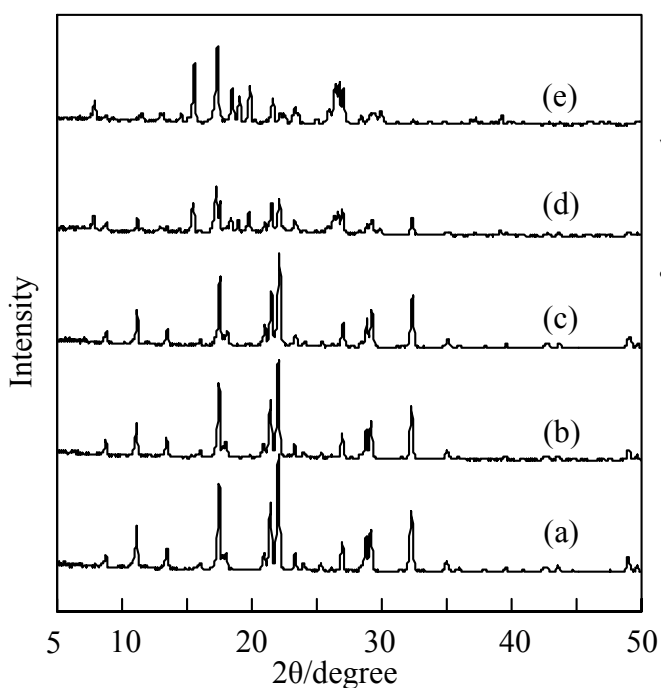


Fig. 3-3 XRD patterns of as-made products obtained from FAU-type zeolites with various Si/Al ratios. Sample Nos.: (a) 6, (b) 7, (c) 8, (d) 9, and (e) 10.

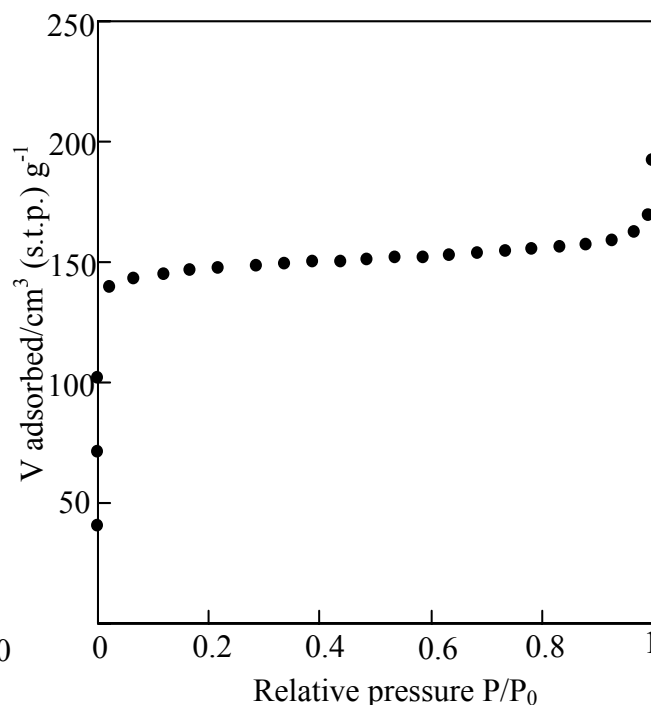


Fig. 3-4 Nitrogen adsorption isotherm of calcined LEV-type zeolite (sample no. 6).

to be  $590 \text{ m}^2\text{g}^{-1}$  and  $0.24 \text{ cm}^3\text{g}^{-1}$ , respectively.

Next, to clarify the role of fluoride anions in interzeolite conversion, the amount of  $\text{NH}_4\text{F}$  was varied. As can be seen in Table 3-2, when  $\text{NH}_4\text{F}$  was not added to the synthesis mixture, there was hardly any decomposition/dissolution of FAU-type zeolite even after 14 days of hydrothermal treatment (sample no. 11). In the case of  $\text{NH}_4\text{F}/\text{SiO}_2 = 0.05$ , FAU-type zeolite converted efficiently into LEV-type zeolite. Under the condition of  $\text{NH}_4\text{F}/\text{SiO}_2 = 0.5$  (sample no. 12), however, the FAU-type zeolite did not convert into LEV-type zeolite, but rather, into DDR-type zeolite. When NaF was used instead of  $\text{NH}_4\text{F}$ , highly crystalline LEV-type zeolite was also obtained (sample no. 13), as shown in the SEM image in Fig. 3-1(f). There were no differences between the bulk Si/Al ratio, BET surface area, and pore volume of LEV-type zeolites synthesized with  $\text{NH}_4\text{F}$  and NaF.

To clarify the advantage of using FAU-type zeolite for the synthesis of LEV-type zeolite, I also attempted to synthesize LEV-type zeolite from amorphous  $\text{SiO}_2/\text{Al}(\text{OH})_3$  (sample no. 14) and amorphous  $\text{SiO}_2/\gamma\text{-Al}_2\text{O}_3$  (sample no. 15). Pure LEV-type zeolite was not obtained, however, which indicates both the advantage and uniqueness of the interzeolite conversion of FAU-type zeolite.

The characteristics of organic molecules occluded in the zeolitic pores of LEV-type zeolite were investigated by  $^{13}\text{C}$  CP/MAS NMR and thermal analysis. As can be seen in Fig. 3-5, the  $^{13}\text{C}$  CP/MAS NMR spectrum consists of four resonances centered at ca. 29, 35, 42, and 57 ppm. This spectrum differs from that observed for 1-adamantanamine in the solid state and is similar to the solution-state spectrum of the protonated 1-adamantanamine cation, which indicates that the amine is protonated [23,24]. The resonance at 29 ppm is assigned to  $\text{H-CC}_3$  of the 1-adamantanamine cation, while the

resonances at 35 and 42 ppm are assigned to C-CH<sub>2</sub>-C. The resonance at 57 ppm corresponds to N-CC<sub>3</sub>. Therefore, the 1-adamantanamine cation was the only organic species existing in the LEV-type zeolite pores. From the TG curves, the amount of 1-adamantanamine cation was calculated to be ca. 23 wt%, implying the presence of ca. 6 molecules of 1-adamantanamine cation/u.c., which is consistent with the number of choline cations in LEV-type zeolite synthesized with choline hydroxide as a SDA.

The chemical states of the aluminum in the obtained LEV-type zeolite were investigated by <sup>27</sup>Al MAS NMR. The <sup>27</sup>Al MAS NMR spectrum of the as-made LEV-type zeolite is shown in Fig. 3-6. It is clear that only one resonance centered at ca. 53 ppm was observed, while a resonance corresponding to that of octahedrally coordinated aluminum species, namely an extra-framework aluminum species, was not observed around 0 ppm. This means that all the aluminum species present in LEV-type zeolite obtained by the interzeolite conversion of starting FAU-type zeolite in the presence of fluoride anions exist within the zeolitic framework. The <sup>29</sup>Si MAS NMR spectrum of the as-made LEV-type zeolite is shown in Fig. 3-7(A). As compared to the <sup>29</sup>Si MAS NMR spectrum of LEV-type zeolite synthesized with choline hydroxide as a SDA, the intensities of the peaks at -99 and -104, and particularly of the peak at -99 ppm, were relatively weak. The <sup>29</sup>Si MAS NMR spectra of calcined LEV-type zeolites are shown in Fig. 3-7(B). The intensities of the peaks at -99 and -104 ppm decreased with calcination at 550 °C. In the CP spectrum of the LEV-type zeolite (Fig. 3-7(C)), the peak intensities at -99 and -104 ppm were enhanced. The degree of enhancement, however, was relatively smaller than that of LEV-type zeolite synthesized using choline hydroxide (Fig. 3-2(C)), which indicates fewer connectivity defects.

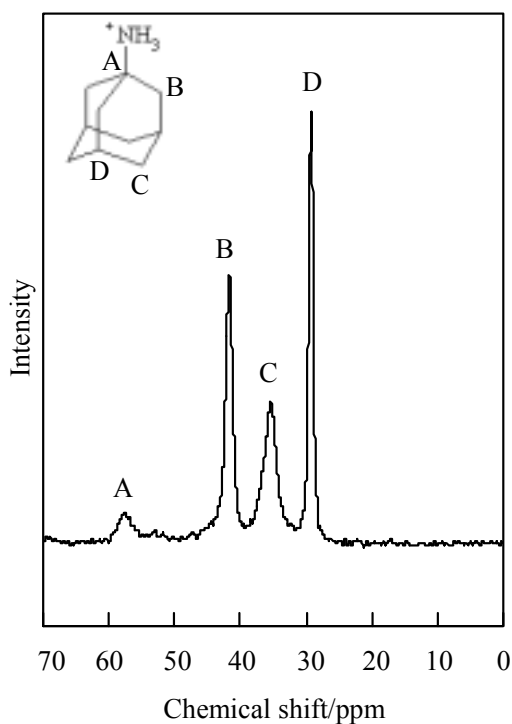


Fig. 3-5  $^{13}\text{C}$  CP/MAS NMR spectrum of LEV-type zeolite synthesized using  $\text{NH}_4\text{F}$  and 1-adamantanamine as SDA (sample no. 6).

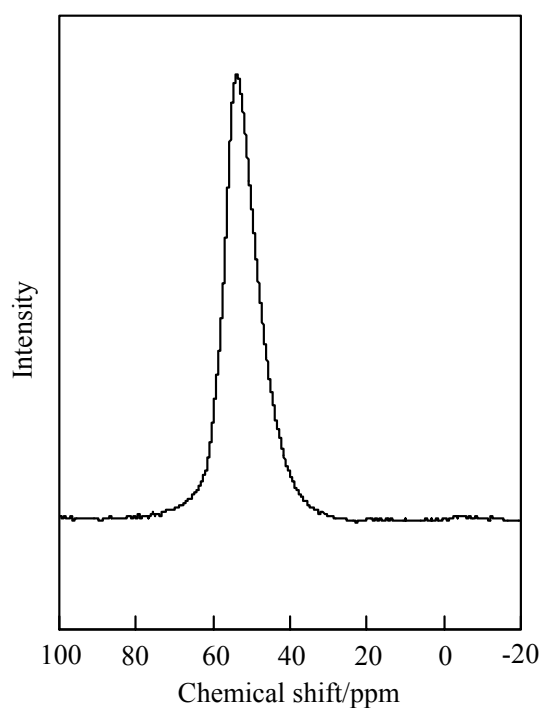


Fig. 3-6  $^{27}\text{Al}$  MAS NMR spectrum of as-made LEV-type zeolite synthesized with  $\text{NH}_4\text{F}$  and 1-adamantanamine as SDA (sample no. 6).

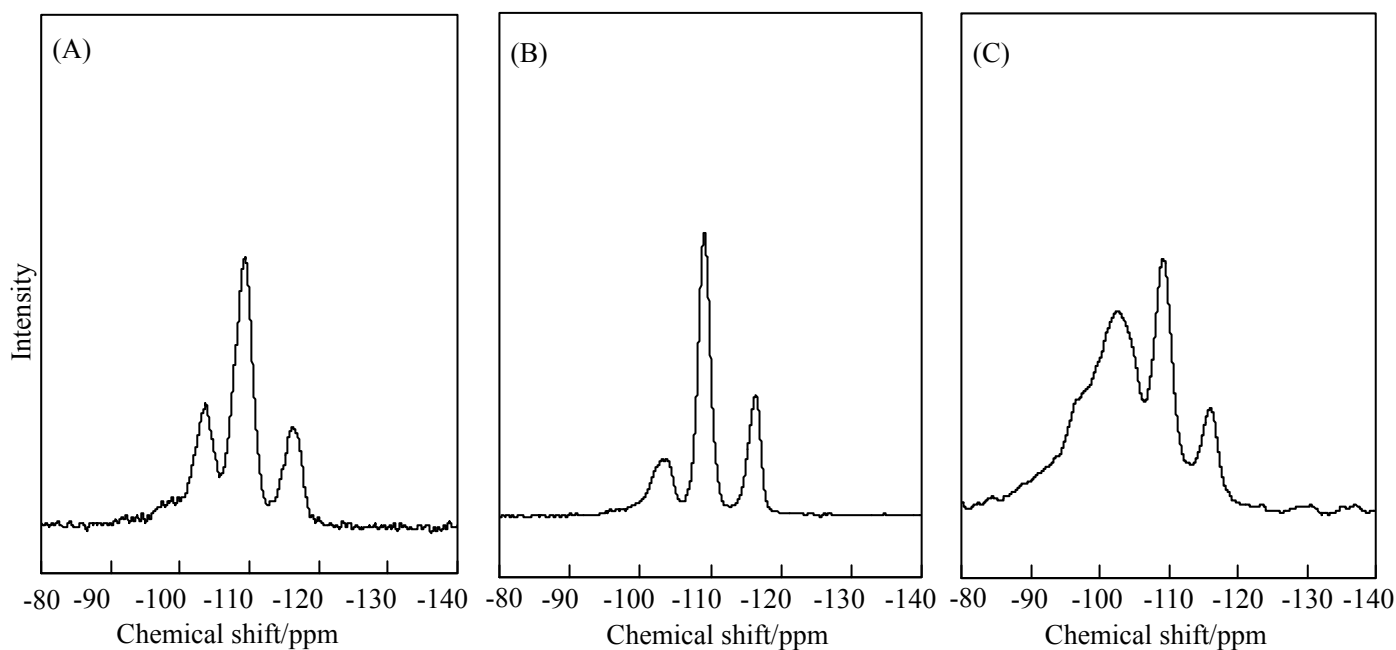


Fig. 3-7  $^{29}\text{Si}$  MAS NMR spectra measured without and with CP for LEV-type zeolites synthesized using  $\text{NH}_4\text{F}$  and 1-adamantanamine as SDA. (A) As-made sample measured without CP, (B) calcined sample measured without CP, and (C) calcined sample measured with CP (sample no. 6).

### 3.3. Thermal stability

To investigate the thermal stability of the obtained LEV-type zeolites, the XRD patterns before and after calcination at 700–1050 °C for 1 h were measured. It is assumed that the thermal stability of LEV-type zeolite can be evaluated by comparing the change in the intensities of the peaks at  $2\theta = 11.2, 13.7, 17.7, 21.4, 22.4, 29.0$  and  $32.8$  of samples before and after calcination. Fig. 3-8 shows the XRD patterns of LEV-type zeolites after calcination at various temperatures, that were synthesized using 1-adamantanamine as a SDA in the presence of  $\text{NH}_4\text{F}$  (sample no. 6,  $\text{Si}/\text{Al}=12.8$ ). For comparison, the XRD patterns of LEV-type zeolites synthesized using choline hydroxide in the absence of fluoride anions were also shown (sample no. 4,  $\text{Si}/\text{Al}=12.0$ ). For LEV-type zeolite synthesized using 1-adamantanamine, no reduction in peak intensity was observed in the temperature range of 700–900 °C, although it became clear from  $^{27}\text{Al}$  MAS NMR measurement that a large degree of dealumination was observed for the LEV-type zeolite after calcination at 900 °C. On the other hand, for LEV-type zeolite synthesized using choline hydroxide, a marked reduction in peak intensity was observed even after calcination at 700 °C, and the zeolite framework structure completely collapsed at 800 °C. Fig. 3-9 shows the relationship between the calcination temperature and the relative crystallinity of LEV-type zeolite after calcination. For comparison, the relative crystallinities of LEV-type zeolites synthesized with choline hydroxide as a SDA in both the absence and presence of fluoride anions (sample nos. 1, 3 and 4) are also shown. For all samples, a great reduction in the relative crystallinity was observed even after calcination at 700 °C and the zeolite framework structure completely collapsed at 800 °C. Because the  $\text{Si}/\text{Al}$  ratios of these zeolites are similar, these results strongly indicate that the LEV-type zeolite that was synthesized

using 1-adamantanamine in the presence of fluoride anions has a higher thermal stability than that which was synthesized using choline hydroxide, probably due to fewer connectivity defects.

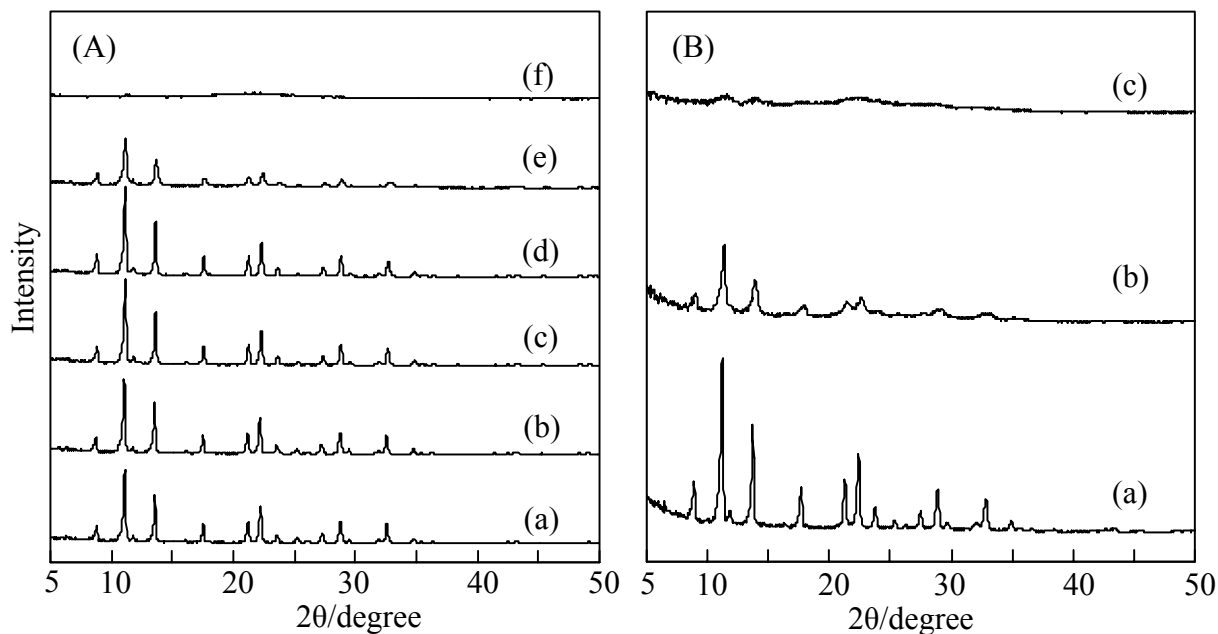


Fig. 3-8. XRD patterns of LEV-type zeolites after calcination at various temperatures for 1 h. (A) Using NH<sub>4</sub>F and 1-adamantanamine (sample no. 6), and (B) using choline hydroxide (sample no. 4). (a) After calcination at 550 °C (A) or 450 °C (B), (b) 700 °C, (c) 800 °C, (d) 900 °C, (e) 1000 °C, and (f) 1050 °C.

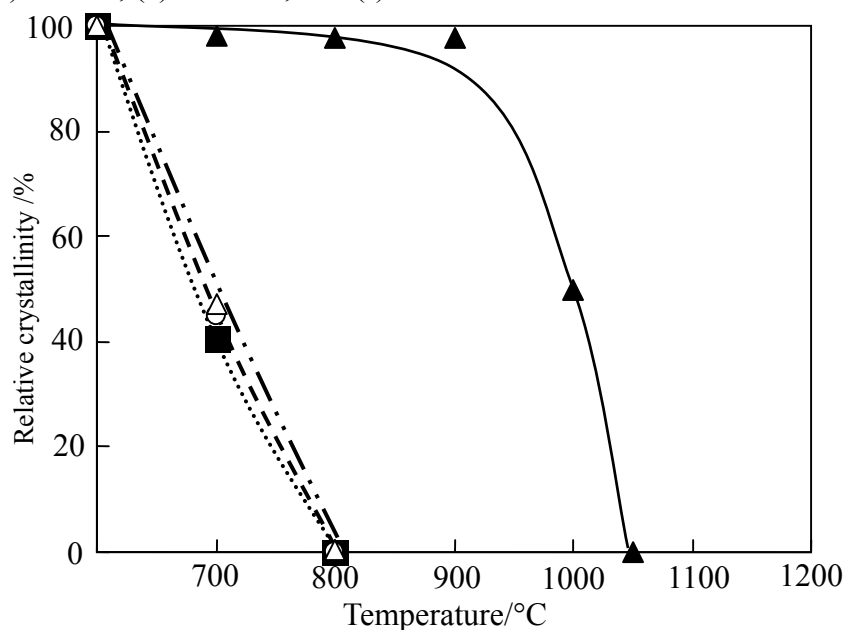


Fig. 3-9. Relative crystallinity of LEV-type zeolite after calcination at various temperatures for 1 h. ▲: sample no. 6 (NH<sub>4</sub>F and 1-adamantanamine), △: sample no. 1 (choline and NaF), ○: sample no. 3 (NH<sub>4</sub>F and choline), ■: sample no. 4 (choline).

### 3.4. Interzeolite conversion process

As described above, there are some differences between the characteristics of LEV-type zeolites synthesized using choline hydroxide and those using 1-adamantanamine as a SDA. To clarify the difference in the FAU–LEV interzeolite conversion process, therefore, the crystallization process was monitored by XRD. XRD data were taken after 2, 3, 4, 5, and 7 days of hydrothermal treatment (Fig. 3-10). In the case in which choline hydroxide was used (Fig. 3-10(B)), the typical diffraction peaks corresponding to FAU-type zeolite completely disappeared after 2 days of hydrothermal treatment and an amorphous halo centered at  $2\theta = 22^\circ$  was observed. After 3 days of hydrothermal treatment, diffraction peaks that correspond to LEV-type zeolite became observable, implying that the nucleation of LEV-type zeolite occurred during the first 3 days of treatment. Highly crystalline LEV-type zeolite was obtained after 7 days of hydrothermal treatment. On the other hand, when 1-adamantanamine was used in the presence of fluoride anions, the process of interzeolite conversion differed substantially from the conversion process in which choline hydroxide was used. As can be seen in Fig. 3-10(A), during interzeolite conversion, diffraction peaks corresponding to FAU-type zeolite can be clearly observed. After 3 days of hydrothermal treatment, diffraction peaks corresponding to LEV-type zeolite became observable. Highly crystalline LEV-type zeolite with no impurity was obtained after 7 days of hydrothermal treatment. I now consider these differences in the FAU–LEV interzeolite conversion process to be as follows. In interzeolite conversion in the presence of hydroxide anions, the rates of nucleation and crystal growth of LEV-type zeolite are slower than the rate of decomposition/dissolution of the starting FAU-type zeolite into nanoparts. On the other

hand, in interzeolite conversion with fluoride anions, there is no great difference between the rates of decomposition/dissolution of FAU-type zeolite and those of the nucleation and crystal growth of LEV-type zeolite [16].

In general, the mineralizing power of fluoride anions is less than that of hydroxide anions, so that the solubility and supersaturation of silicate and aluminosilicate species are lower [22,23]. In addition, in the synthesis of LEV-type zeolite using 1-adamantanamine, the amount of  $\text{NH}_4\text{F}$  was very small. In the case of 1-adamantanamine, therefore, the rate of decomposition/dissolution of the starting FAU-type zeolite is slower than it is in the presence of hydroxide anions. Consequently, the nucleation and crystal growth of LEV-type zeolite proceeds simultaneously with the decomposition/dissolution of the starting FAU-type zeolite. On the other hand, in the presence of choline hydroxide, the decomposition/dissolution of the starting FAU-type zeolite proceeds easily because of the great mineralizing ability of hydroxide anions. Considering the Si/Al ratio of the LEV-type zeolite obtained using choline hydroxide

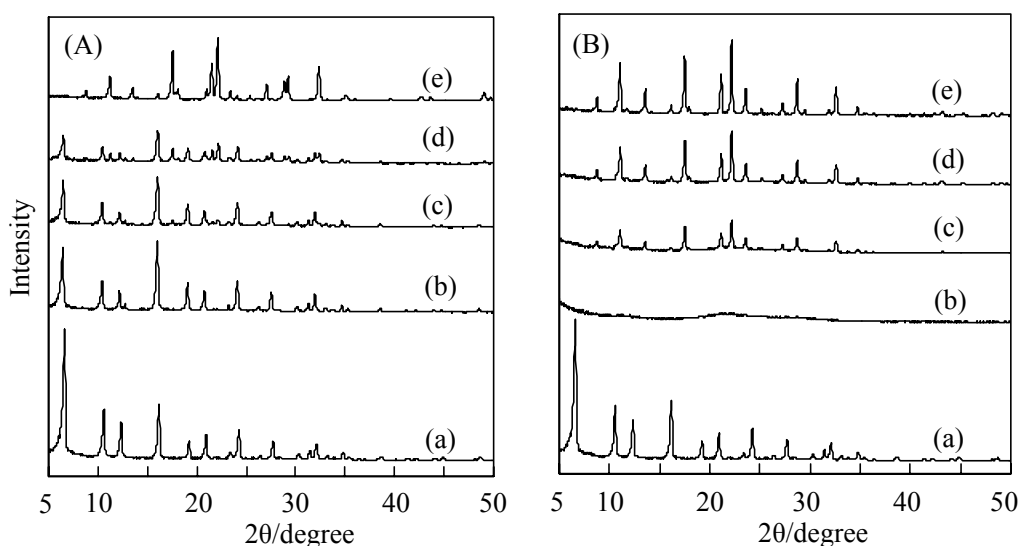


Fig. 3-10. XRD patterns of products obtained from FAU-type zeolite after various crystallization times. (A) Using  $\text{NH}_4\text{F}$  and 1-adamantanamine (sample no. 6), and (B) using choline hydroxide (sample no. 4). (a) Starting FAU-type zeolite (Si/Al = 22), (b) 2 days, (c) 3 days, (d) 4 days, and (e) 7 days.

was lower than that of the starting FAU-type zeolite, I may also deduce the higher solubility of silicate and aluminosilicate species in the aqueous phase.

#### 4. Conclusions

I have investigated the influence of fluoride anions on the interzeolite conversion of FAU-type zeolite into LEV-type zeolite. When choline hydroxide was employed as a SDA, there was no difference between the characteristics and thermal stability of LEV-type zeolites synthesized in the presence and absence of fluoride anions, which indicates that fluoride anions do not play pronounced role in the process. When 1-adamantanamine was employed instead of choline hydroxide, however, the fluoride anions exerted a pronounced influence. I succeeded in the synthesis of high silica LEV-type zeolites (Si/Al ratio = 13–29). In addition, the interzeolite conversion of FAU-type zeolite into LEV-type zeolite in the presence of fluoride anions was shown to occur in a short crystallization time (7–10 days), which is one of the advantages of zeolite synthesis that uses the interzeolite conversion method. A marked enhancement in the thermal stability of LEV-type zeolite synthesized in the presence of fluoride anions was also observed, which I attribute to fewer connectivity defects.

The largest differences in the FAU–LEV interzeolite conversion process were observed when choline hydroxide and 1-adamantanamine were used. In the case in which choline hydroxide is used, the decomposition/dissolution rate of FAU-type zeolite was relatively faster than the nucleation and crystal growth rates of LEV-type zeolites. In the case in which 1-adamantanamine was used in a fluoride medium, however, XRD diffraction patterns of the starting FAU-type zeolite were clearly

observed during the FAU–LEV interzeolite conversion process. This takes place because of the difference between the mineralizing power of fluoride anions and hydroxide anions. That is, the rate of decomposition/dissolution of the starting FAU-type zeolite in the presence of fluoride anions is slower than that in the presence of hydroxide anions, and as a consequence, the nucleation and crystal growth of LEV-type zeolite proceeds simultaneously with the decomposition/dissolution of the starting FAU-type zeolite.

## References

- [1] G. Gottardi, E. Galli, *Natural Zeolites*, Springer, Berlin, 1825, p. 192.
- [2] G.T. Kerr, US Pat. 3 459 676, 1969.
- [3] G.D. Shorte, T.V. Whittam, E.P. 0040016, 1981.
- [4] T.R. Cannon, M.T. Brent, E.M. Flanigen, E.P. 0091048A1, 1983.
- [5] E.J. Rosinski, M.K. Rubin, E.P. 0107370A1, 1983.
- [6] G.H. Kuehi, US Pat. 4 495 303, 1985.
- [7] B. Han, S. Lee, C. Lee, C. Shin, P.A. Cox, S.B. Hong, *Chem. Mater.* 17 (2005) 477.
- [8] C.S. Cundy, P.A. Cox, *Micropor. Mesopor. Mater.* 28 (2005) 1.
- [9] F. Fajula, M. Vera-Pacheco, F. Figueras, *Zeolites* 7 (1987) 203.
- [10] T. Inoue, M. Itakura, H. Jon, A. Takahashi, T. Fujitani, Y. Oumi, T. Sano, *Micropor. Mesopor. Mater.* 122 (2009) 149.
- [11] E.M. Flanigen, R. L. Patton, US Patent 4, 073, 865 (1978).
- [12] P. Caullet, J. -L. Paillaud, A. Simon-Masseron, M. Soulard, J. Patarin, C. R. *Chimie* 8 (2005) 245.
- [13] T. Blasco, M. A. Camblor, A. Corma, P. Esteve, A. Martínez, C. Prieto, S. Valencia, *Chem. Commun.* (1996) 2367.
- [14] M.A. Camblor, L. A. Villaescusa. M. J. Díaz-Cabañas, *Top. Catal.* 9 (1999) 59.
- [15] J.M. Chezeau, L. Delmotte, J. L. Guth, M. Soulard, *Zeolites* 11 (1989) 78.
- [16] B.-W. Lu, Y. Oumi, K. Itabashi, T. Sano, *Micropor. Mesopor. Mater.* 81 (2005) 365.
- [17] P. Lentz, J.B. Nagy, L. Delevoye, Y. Dumazy, C. Fernandez, J.-P. Amoureux, C.V. Tuoto, A. Nastro, *Colloid Surf. A* 158 (1999) 13.

- [18] L.B. McCusker, *Mat. Sci. Forum* 133 (1993) 423.
- [19] M.J. den Exter, J.C. Jansen, H. van Bekkum, A. Zikánova, *Zeolites* 19 (1997) 353.
- [20] H. Gies, B. Marler, *Zeolites* 12 (1992) 42.
- [21] P. Caullet, L. Delmotte, A.C. Faust, J.L. Guth, *Zeolites* 15 (1995) 139.
- [22] R.A. Hearmon, A. Stewart, *Zeolites* 10 (1990) 608.
- [23] E.J.P. Feijen, J.A. Martens, P.A. Jacobs, in: *Zeolites and Related Materials: State and The Art 1994*. J. Weitkamp, H. G. Karge, H. Pfeifer, W. Hölderich (Eds.), *Stud. Surf. Sci. Catal.* 84 (1994) 3.
- [24] J.L. Guth, *P 3 Conv. Naz. Sci. Tec* (1995) 13.

## Chapter 4

# Synthesis of high-silica CHA-type zeolite from FAU-type zeolite and its catalytic application for ethanol to olefin reaction and membrane application for dehydration of acetic acid aqueous solution

### 1. Introduction

Aluminosilicate zeolite chabazite (CHA) with Si/Al ratios of 2–3 has a three-dimensional pore system with ellipsoidal-shaped large cages ( $6.7 \times 10 \text{ \AA}$ ) that are accessible via 8-membered ring windows ( $3.8 \times 3.8 \text{ \AA}$ ). High-silica chabazite SSZ-13 and silicoaluminophosphate zeolite SAPO-34 characterized by CHA structure have attracted great interest because they exhibit specific shape selectivity for the conversion of methanol [1–3] or bioethanol [4,5] into light olefins such as ethylene and propylene. Pure silica chabazite also has potential applications involving adsorption and separation of organic molecules and gas storage on account of a larger void space attributable to the absence of counter cations in the pores and to its extreme hydrophobicity. SSZ-13 and pure silica chabazite have been synthesized only in alkali or fluoride media using expensive *N,N,N*-trimethyl-adamantammonium cation (TMAda<sup>+</sup>) as a structure-directing agent (SDA) [6,7]. Falconer et al. reported that the SSZ-13 zeolite membrane could separate light-gas mixtures of CO/N<sub>2</sub>, CO<sub>2</sub>/CH<sub>4</sub>, H<sub>2</sub>/CH<sub>4</sub>, and H<sub>2</sub>/n-C<sub>4</sub>H<sub>10</sub> with

notably higher selectivity than that allowed by the Knudsen mechanism [8]. Hasegawa et al. also found that the CHA-type zeolite membrane exhibited excellent dehydration performance for water/alcohol mixtures [9,10]. As the SSZ-13 zeolite has only been synthesized using expensive TMAda<sup>+</sup> as a structure-directing agent (SDA), several research efforts have been applied to generating improved methods for the synthesis of high-silica CHA-type zeolite using a reduced amount of TMAda<sup>+</sup> or other inexpensive SDAs [11,12].

In general, it is well known that adding seed crystals of the desired zeolite phase to the starting synthesis gel can enhance the crystallization rate [13–16]. Moreover, it is also possible to control the crystal size distribution in this manner [17,18]. Although the mechanism of the crystallization rate enhancement has not been clarified, two explanations have been offered [19]: (1) the increase in the surface area due to the addition of the seed crystals results in an increased and faster consumption of reagents and (2) seeds promote nucleation through some secondary nucleation mechanism.

Interzeolite conversion method has also attracted much attention as an alternative synthesis method for enhancement of crystallization rate. The highly crystalline and pure \*BEA-, RUT-, and MTN- type zeolites were obtained from FAU-type zeolite faster than amorphous materials in the presence of tetraethylammonium hydroxide, tetramethylammonium hydroxide, and benzyltrimethylammonium hydroxide (BTMAOH), respectively [20–23]. Here I report the synthesis of high-silica chabazite from FAU-type zeolite using BTMAOH. To the best of my knowledge, this is the first high-silica CHA-type zeolite synthesized with a SDA other than TMAda<sup>+</sup> cation, although it is already reported that the conventional aluminous CHA-type zeolite is obtained from FAU-type zeolite in a KOH solution [24]. Moreover, the catalytic

performance of the obtained high-silica CHA-type zeolite was investigated based on ethanol conversion reactions. The acid-resistance of CHA-type zeolite synthesized by the interzeolite conversion of FAU-type zeolite in acid media was further investigated in the context of previous research in this chapter. Furthermore, the CHA-type zeolite membrane was prepared on the outer surface of a porous  $\alpha$ -alumina tube by the interzeolite conversion method, and the dehydration performance was subsequently evaluated by pervaporation with a water/acetic acid mixture.

## 2 Experimental

### 2.1 Synthesis of high-silica CHA-type zeolite by interzeolite conversion of FAU-type zeolite with BTMA<sup>+</sup>

CHA-type zeolites were synthesized according to three methods. Table 4-1 lists the chemical compositions of starting mixtures and crystallization conditions.

Starting FAU-type zeolites with various Si/Al ratios were prepared from NH<sub>4</sub>-Y zeolite (Si/Al = 2.8, Tosoh Co., Japan) through dealumination treatment involving a combination of steaming at 700 °C and the administration of H<sub>2</sub>SO<sub>4</sub> (0.74–0.85 M) at 75 °C for 4 h. Seed crystals were calcined at 600 °C for 10 h. Hydrothermal conversion was performed as follows. The dealuminated FAU-type zeolite was thoroughly mixed with an aqueous solution containing the SDA BTMAOH (40 wt%, Aldrich, USA), seed crystals, and, an optional additive, namely, NaOH (>99%, Merck Chemicals, Inc., Japan), NaF (99%, Wako Pure Chemical Ind., Ltd., Japan) or NaCl (>99.5%, Kanto Chemical Co., Inc., Japan). For the synthesis of low-silica CHA-type zeolite, Al(OH)<sub>3</sub> (Wako Pure Chemical Ind., Ltd., Japan) was also added to the starting mixture.

Subsequently, the resultant mixture was placed to a 30 cm<sup>3</sup> Teflon-lined stainless steel autoclave.

Hydrothermal conversion was conducted at 125 °C for 7–14 days in a convection oven. After crystallization, the reaction mixture was cooled to room temperature, and the solid phase was separated from the liquid phase by centrifugation. The solid product was washed thoroughly with deionized water until a near neutral pH was achieved, and the material was then dried overnight at 70 °C and calcined at 600 °C for 10 h to remove any remaining SDA cations that caused zeolite pores to be occluded.

## **2.2 Synthesis of SSZ-13 using TMAda<sup>+</sup>**

SSZ-13 zeolite was prepared at 150 °C for 5 days according to the method previously outlined in the literature with only a slight modification [25], including the use of fumed silica (Cab–O–Sil M5, Cabot) and Al(OH)<sub>3</sub> as Si and Al sources as well as TMAdaOH as a SDA.

## **2.3 Synthesis of CHA-type zeolite with high Al content**

CHA-type zeolite with high Al content was synthesized at 95 °C for 100 h from FAU-type zeolite and KOH according to the method described in “Verified Syntheses of Zeolitic Materials” published by the International Zeolite Association [26].

## **2.4 Characterization**

Powder X-ray diffraction (XRD) patterns of the solid products were collected on a Rigaku Mini Flex diffractometer with curved graphite monochromatized Cu-K $\alpha$  radiation operated at 30 kV and 15 mA. The bulk Si/Al ratios were determined using

inductively coupled plasma optical emission spectroscopy (ICP, Seiko SPS7000) or using the dilithium tetraborate ( $\text{Li}_2\text{B}_4\text{O}_7$ ) method with the X-ray fluorescence (XRF) technique (Philips PW 2400). In these experiments, 0.5 g of sample was fused with 5 g of  $\text{Li}_2\text{B}_4\text{O}_7$  at 1100 °C. The Si/Al ratio was calculated from the Si and Al concentrations, which were determined by the corresponding calibration curves that were prepared using high purity  $\text{SiO}_2$  (99.999%) and  $\gamma\text{-Al}_2\text{O}_3$  (99.999%). The crystal morphology and the surface Si/Al ratio were measured using scanning electron microscopy (SEM, Hitachi S-4800) and energy-dispersive X-ray analysis (EDX). The  $^{27}\text{Al}$  magic angle spinning (MAS) NMR and  $^{29}\text{Si}$  MAS NMR spectra were recorded at 104.2 MHz and 79.5 MHz, respectively, on a Varian 600PS solid NMR spectrometer, using a 3.2-mm-diameter zirconia rotor for  $^{27}\text{Al}$  MAS NMR and a 6-mm-diameter zirconia rotor for  $^{29}\text{Si}$  MAS NMR. The rotor was spun at 15 kHz for  $^{27}\text{Al}$  MAS NMR and at 6 kHz for  $^{29}\text{Si}$  MAS NMR. The spectra were acquired using 2.3  $\mu\text{s}$  pulses, a 1 s recycle delay, and 1000 scans for  $^{27}\text{Al}$  MAS NMR, and 5  $\mu\text{s}$  pulses, a 100 s recycle delay, and 1000 scans for  $^{29}\text{Si}$  MAS NMR.  $\text{Al}(\text{NO}_3)_3 \cdot 9\text{H}_2\text{O}$  and  $\text{Si}(\text{CH}_3)_4$  were used as chemical shift references for  $^{27}\text{Al}$  and  $^{29}\text{Si}$  MAS NMR, respectively. Prior to the  $^{27}\text{Al}$  MAS NMR measurements, the samples were moisture equilibrated over a saturated solution of  $\text{NH}_4\text{Cl}$  for 24 h. Thermal analyses were carried out using a TG/DTA apparatus (SSC/5200 Seiko Instruments). A sample (ca. 7 mg) was heated in a flow of air (50 mL  $\text{min}^{-1}$ ) at a heating rate of 5 °C  $\text{min}^{-1}$  from room temperature to 800 °C. Micropore volume and surface area were determined by nitrogen physisorption using the t-plot and Brunauer–Emmett–Teller (BET) methods, respectively. Nitrogen adsorption isotherms at -196 °C were obtained using a conventional volumetric apparatus (Bel Japan, BELSORP-mini).

## 2.5 Catalytic testing

The catalytic performance of the protonated CHA type zeolite (H-CHA) for the ethanol conversion reaction was tested using a quartz fixed-bed reactor at 400 °C and atmospheric pressure. The protonated form was prepared using an ion-exchange method with a 1M NH<sub>4</sub>NO<sub>3</sub> solution, followed by calcination at 450 °C for 10 h. The reaction gas, EtOH/N<sub>2</sub> (50/50 vol.%), was fed at a W/F (g(H-CHA)/mL (EtOH/N<sub>2</sub>) per min) of 0.0125–0.03 g min mL<sup>-1</sup>. The gaseous products were analyzed through on-time GC equipped with TCD- and FID-type detectors, on Shincarbon ST (Shinwa Chem. Ind. Ltd., Japan) for N<sub>2</sub>, H<sub>2</sub>, and CO<sub>2</sub>; on Gaskropack54 (GL Sciences, Japan) for ethanol; and on RT-alumina PLOT (Restek, USA) for C<sub>1</sub>–C<sub>4</sub> hydrocarbons. The product yields were calculated using N<sub>2</sub> as an internal standard.

## 2.6. Acid stability (structure stability and composition stability)

The structure stability of the resultant CHA-type zeolites was evaluated by XRD analysis by the comparison of the peak intensity changes in the intensities at  $2\theta = 9.4(1\ 0\ 0)$ ,  $20.5(2\ 0\ -1)$ , and  $30.4(3\ -1\ -1)$  in samples prior and subsequent to acid treatment at 75 °C for 2 h–30 days. CH<sub>3</sub>COOH, HCl, HNO<sub>3</sub>, H<sub>2</sub>SO<sub>4</sub>, and H<sub>3</sub>PO<sub>4</sub> aqueous solutions were employed for acid treatment. The relative crystallinity was determined as follows:

Relative crystallinity (%) =

$$\frac{\text{Sum of intensities of the peaks at } 2\theta = 9.4, 20.5, \text{ and } 30.4 \text{ after acid treatment}}{\text{Sum of intensities of the peaks at } 2\theta = 9.4, 20.5, \text{ and } 30.4 \text{ before acid treatment}} \quad (1)$$

The Si/Al ratios of samples after acid treatment were employed as an index of the composition stability.

## 2.7. Fabrication of CHA-type zeolite membrane

Polycrystalline high-silica CHA-type zeolite membranes were formed by the secondary growth of seed crystals on the outer surface of a porous  $\alpha$ -alumina tube with a 2.0 mm outer diameter, 1.6 mm inner diameter, 210 mm length, 42% porosity, and 150 nm mean pore diameter. The seed crystals were synthesized by the interzeolite conversion method. Seed crystals were applied to the outer surface of the support tube by rubbing with a Si/Al ratio of 16 in order to implant the seed crystals for nucleation. The secondary growth solution with a chemical composition of  $\text{SiO}_2$ :  $0.03\text{Al}_2\text{O}_3$ :  $0.2\text{BTMA}$ :  $0.1\text{NaCl}$ :  $10\text{H}_2\text{O}$  was prepared from the dealuminated FAU, BTMAOH, NaCl, and distilled water. Thereafter, a hydrothermal reaction was carried out at  $130\text{ }^\circ\text{C}$  for 7 days using a  $45\text{ cm}^3$  Teflon-lined autoclave. After cooling the autoclave, the support tube was recovered, washed with distilled water, and dried overnight in air at room temperature. Finally, the support tube was calcined at  $550\text{ }^\circ\text{C}$  for 20 h.

## 2.8. Dehydration performance

The high-silica CHA-type zeolite membrane prepared on the  $\alpha$ -alumina tube was connected with the SUS tube using heat shrink tubing, and the tube was subsequently set in the conventional batch-type pervaporation apparatus. An acetic acid aqueous solution (50/50 wt%) was used as the feed at  $75\text{ }^\circ\text{C}$ . Liquid nitrogen was used as a cooling agent for the cold trap. The compositions of the feed and the permeate were determined by FID-gas-chromatography (Shimadzu GC-8A 5MS, capillary column). The permeation flux and separation factor,  $\alpha(\text{H}_2\text{O}/\text{CH}_3\text{COOH})$ , were calculated from the following equations:

$$\text{Flux (kg m}^{-2}\text{ h}^{-1}\text{)} = \frac{\text{(weight of permeate /kg)}}{\text{(membrane area /m}^2\text{)} \times \text{(collection time /h)}} \quad (2)$$

$$\alpha(\text{H}_2\text{O}/\text{CH}_3\text{COOH}) = \frac{(\text{C}_{\text{H}_2\text{O}}/\text{C}_{\text{CH}_3\text{COOH}})_{\text{Permeate}}}{(\text{C}_{\text{H}_2\text{O}}/\text{C}_{\text{CH}_3\text{COOH}})_{\text{Feed}}} \quad (3)$$

### 3 Results and discussion

#### 3.1. Synthesis and characterization of CHA-type zeolite

The detailed hydrothermal conversion conditions and products are listed in Table 4-1. The hydrothermal conversion of FAU-type zeolite without any additives other than BTMAOH gave amorphous materials. When a small amount of NaCl (NaCl/SiO<sub>2</sub> ratio of 0.05) was added to the mixture, the highly crystalline and pure clathrasil zeolite MTN was obtained [23]. Under a further increase in the NaCl/SiO<sub>2</sub> ratio and lower synthesis temperatures, the pure CHA-type zeolite was successfully synthesized. Fig. 4-1(a) and 2(b) show the XRD pattern and SEM image of calcined CHA-type zeolite, respectively. It shows the typical diffraction pattern of CHA-type zeolite, which contains no impurities coming from the unconverted starting FAU-type zeolite and/or the cocrystallized phase. The obtained CHA-type zeolite has an ellipsoidal plate-like crystal shape with 1–1.5 mm in size. When the hydrothermal conversion of FAU-type zeolite was carried out in the absence of seed crystals, a prolonged crystallization time (21 days) was required for synthesis of highly crystalline CHA-type zeolite (sample no. 4 in Table 4-1). The FAU–CHA interzeolite conversion did not occur when the Si/Al ratio of the starting FAU-type zeolite was 25 (sample no. 6). When the 2 wt.% seed crystals were added to the starting gel, however, highly crystalline CHA-type zeolite was obtained after hydrothermal treatment for only 7 days (sample no. 9). The yield of CHA type zeolite was ca. 92% based on the weight of the FAU-type zeolite.

Table 4-1 Hydrothermal conversion of FAU-type zeolite and products obtained.

Sample no.	Hydrothermal synthesis condition							Products			
	Si & Al sources (Si/Al)	SDA/SiO <sub>2</sub>	Additive/SiO <sub>2</sub>	H <sub>2</sub> O/SiO <sub>2</sub>	Seed content	Temp./°C	Time/days	Phase	Bulk Si/Al	S <sub>BET</sub> /m <sup>2</sup> g <sup>-1</sup>	V <sub>pore</sub> /cm <sup>3</sup> g <sup>-1</sup>
1	FAU(21)	0.2(BTMAOH)	0.05(NaCl)	5		170	10	MTN	21.5		
2	FAU(21)	0.2(BTMAOH)	0.05(NaCl)	5		140	21	MTN,CHA			
3	FAU(21)	0.2(BTMAOH)	0.05(NaCl)	5		120	21	Am.,FAU			
4	FAU(21)	0.2(BTMAOH)	0.1(NaCl)	5		120	21	CHA	16.9	590	0.29
5	SiO <sub>2</sub> /γ-Al <sub>2</sub> O <sub>3</sub> (21)	0.2(BTMAOH)	0.1(NaCl)	5		120	21	Am.			
6	FAU(25)	0.2(BTMAOH)	0.1(NaCl)	5		120	21	Am.			
7	FAU(16)	0.2(BTMAOH)	0.1(NaCl)	5	2	125	7	FAU,CHA,Am.			
8	FAU(16)	0.2(BTMAOH)	0.1(NaCl)	5	2	125	14	CHA	14.5		
9	FAU(22)	0.2(BTMAOH)	0.1(NaCl)	5	2	125	7	CHA	18.2	630	0.29
10	FAU(30)	0.2(BTMAOH)	0.1(NaCl)	5	2	125	14	CHA	21.5		
11	FAU(44)	0.2(BTMAOH)	0.1(NaCl)	5	2	125	14	CHA,Am.			
12	FAU(16)	0.2(BTMAOH)	0.1(NaOH)	5	2	125	7	CHA	14.7		
13	FAU(22)	0.2(BTMAOH)	0.1(NaOH)	5	2	125	7	CHA	14.7	590	0.30
14	FAU(81)	0.2(BTMAOH)	0.1(NaOH)	5	2	125	7	CHA	21.3		
15	FAU(95)	0.2(BTMAOH)	0.1(NaOH)	5	2	125	7	CHA	19.6		
16	FAU(24)	0.3(BTMAOH)		5	2	125	14	Am.,CHA			
17	FAU(24)	0.3(BTMAOH)		5	5	125	14	CHA	14.0		
18	FAU(22)	0.3(BTMAOH)		5	10	125	7	CHA	13.6	620	0.29
19	FAU(97)	0.3(BTMAOH)		5	10	125	7	CHA	18.6		
20	SiO <sub>2</sub> /γ-Al <sub>2</sub> O <sub>3</sub> (22)	0.2(BTMAOH)	0.1(NaCl)	5	2	125	14	Layer,Am.			
21	FAU(2.6)		0.8(KOH)	35		100	5	CHA	2.5	340	0.17
22	FAU+Al(OH) <sub>3</sub> (5)	0.2(BTMAOH)	0.1(NaOH)	5	2	125	7	CHA	5.2	530	0.27
23	FAU+Al(OH) <sub>3</sub> (10)	0.2(BTMAOH)	0.1(NaOH)	5	2	125	7	CHA	8.4	600	0.24
25	FAU(22)	0.2(BTMAOH)	0.1(NaF)	5	2	125	14	CHA	17	600	0.29
26	FAU(27)	0.2(BTMAOH)	0.1(NaCl)	5	2	125	14	CHA	21	630	0.28
27	SiO <sub>2</sub> /Al(OH) <sub>3</sub> (10)	0.2(TMAdaOH)	0.2(NaOH)	45		150	5	CHA	8.1	560	0.27
28	SiO <sub>2</sub> /Al(OH) <sub>3</sub> (20)	0.2(TMAdaOH)	0.2(NaOH)	45		150	5	CHA	12	520	0.25
29	SiO <sub>2</sub> /Al(OH) <sub>3</sub> (50)	0.2(TMAdaOH)	0.2(NaOH)	45		150	5	CHA	17	580	0.28

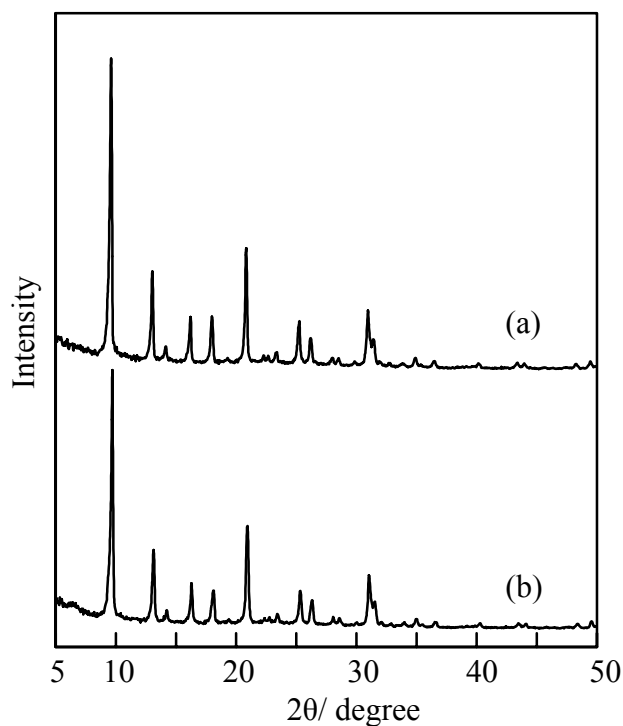


Fig. 4-1 XRD patterns of CHA-type zeolites obtained (a) without seed crystals (sample no. 4) and (b) with seed crystals (sample no. 9).

Fig. 4-1 provides the XRD patterns of the CHA-type zeolites obtained in the absence and in the presence of seed crystals. There was no difference in the peak intensity of the two CHA-type zeolites. For comparison, I attempted to synthesize CHA-type zeolite from amorphous  $\text{SiO}_2/\gamma\text{-Al}_2\text{O}_3$  as the starting material (sample nos. 5 and 20). However, CHA-type zeolite was not obtained, demonstrating the advantage and uniqueness of the hydrothermal conversion of FAU-type zeolite.

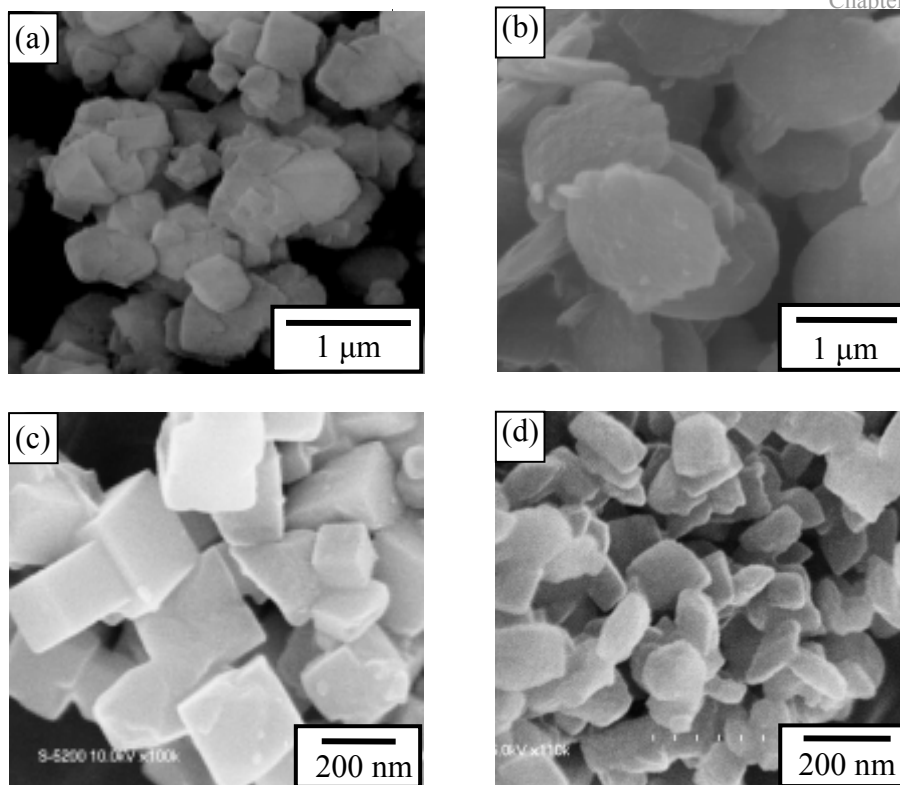


Fig. 4-2 SEM images of starting FAU-type zeolite and various CHA-type zeolites obtained. (a) FAU-type zeolite, (b) CHA-type zeolite obtained without seed crystals (sample no. 1), (c) CHA-type zeolite obtained with seed crystals (sample no. 5), and (d) CHA-type zeolite obtained with seed crystals in the absence of  $\text{Na}^+$  cations (sample no. 15).

The previous results concerning the interzeolite conversion showed that the conversion was strongly dependent on the Si/Al ratio of the starting FAU-type zeolite [20–23]. In order to study the influence of the Si/Al ratio of the starting FAU-type zeolite on the synthesis of CHA type zeolite, FAU-type zeolites with various Si/Al ratios (Si/Al = 16–95) were prepared through dealumination treatment and were subjected to hydrothermal treatment. Only FAU-type zeolites with Si/Al ratios of 21 could be converted into pure CHA-type zeolites, indicating a very narrow synthesis region without seed crystal (sample no. 4). By seeding, for the FAU-type zeolites with Si/Al ratios of 16 and 30, CHA-type zeolite was obtained while a prolonged synthesis time (14 days) was needed (sample nos. 8 and 10). However, for the Si/Al ratio of 44, pure CHA-type zeolite was not obtained (sample no. 11). When NaOH was used as an

additive instead of NaCl, pure CHA-type zeolites were obtained from starting FAU-type zeolites with higher Si/Al ratios (sample nos. 14 and 15). However, the Si/Al ratios of the obtained CHA-type zeolites were considerably smaller than those of the starting FAU-type zeolites. The lower Si/Al ratio is probably due to the hydrothermal conversion under higher alkalinity condition, namely, an increase of silicon concentration in the liquid phase.

Fig. 4-2 presents SEM images of CHA-type zeolites obtained from FAU-type zeolite, together with the starting FAU-type zeolite. After thorough observation, I did not find any crystals of the starting FAU-type zeolite or impurities. In the SEM image of the CHA type zeolite obtained with seed crystals, cubic morphology, and the crystal size was 100–200 nm (Fig. 4-2c) was observed. The morphology of CHA crystal was altered by existence of seed crystal.

Figure 4-3 shows the  $^{13}\text{C}$  CP/MAS NMR spectrum of synthesized CHA-type zeolite. Three resonances were observed at ca. 54, 72, and 132 ppm, which correspond to the methyl carbon, methylene carbon, and phenyl carbon of BTMA<sup>+</sup> cation, respectively. It was found that the SDA molecule exists intact within the pores of high-silica CHA zeolite. Although Zones and van Nordstand have already reported the hydrothermal conversions of cubic P zeolite and faujasite to high-silica chabazite SSZ-13 using expensive TMA<sup>+</sup> cation as SDA, these zeolites was employed only as the aluminium source [11,27]. Next, to clarify the chemical states of aluminum and silicon in the obtained CHA type zeolite,  $^{27}\text{Al}$  and  $^{29}\text{Si}$  MAS NMR measurements were performed. Fig. 4-4(A) provides the  $^{27}\text{Al}$  MAS NMR spectra of CHA-type zeolites obtained without and with seed crystals. Regardless of the presence of seed crystals, only one peak centered at ca. 55 ppm was observed, corresponding to tetrahedrally coordinated

aluminum species. The peak corresponding to octahedrally coordinated aluminum species, i.e., extra-framework aluminum species, was not observed at around 0 ppm. This means that all of the aluminum species present in both CHA-type zeolites resulting from hydrothermal conversion of FAU-type zeolite exist within the zeolite framework. The  $^{29}\text{Si}$  MAS NMR spectra of these CHA-type zeolites are also shown in Fig. 4-4(B). Three peaks were observed centered at ca.  $-110$ ,  $-105$ , and  $-100$  ppm, and they are assigned to  $\text{Q}^4(0\text{Al})$ ,  $\text{Q}^4(1\text{Al})$ , and  $\text{Q}^4(2\text{Al}) + \text{Q}^3(0\text{Al})$ , respectively (Fig. 4-4(B)) [28,29]. The difference in the intensity of the peak at ca.  $-105$  ppm of the CHA-type zeolites is due to the difference in the aluminum content. The BET surface area and the micropore volume of the CHA-type zeolite obtained with seed crystals were calculated to be  $630 \text{ m}^2 \text{ g}^{-1}$  and  $0.29 \text{ m}^3 \text{ g}^{-1}$ , respectively, and those calculated from the CHA-type zeolite obtained without seed crystals were  $590 \text{ m}^2 \text{ g}^{-1}$  and  $0.29 \text{ m}^3 \text{ g}^{-1}$  (shown in Table 4-1).

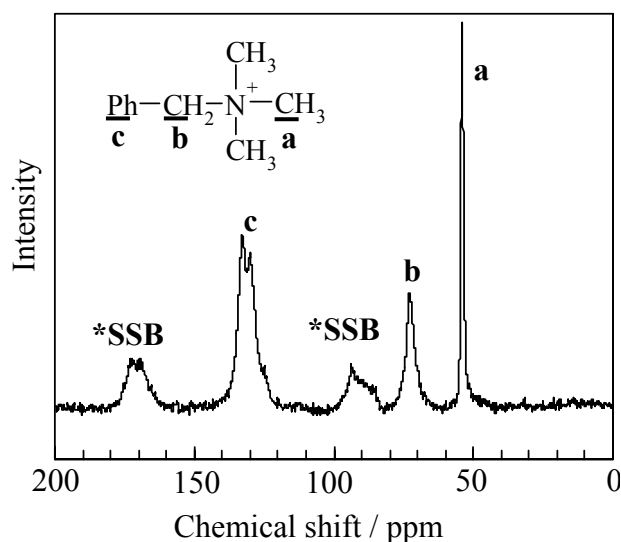


Fig. 4-3  $^{13}\text{C}$  CP/MAS NMR spectrum of CHA-type zeolite obtained (sample no. 4). Asterisks denote spinning sidebands (SSB).

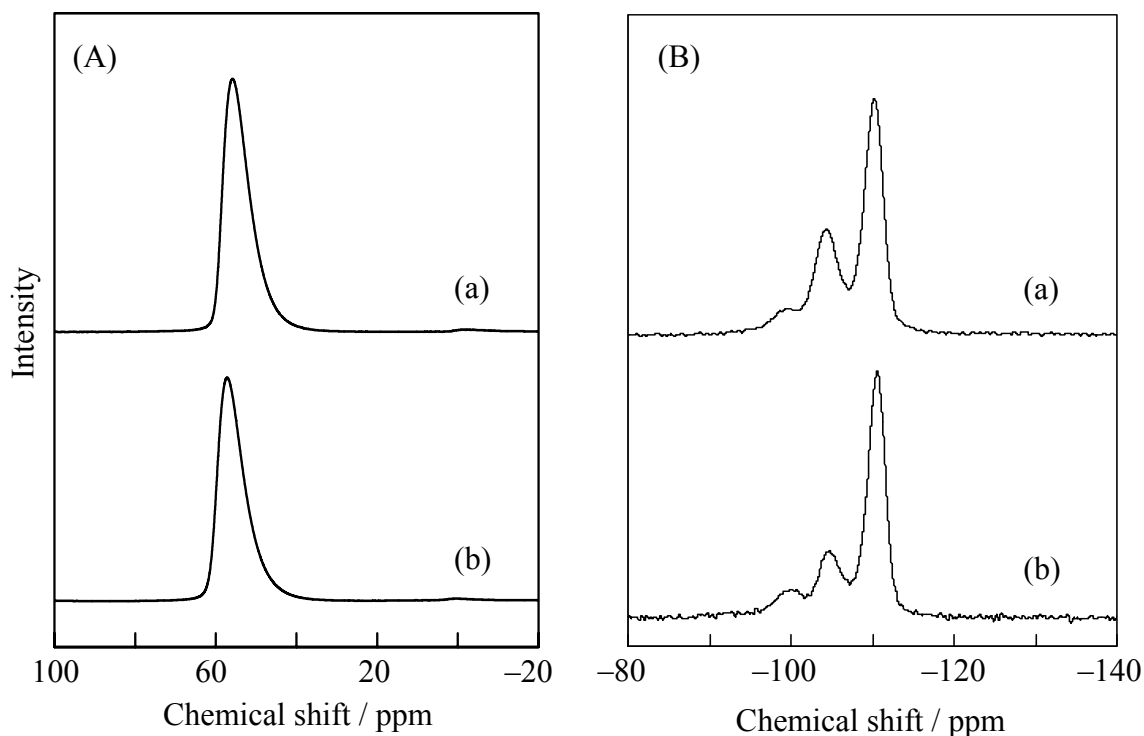


Fig. 4-4 (A)  $^{27}\text{Al}$  and (B)  $^{29}\text{Si}$  MAS NMR spectra of CHA-type zeolites obtained (a) without seed crystals (sample no. 4) and (b) with seed crystals (sample no. 9).

In my previous studies, alkaline metal cations, especially  $\text{Na}^+$  cations, were required for synthesis of LEV-, MTN-, and OFF-type zeolites from FAU-type zeolite [30]. To clarify the role of  $\text{Na}^+$  cations in the FAU–CHA interzeolite conversion process, the interzeolite conversion was carried out in the absence of  $\text{NaCl}$ . Although a higher BTMAOH/ $\text{SiO}_2$  ratio and seed content were needed, the FAU–CHA interzeolite conversion proceeded effectively (sample nos. 17–19 in Table 4-1). It was thereby found that  $\text{Na}^+$  cations are not required for interzeolite conversion in the presence of seed crystals. To my knowledge, this is the first report on alkaline metal cation-free synthesis of high-silica CHA-type zeolite. As can be seen in Fig. 4-2(d), the crystal size

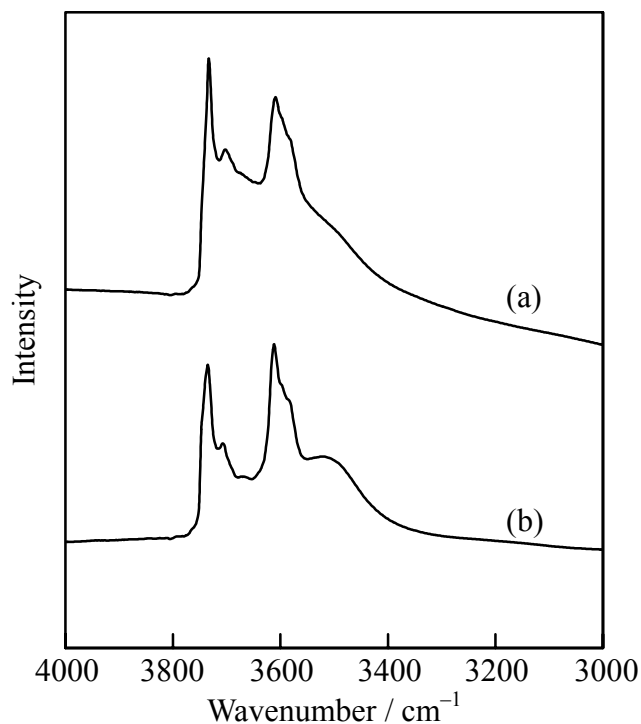


Fig. 4-5 FT-IR spectra of H-CHA-type zeolites. (a) CHA-type zeolite obtained with seed crystals in the presence of NaCl (sample no. 9) and (b) Na<sup>+</sup> cation-free CHA-type zeolite obtained with seed crystals (sample no. 19).

of Na<sup>+</sup> cation-free CHA-type zeolite was considerably smaller than that obtained in the presence of Na<sup>+</sup> cations, suggesting an enhancement of nucleation. Fig. 4-5 presents FTIR spectra in the hydroxyl groups region of the protonated CHA-type zeolites (H-CHA) obtained in the absence and in the presence of Na<sup>+</sup> cations. The CHA-type zeolite obtained in the presence of Na<sup>+</sup> cations was protonated by ion-exchange with a 1 M NH<sub>4</sub>NO<sub>3</sub> solution, followed by calcination at 450 °C for 10 h. On the other hand, the Na<sup>+</sup> cation-free CHA type zeolite was protonated only by calcination. The IR spectrum of the H-CHA type zeolite obtained in the presence of Na<sup>+</sup> cations exhibited four peaks at approximately 3730, 3680, 3610, and 3500 cm<sup>-1</sup>. The two peaks at 3730 and 3610

$\text{cm}^{-1}$  are assigned to isolated silanol groups and to the acidic bridged OH of  $\text{Si}(\text{OH})\text{Al}$ , respectively, whereas the peaks at 3680 and 3500  $\text{cm}^{-1}$  are assigned to internal silanol groups of hydroxyl nests [23]. The intensity of the peak at 3500  $\text{cm}^{-1}$  was slightly strong in the spectrum of the H-CHA-type zeolite obtained in the absence of  $\text{Na}^+$  cations. These results indicate that the H-CHA-type zeolite in the absence of  $\text{Na}^+$  cations is higher in framework defects.

### 3.2. Ethanol to olefins reaction

Regarding the high-silica CHA-type zeolites with a wide range of Si/Al ratios that were obtained by interzeolite conversion of FAU-type zeolite in the presence of seed crystals, their catalytic performance for ethanol conversion to light olefins was evaluated using a fixed-bed reactor at atmospheric pressure and a temperature of 400 °C, with  $W/F = 0.0125 \text{ g min mL}^{-1}$ . The typical results over CHA-type zeolites obtained with and without seed crystals are shown in Fig. 4-6. For both H-CHA-type zeolites, the ethanol conversion was 100%, even after 3 h time on stream. The initial propylene yield for CHA-type zeolite obtained with seed crystals (sample no. 9) was ca. 10 C-% higher than that for CHA-type zeolite obtained without seed crystals (sample no. 4). The yields of products obtained on the CHA-type zeolite synthesized with seed crystals were as follows: 37.1 C-% ethylene, 45.4 C-% propylene, 3.0 C-% butene, 6.0 C-%  $\text{C}_1\text{-C}_5$  paraffins and 7.4 C-%  $\text{C}_5^+$  species. However, rapid deactivation by the poisoning of acid sites due to the accumulation of carbonaceous deposits was observed. The amounts of carbonaceous deposits after a reaction lasting 3 h, evaluated by TG analysis, were 19.8% and 16.9% for CHA-type zeolites obtained with and without seed crystals, respectively.

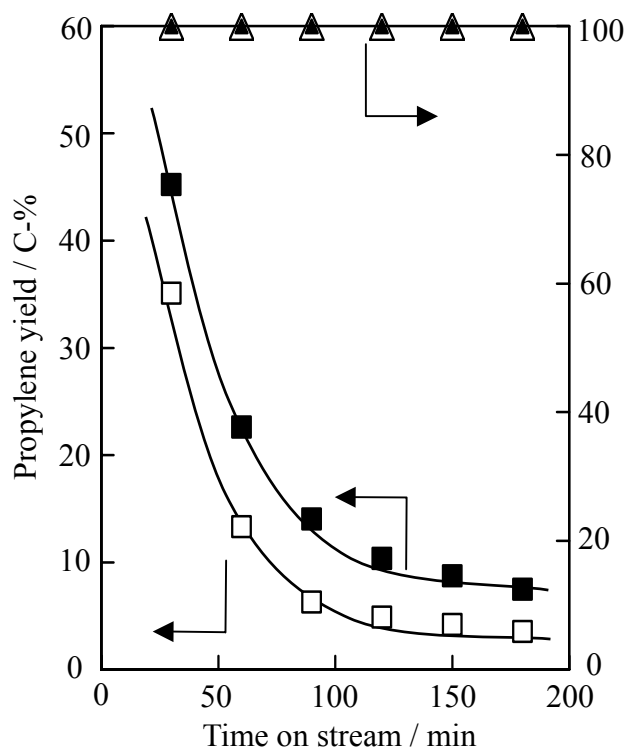


Fig. 4-6 Time on stream of propylene yield and ethanol conversion of CHA-type zeolites obtained with seed crystals (■, ▲), sample no. 9, and without seed crystals (□, △), sample no. 4.

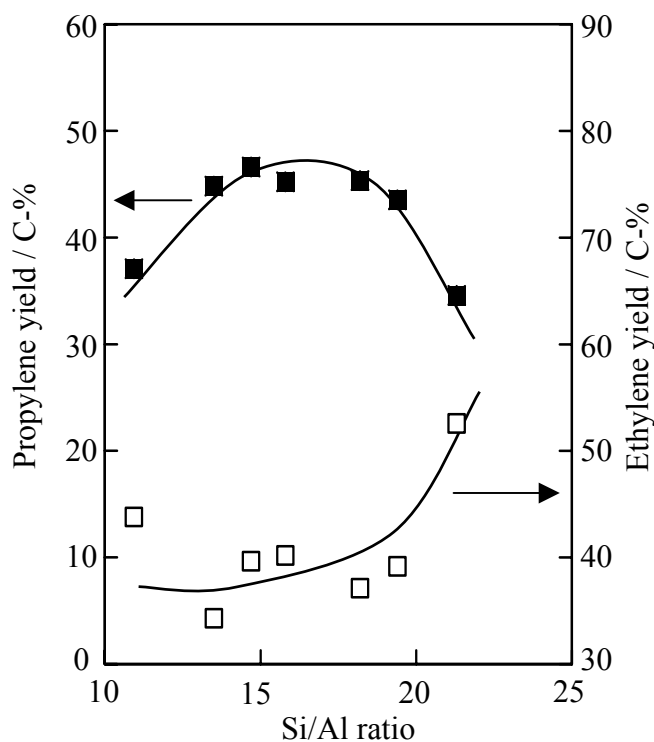


Fig. 4-7 Relationship between Si/Al ratio of CHA-type zeolite and yield of light olefins ((□) ethylene and (■) propylene).

Fig. 4-7 shows the relationship between the Si/Al ratio of CHA-type zeolite obtained with seed crystals and initial ethylene and propylene yields at 0.5 h time on stream. The ethylene and propylene yields were strongly dependent on the Si/Al ratio, and the maximum propylene yield of ca. 48 C-% was obtained at the Si/Al ratio of ca. 15. On the other hand, the ethylene yield tended to increase with an increase in the Si/Al ratio. As it is well known that the product distribution in the zeolitic ethanol conversion process strongly depends on the acidity as well as the channel structure of zeolite and that ethanol is considered to first convert to ethylene and then subsequently to higher hydrocarbons, the observed relationship between the Si/Al ratio and initial ethylene and propylene yields seems to be related with the oligomerization ability of ethylene on the

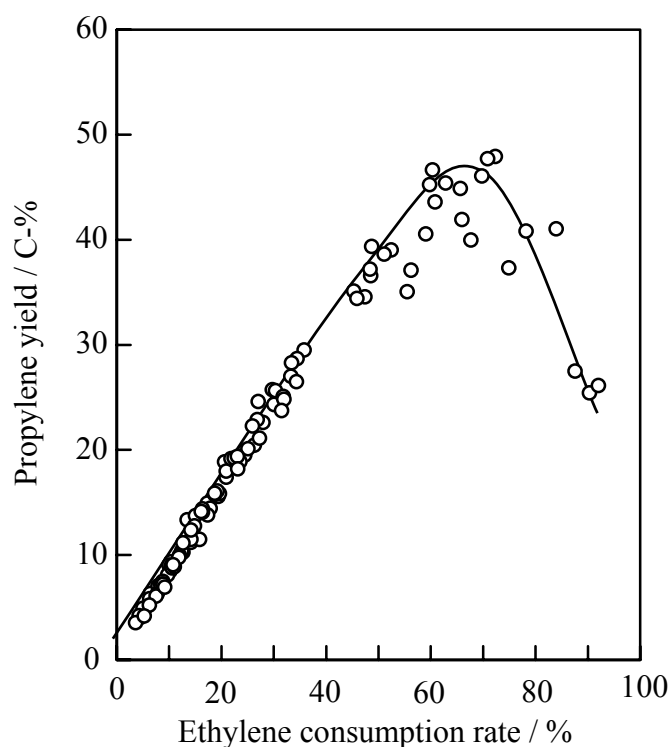


Fig. 4-8 Propylene yield as a function of ethylene consumption rate for CHA-type zeolite obtained with seed crystals.

acid sites. Next, therefore, the effect of ethylene consumption on the propylene yield was investigated [31]. The propylene yield was plotted against the ethylene consumption rate (%),  $100 - \text{yield of ethylene}$ , as shown in Fig. 4-8. To obtain a variety of ethylene consumption values, the ethanol conversion reaction was carried out at  $400\text{ }^{\circ}\text{C}$  while varying the W/F ratio. The propylene yield increased with an increase in the ethylene consumption rate, and it reached a maximum yield of ca. 48 C-% at ca. 72% ethylene consumption rate. This value is similar to that of SAPO-34 (52.2 C-% at 71.2% ethylene consumption) having a CHA-type structure [4].

### 3.3. Acid stability

In order to ascertain the acid-resistance of CHA-type zeolites, the CHA-type zeolite samples were treated with a 90 vol% acetic acid aqueous solution at  $75\text{ }^{\circ}\text{C}$  for 5 days.

The structure stability was evaluated by the comparison of peak intensity changes at  $2\theta = 9.4(100)$ ,  $20.5(20-1)$ , and  $30.4(3-1-1)$  for samples prior and subsequent to the treatment. Fig. 4-9B shows the XRD patterns of CHA-type zeolites after acid treatment. No reductions in peak intensities were observed in CHA-type zeolites synthesized by interzeolite conversion (sample no. 13) and SSZ-13 (sample no. 29), whereas the CHA-type zeolite structure of sample no. 21 collapsed completely upon acid treatment. These results suggest the high structure stability of sample nos. 13 and 29. The acid stability of zeolites has been comprehensively documented for its dependence upon the Si/Al ratio of the zeolite framework to resist acid degradation. In order to examine the mechanism of the Si/Al ratio's influence on zeolite acid stability, CHA-type zeolites with various Si/Al ratios were synthesized and subjected to treatment with a 90 vol% acetic acid aqueous solution at 75 °C for 5 days. Since no reductions in XRD peak intensities were observed for CHA-type zeolites with various Si/Al ratios and particle sizes (not shown), it was found that both CHA-type zeolite synthesized by interzeolite conversion and SSZ-13 possess the high structure stability. Fig. 4-10 shows the relationship between the Si/Al ratio prior to the acetic acid treatment and the Si/Al ratio subsequent to the acetic acid treatment. No differences were observed between the Si/Al ratios prior and subsequent to acid treatment for CHA-type zeolites synthesized by the interzeolite conversion method. Conversely, notable differences were observed in the SSZ-13 zeolite, particularly the SSZ-13 possessing a Si/Al ratio of 17. Specifically, the acid treatment enhanced dealumination of the SSZ-13. These results indicate that the high-silica CHA-type zeolite synthesized by the interzeolite conversion of FAU-type zeolite has superior composition stability as compared to the SSZ-13 zeolite. The high acid stability of CHA-type zeolite synthesized by interzeolite conversion were also

confirmed by the long acid stability test (not shown), which revealed no reduction in the relative crystallinity even after acid treatment for 30 days. However, slight dealumination was observed. The high acid stability of the high-silica CHA-type

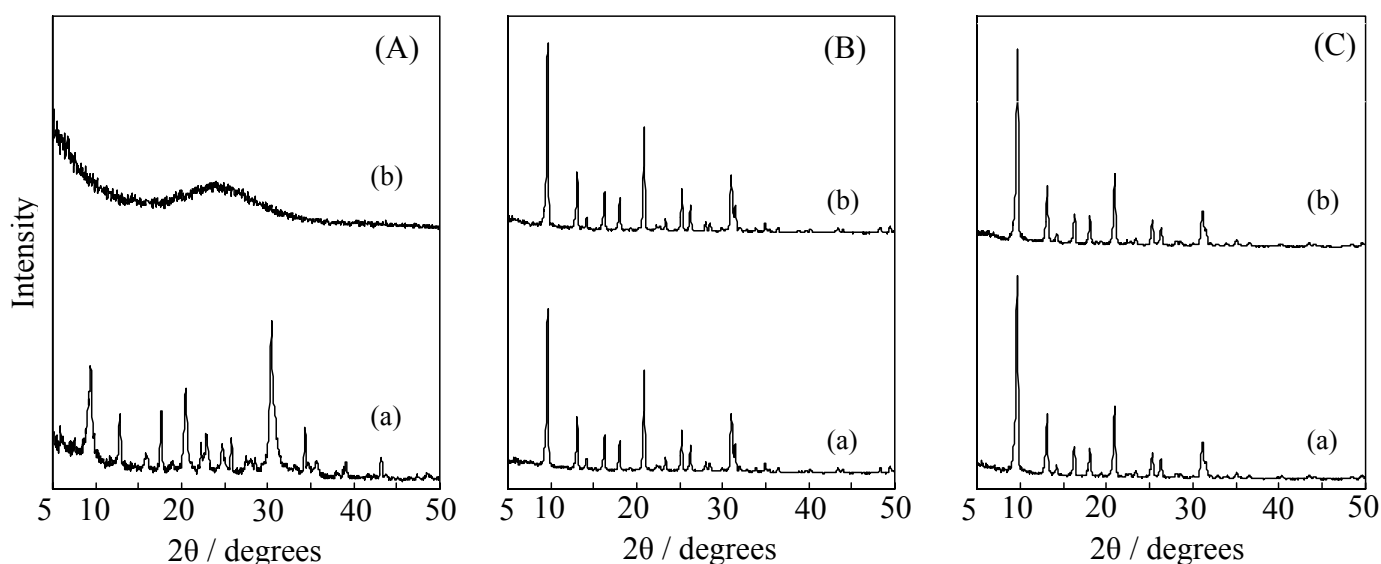


Fig. 4-9. XRD patterns of various CHA-type zeolites (a) before and (b) after acetic acid treatment. Sample Nos.: (A) 21, (B) 13, and (C) 29.

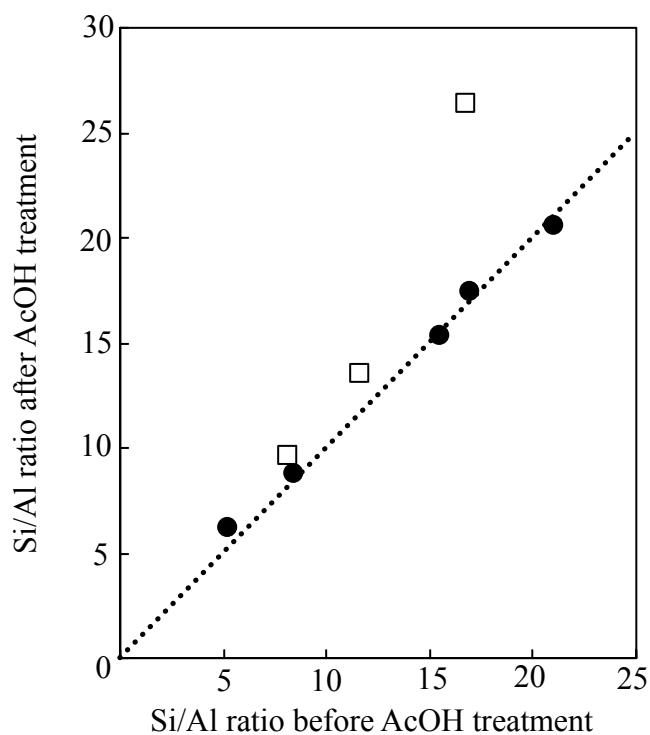


Fig. 4-10 Bulk Si/Al ratios before and after acetic acid treatment. (●) CHA-type zeolite synthesized by interzeolite conversion and (□) SSZ-13.

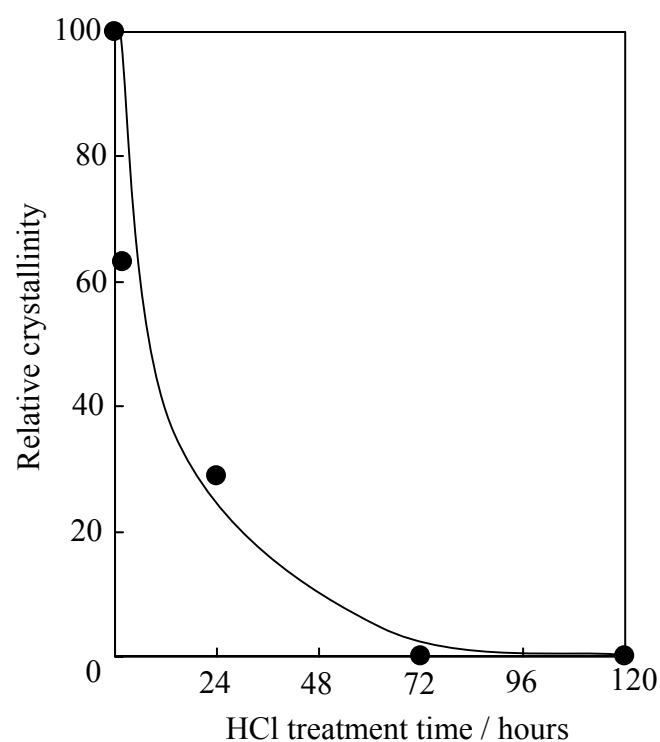


Fig. 4-11 Effect of HCl treatment time on relative crystallinity of CHA-type zeolite with Si/Al ratio of 8.4.

zeolites synthesized by the interzeolite conversion method was further confirmed by treatment with several mineral acid solutions, including 5 M HCl, H<sub>2</sub>SO<sub>4</sub>, HNO<sub>3</sub>, and H<sub>3</sub>PO<sub>4</sub> at 75 °C for 2 h–5 days. Fig. 4-11 shows the time-course of the relative crystallinity of the CHA-type zeolite with a Si/Al ratio of 8.4 (Sample no. 23) during 5 M HCl treatment at 75 °C. A rapid decrease in the relative crystallinity was observed in the initial stage of HCl treatment, and the zeolite structure collapsed completely after 3 days of HCl treatment. The relative crystallinities and the Si/Al ratios of CHA-type zeolite samples after acid treatment with various mineral acids are summarized in Table 4-2. Treatment of the CHA-type zeolite with a Si/Al ratio of 11 with 5 M HCl for 1 day produced a relative crystallinity decrease to ca. 81%, and half of the aluminum atoms were removed from the zeolite. No reduction in the relative crystallinity was observed, however, for zeolites with Si/Al ratios of 16 and 17, although slight dealumination was observed. CHA-type zeolites with Si/Al ratios of 16 and 17 also exhibit high acid stability in the presence of HNO<sub>3</sub> and H<sub>2</sub>SO<sub>4</sub>. Fig. 4-12A shows the nitrogen adsorption isotherm after H<sub>2</sub>SO<sub>4</sub> treatment. No reduction in nitrogen adsorption quantities was observed. However, as listed for Run nos. 6 and 7 in Table 4-2, the H<sub>3</sub>PO<sub>4</sub> treatment produced a slight reduction in the relative crystallinity as well as an increase in the Si/Al ratio. Taking into account the fact that incorporation of phosphorous into zeolite frameworks occurred under dealumination condition (pH < 4) [32], it might be considered that part of phosphorous is incorporated into CHA-type zeolite structure during H<sub>3</sub>PO<sub>4</sub> treatment, giving a relative crystallinity decrease and an increase in the Si/Al ratio. However, I need a further study. In comparison, the SSZ-13 with a Si/Al ratio of 17 was also treated with mineral acids. As can be seen in Fig. 4-12B and Run nos. 8 and 9 in Table 4-2, considerable decrease in nitrogen adsorption quantities and

Table 4-2 Acid treatment of CHA-type zeolites in various 5 M acid solutions.<sup>a</sup>

Run No.	Zeolite (Si/Al)	Treatment conditions		Relative crystallinity/%	Si/Al after acid treatment
		Acid	Time/days		
1	CHA(11)	HCl	1	81	22
2	CHA(16)	HCl	5	100	19
3	CHA(17)	HCl	5	100	21
4	CHA(17)	HNO <sub>3</sub>	5	100	20
5	CHA(17)	H <sub>2</sub> SO <sub>4</sub>	5	100	21
6	CHA(17)	H <sub>3</sub> PO <sub>4</sub>	5	85	25
7	CHA(21)	H <sub>3</sub> PO <sub>4</sub>	5	81	26
8	SSZ-13(17)	H <sub>2</sub> SO <sub>4</sub>	5	23	68
9	SSZ-13(17)	H <sub>3</sub> PO <sub>4</sub>	5	19	104

<sup>a</sup>Treatment temperature: 75 °C.

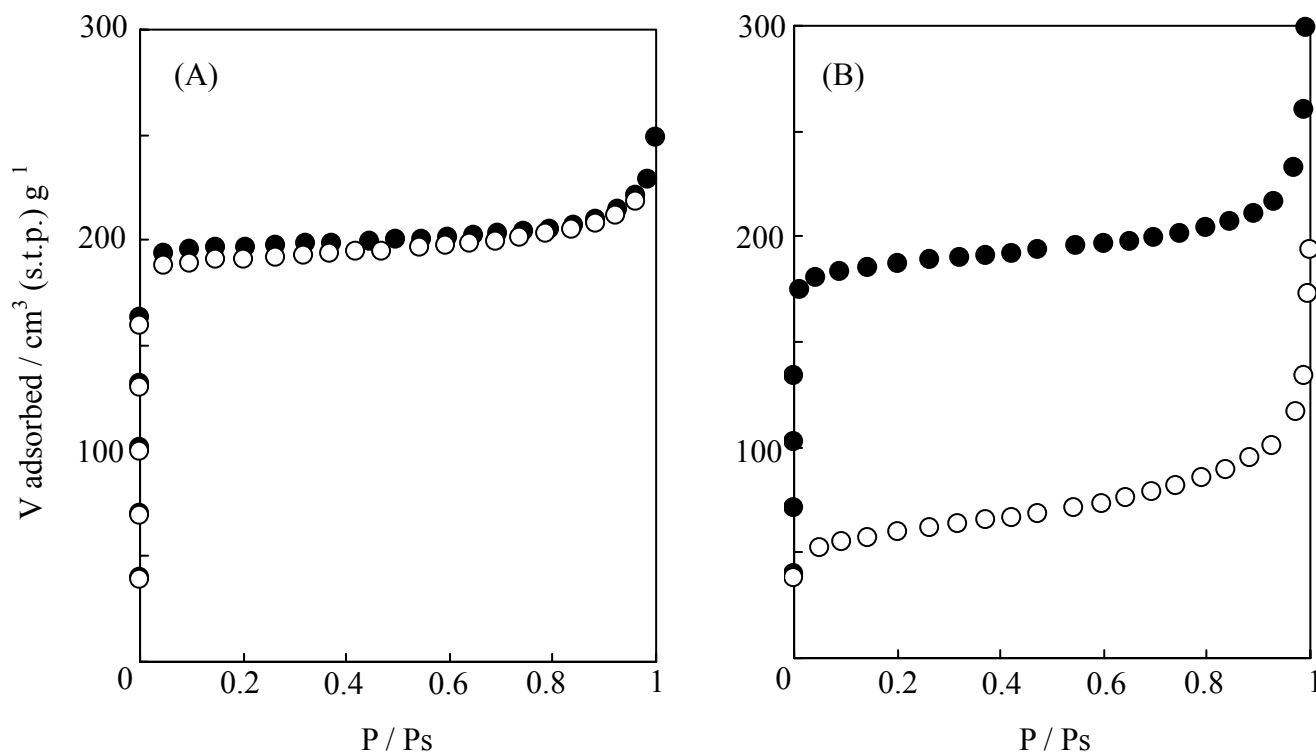


Fig. 4-12 Nitrogen adsorption isotherms of (A) CHA-type zeolite synthesized by interzeolite conversion (Run no. 5) and (B) SSZ-13 (Run no. 8). (●) before and (○) after  $\text{H}_2\text{SO}_4$  treatment.

relative crystallinity occurred upon acid treatment, indicating reduced acid stability. The above results indicate that the CHA-type zeolite obtained by the interzeolite conversion of FAU-type zeolite exhibits higher acid stability than SSZ-13.

In the previous study, I found that a dealumination rate of MFI-type zeolite with a

large number of silanol groups (structure defects) is larger than that of zeolite with small defects [33]. To clarify an influence of structure defects on the acid stability, therefore, the chemical states of the silicon in obtained CHA-type zeolites synthesized by interzeolite conversion and SSZ-13 were investigated by  $^{29}\text{Si}$  MAS NMR both with and without  $^1\text{H}$ - $^{29}\text{Si}$  cross polarization (CP). Fig. 4-13A shows  $^{29}\text{Si}$  MAS NMR spectra of CHA-type zeolite and SSZ-13. Three peaks were observed centered at ca.  $-110$ ,  $-105$ , and  $-100$  ppm, and they are probably assigned to  $\text{Q}^4(0\text{Al})$ ,  $\text{Q}^4(1\text{Al})$ , and  $\text{Q}^4(2\text{Al}) + \text{Q}^3(0\text{Al})$ , respectively [29,34]. In the CP spectrum (Fig. 4-13B), the peak intensity at ca.  $-100$  ppm was enhanced. The degree of enhancement in the CP spectrum of SSZ-13 was relatively larger than that in the CP spectrum of CHA-type zeolite. This strongly indicates a large amount of connectivity defects in the zeolite framework of SSZ-13, resulting in lower acid stability. However, I could not rule out the following possibility. As the CHA-type zeolite is formed by the reassembly of locally ordered aluminosilicate species (nanoparts) generated by decomposition/dissolution of the starting FAU-type zeolite, the stabilization of framework aluminum in the nanoparts takes place through dealumination and realumination during the crystallization process.

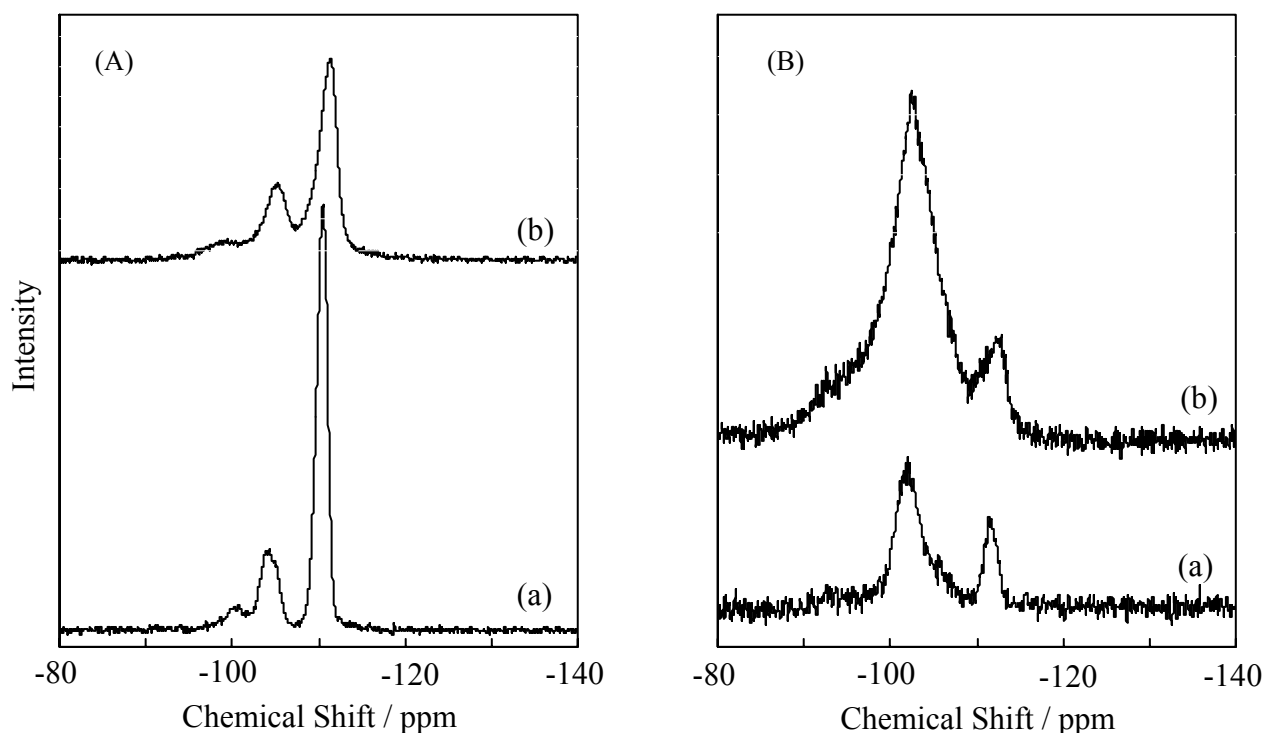


Fig. 4-13 (A)  $^{29}\text{Si}$  MAS and (B)  $^{29}\text{Si}$  CP/MAS NMR spectra of CHA-type zeolites with Si/Al ratio of 15. (a) CHA-type zeolite synthesized by interzeolite conversion, (b) SSZ-13.

### 3.4 Membrane performance

The XRD pattern of the CHA-type zeolite membrane prepared on the porous  $\alpha$ -alumina tube using secondary growth techniques, consisting of deposition of seed crystals on the support followed by crystal growth under the interzeolite conversion condition, is shown in Fig. 14. In addition to the diffraction peaks corresponding to the  $\alpha$ -alumina support, only typical CHA peaks were observed. Fig. 4-15 shows the SEM images of the outer surface and cross section of CHA-type zeolite membrane. The membrane surface was covered with small crystals of a size less than 1  $\mu\text{m}$ . The thickness of the membranes was ca. 2  $\mu\text{m}$ . To analyze the surface Si/Al ratio of the membrane, the zeolite layer was carefully detached from the alumina support by the mechanical method. The surface Si/Al ratio determined by EDX was 16–20, indicating the

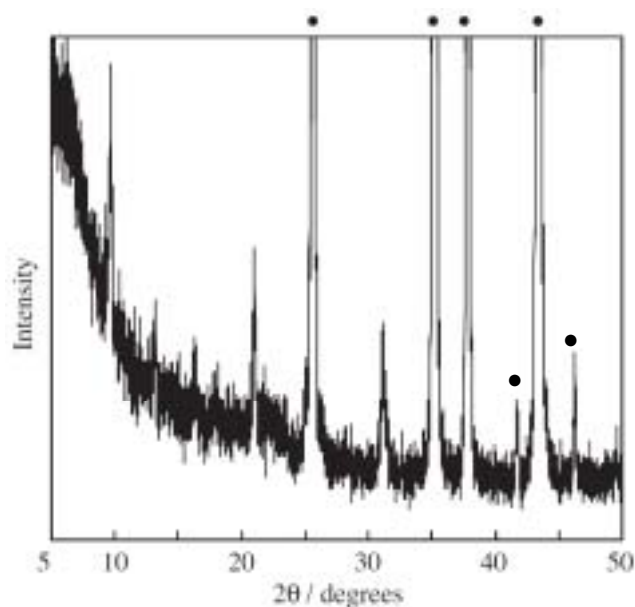


Fig. 4-14 XRD pattern of CHA-type zeolite membrane prepared on a porous  $\alpha$ -alumina tube by interzeolite conversion of FAU-type zeolite (●:  $\alpha$ -alumina substrate).

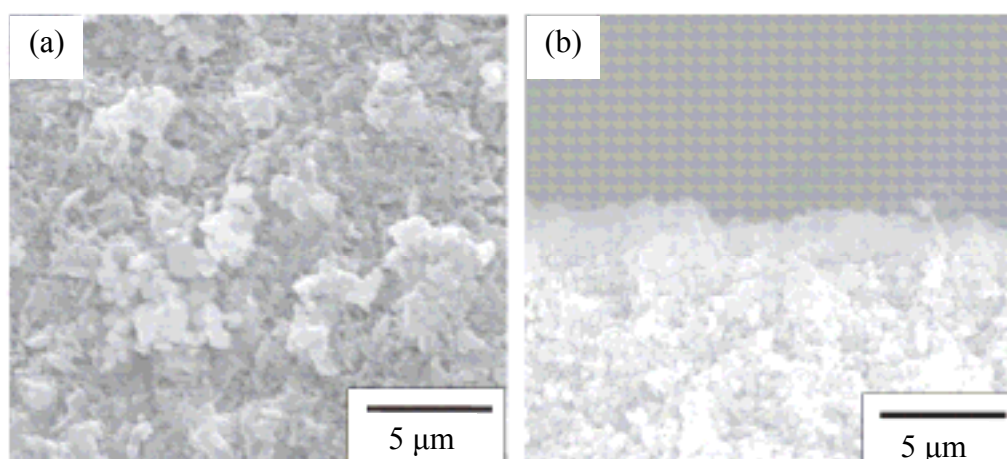


Fig. 4-15 SEM images of the (a) outer surface and (b) cross section of CHA-type zeolite membrane.

formation of a high-silica CHA-type zeolite membrane on the alumina support. The pervaporation performance of the high-silica CHA-type zeolite membrane was evaluated by the dehydration of 50 wt% acetic acid aqueous solution at 75 °C. The permeate flux and separation factor,  $\alpha(\text{H}_2\text{O}/\text{CH}_3\text{COOH})$ , were  $7.9 \text{ kg m}^{-2} \text{ h}^{-1}$  and ca. 2500, respectively, and the membrane performance was identical to that of commercially available NaA-type zeolite membranes used for the dehydration of

alcohol solution [35]. The leak acetic acid concentration was ca. 0.04 wt%. The membrane performance was the highest among the zeolite membranes researched by the authors, such as MFI-, MOR-, T-, and MCM-22-type zeolite membranes previously reported [36–40]. No change in the pervaporation performance was observed in the time-courses of both the flux and the separation factor, indicating the high acetic acid stability of the CHA-type zeolite membrane.

#### 4. Conclusion

High-silica CHA-type zeolite was synthesized by interzeolite conversion method in the presence of BTMAOH. This is the first high-silica CHA-type zeolite synthesized with a SDA other than TMA<sup>+</sup> cation. The CHA-type zeolite was not obtained using amorphous materials. This seems to be due to an existence of locally ordered aluminosilicate species formed by decomposition or dissolution of zeolite. By adding seed crystals, CHA-type zeolites with a wide range of Si/Al ratios (13.4–21.5) were obtained with shorter crystallization time. I also achieved the first successful synthesis of high-silica CHA-type zeolite in the absence of Na<sup>+</sup> cations by using a higher content of seed crystals, indicating that no H<sup>+</sup> ion-exchange process is required for the use of a solid acid catalyst. The protonated CHA-type zeolite exhibited good performance in relation to the conversion of ethanol to light olefins. A maximum propylene yield of ca. 48 C-% was achieved at the Si/Al ratio of ca. 15. Furthermore, high acid stability towards several acids, such as acetic acid, HCl, H<sub>2</sub>SO<sub>4</sub>, and HNO<sub>3</sub>, was confirmed. The acid stability of CHA-type zeolite was higher than that of SSZ-13. The CHA-type zeolite membrane prepared on the porous  $\alpha$ -alumina tube demonstrated the excellent

pervaporation performance for dehydration of water/acetic acid (50/50 wt%) at 75 °C. The membrane showed a high separation factor,  $\alpha(\text{H}_2\text{O}/\text{CH}_3\text{COOH})$ , of ca. 2500 with a permeate flux of ca.  $8 \text{ kg m}^{-2} \text{ h}^{-1}$ . These indicate the potential for the effective future application of CHA-type zeolite membrane synthesized by interzeolite conversion methods

## References

- [1] M. Stöcker, *Micropor. Mesopor. Mater.* 29 (1999) 3.
- [2] J.Q. Chen, A. Bozzano, B. Glover, T. Fuglerud, S. Kvisle, *Catal. Today* 106 (2005) 103.
- [3] Q. Zhu, J.N. Kondo, T. Tatsumi, S. Inagaki, R. Ohnuma, Y. Kubota, Y. Shimodaira, H. Kobayashi, K. Domen, *J. Phys. Chem. C* 111 (2007) 5409.
- [4] H. Oikawa, Y. Shibata, K. Inazu, Y. Iwase, K. Murai, S. Hyodo, G. Kobayashi, T. Baba, *Appl. Catal. A* 312 (2006) 181.
- [5] M. Yamaguchi, Y. Yoshikawa, T. Takewaki, R. Setoyama, *Jpn. Kokai Tokkyo Koho* 291076 (2007).
- [6] M.J. Díaz-Cabañas, P.A. Barrett, M.A. Cambor, *Chem. Commun.* 17 (1998) 1881.
- [7] S.I. Zones, US Patent 4544,538 (1985)
- [8] H. Kalipcilar, T.C. Bowen, R.D. Noble, J.L. Falconer, *Chem. Mater.* 14 (2002) 3458.
- [9] Y. Hasegawa, H. Hotta, K. Sato, T. Nagase, F. Mizukami, *J. Membr. Sci.* 347 (2010) 193.
- [10] Y. Hasegawa, C. Abe, M. Nishioka, K. Sato, T. Nagase, T. Hanaoka, *J. Membr. Sci.* 363 (2010) 256; 364 (2010) 318.
- [11] S.I. Zones, *J. Chem. Soc. Faraday Trans.* 87 (1991) 3709.
- [12] Y. Kubota, H. Maekawa, S. Miyata, T. Tatsumi, Y. Sugi, *Micropor. Mesopor. Mater.* 101 (2007) 115.
- [13] G.T. Kerr, *J. Phys. Chem.* 70 (1966) 1047.
- [14] G.T. Kerr, *J. Phys. Chem.* 72 (1968) 1385.
- [15] J. Warzywoda, R.W. Thompson, *Zeolites* 11 (1991) 577.

- [16] B. Lu, T. Tsuda, Y. Oumi, K. Itabashi, T. Sano, *Micropor. Mesopor. Mater.* 76 (2004) 1.
- [17] C.S. Cundy, P.A. Cox, *Micropor. Mesopor. Mater.* 82 (2005) 1.
- [18] C.S. Cundy, J.O. Forrest, *Surf. Sci. Catal.* 135 (2001) 185.
- [19] K. Nishi, R.W. Thompson, in: K. Schüth, S.W. Sing, J. Weitkamp (Eds.), *Handbook of Porous Solids*, vol. 2, WILEY-VCH, Germany, 2002, p. 736.
- [20] H. Jon, K. Nakahata, B. Lu, Y. Oumi, T. Sano, *Micropor. Mesopor. Mater.* 96 (2006) 72.
- [21] H. Jon, S. Takahashi, H. Sasaki, Y. Oumi, T. Sano, *Micropor. Mesopor. Mater.* 113 (2008) 56.
- [22] H. Jon, N. Ikawa, Y. Oumi, T. Sano, *Chem. Mater.* 20 (2008) 4135.
- [23] H. Sasaki, H. Jon, M. Itakura, T. Inoue, T. Ikeda, Y. Oumi, T. Sano, *J. Porous Mater.* 16 (2009) 465.
- [24] H. Robson (Eds.), *Verified Syntheses of Zeolitic Materials*, Elsevier, 2001, p. 123.
- [25] Q. Zhu, J.N. Kondo, R. Ohmura, Y. Kubota, M. Yamaguchi, T. Tatsumi, *Micropor. Mesopor. Mater.* 112 (2008) 153.
- [26] H. Robson, K.P. Lillerud, *Verified Syntheses of Zeolitic Materials*, second ed., Elsevier, Amsterdam, 2001. p. 123.
- [27] S.I. Zones, R. A. van Nordstand, *Zeolites* 8 (1988) 166.
- [28] D.E. Akporiaye, I.M. Dahl, H.B. Mostad, R. Wendelbo, *J. Phys. Chem.* 100 (1996) 4148.
- [29] M.A. Camblor, A. Corma, M.-J. Díaz-Cabañas, *J. Phys. Chem. B* 102 (1998) 44.
- [30] G.L. Wooley, L.B. Alernany, R.M. Dessau, A.W. Chester, *Zeolites* 6 (1986) 14.
- [31] Y. Iwase, K. Motokura, T. Koyama, A. Miyaji, T. Baba, *Phys. Chem. Chem. Phys.*

11 (2009) 9268.

[32] T. Ida, Jpn. Kokai Tokkyo Koho 7-53209, 1995.

[33] T. Sano, H. Ikeya, T. Kasuno, Z.B. Wang, Y. Kawakami, K. Soga, *Zeolites* 19 (1997) 80.

[34] D.E. Akporiaye, I.M. Dahl, H.B. Mostad, R. Wendelbo, *J. Phys. Chem.* 100 (1996) 4148.

[35] K. Sato, K. Sugimoto, T. Nakane, *J. Membr. Sci.* 307 (2008) 181.

[36] G. Li, E. Kikuchi, M. Matsukata, *J. Membr. Sci.* 218 (2003) 185.

[37] G. Li, E. Kikuchi, M. Matsukata, *Sep. Purif. Technol.* 32 (2003) 199.

[38] Y. Cui, H. Kita, K. Okamoto, *J. Membr. Sci.* 236 (2004) 17.

[39] K. Sato, K. Sugimoto, T. Kyotani, N. Shimotsuma, T. Kurata, *J. Membr. Sci.* 385 (2011) 20.

[40] K. Makita, Y. Hirota, Y. Egashira, K. Yoshida, Y. Sasaki, N. Nishiyama, *J. Membr. Sci.* 372 (2011) 269.

## Chapter 5

### Synthesis of high-silica OFF-type zeolite by the interzeolite conversion method

#### 1. Introduction

Zeolite is a class of microporous crystalline aluminosilicate, which has been widely used in adsorption, catalysis and ion-exchange applications [1–3]. These applications are based on their unique properties such as solid acidity, high internal surface and molecular sieving.

The framework structure of offretite (OFF) and erionite (ERI) are closely related. Their distinction between OFF- and ERI-type zeolites is caused by stacking of cancrinite cages (composite building unit of OFF- and ERI-type zeolites). In OFF-type zeolite, cancrinite cages are regularly stacked to form columns that originate channels with 12-membered ring (12MR) windows in the c-direction as well as 8-membered ring (8MR) windows in the a-direction. By contrast, in ERI-type zeolite, cancrinite cages are alternately rotated by  $60^\circ$  giving only 8MR windows in the a-direction. Therefore, stacking faults or intergrowth of these two zeolites are very common, such as zeolite T and ZSM-34 [4,5]. As it is known that the catalytic performances such as methanol conversion, dewaxing and oligomerization are strongly affected by the distribution of ERI within the crystals and the framework Si/Al ratio [6–8], a lot of efforts concerning the synthesis of OFF-type zeolite have still been made by several researchers [9–11].

Although the degree of intergrowth of OFF- and ERI-type zeolites can be achieved by changing the organic structure-directing agent (SDA), there are few reports concerning the synthesis of pure OFF-type zeolite [12]. Moreover, the synthesis commonly requires prolonged crystallization time as well as both cations of sodium and potassium, and the framework Si/Al ratio is not so high (3–5).

Generally, zeolite is synthesized using an amorphous aluminosilicate gel as a starting material in the presence of organic or inorganic SDA. However, the formation of a zeolite phase is preceded with another phase as an intermediate during the course of zeolite crystallization [13]. As this phenomenon can be considered to be an alternative synthesis strategy for the hydrothermal conversion of one zeolite into another, i.e., interzeolite conversion, this method has attracted much attention. Subotić et al. synthesized P-type zeolite (GIS) and sodalite (SOD) using A-type zeolite (LTA) as a starting material [14–16]. Zones et al. reported the conversion of various zeolites, for instance Y-type zeolite (FAU) to SSZ-13; B-\*BEA to B-SSZ-24, B-SSZ-31 and B-SSZ-33; Al-\*BEA to Al-SSZ-24 and Al-SSZ-31 in the presence of adamantammonium cation and its derivatives [17–19]. Kubota et al. also succeeded in the interconversion of Al-\*BEA and Ti-\*BEA into Al-SSZ-31 and Ti-SSZ-24, respectively [20,21].

Jon et al. have also investigated the potential of the interzeolite conversion method. In the hydrothermal conversion of FAU-type zeolite into \*BEA-type zeolite, it was found that when tetraethylammonium hydroxide (TEAOH) is employed as an alkali source, the use of FAU-type zeolite as a starting material shows the enhanced crystallization rate of \*BEA-type zeolite as compared to amorphous silica/alumina [22]. It was also indicated from the recent results that the enhancement in the crystallization rate of

\*BEA-type zeolite is due to the locally ordered aluminosilicate species (nanoparts) produced by decomposition/dissolution of FAU-type zeolite [23]. Namely, their assembly under a specific SDA gives rise to a fast crystallization rate and a high selectivity to a particular zeolite. These results led us to the hypothesis that the structure of nanoparts produced is alterable by changing a kind of SDA. The hydrothermal conversion of FAU-type zeolite was carried out with a variety of SDAs. Consequently, the highly crystalline RUT-, MTN-, CHA- and LEV-type zeolites other than \*BEA-type zeolite were obtained from FAU type-zeolite in the presence of tetramethylammonium hydroxide (TMAOH) [24], benzyltrimethylammonium hydroxide (BTMAOH) [25, 26] and choline hydroxide [27], respectively. The enhancement of crystallization rate was also observed for these zeolites.

From such viewpoints, in this work, I applied the interzeolite conversion method to OFF-type zeolite synthesis and succeeded in the synthesis of high-silica OFF-type zeolite with no or very little amount of ERI in the presence of both BTMAOH and the structure-forming alkali metal cations such as  $\text{Li}^+$  and  $\text{Na}^+$ .

## **2. Experimental**

### **2.1. Synthesis of OFF-type zeolite**

The starting FAU-type zeolites with various Si/Al ratios were prepared from  $\text{NH}_4\text{-Y}$  zeolite (Si/Al = 2.8, Tosoh Co., Japan) through dealumination treatment involving a combination of steaming at 700 °C and  $\text{H}_2\text{SO}_4$  (0.74–0.85 M) treatment at 75 °C for 4 h. The hydrothermal conversion was performed as follows. The dealuminated FAU-type zeolite was mixed well with an aqueous solution containing BTMAOH and alkali metal

hydroxide (MOH,  $M^+ = Li^+, Na^+, K^+$  and  $Rb^+$ ), and then the mixture was placed into 30 cm<sup>3</sup> Teflon-lined stainless steel autoclave. The hydrothermal conversion was conducted at 125 °C for 2 h–21 days in the convection oven. After crystallization, the solid product was collected by centrifugation and washed thoroughly with deionized water until near neutral, and then dried overnight at 70 °C. For comparison, the starting gels from amorphous silica powder produced by wet process ( $SiO_2 = 88$  wt%,  $Al_2O_3 = 0.27$  wt%, Nipsil, Nippon Silica Ind. Japan) and  $\gamma$ - $Al_2O_3$  (JGC Catalysts and Chemicals Ltd. Japan) or  $Al(OH)_3$  (Wako Pure Chemical Ind., Ltd. Japan) as other Si and Al sources respectively were also prepared. The detailed hydrothermal conversion conditions are listed in Table 5-1.

## 2.2 Characterization

The powder X-ray diffraction (XRD) patterns of the solid products were collected on a Rigaku Mini Flex diffractometer with curved-graphite monochromatized Cu  $K\alpha$  radiation operated at 30 kV and 15 mA. Si/Al ratios were determined by X-ray fluorescence (XRF, Philips PW 2400). 0.5 g of sample was fused with 5 g of dilithium tetraborate ( $Li_2B_4O_7$ ) at 1100 °C. The Si/Al ratio was calculated from Si and Al concentrations determined by the corresponding calibration curves. The crystal morphology was observed using scanning electron microscopy (SEM, JEOL JSM-6320FS). Micropore volume and surface area were determined by nitrogen physisorption using the t-plot and Brunauer–Emmett–Teller (BET) methods, respectively. Nitrogen adsorption isotherms at  $-196$  °C were performed using a conventional volumetric apparatus (Bel Japan, BELSORP 28SA). Benzene adsorption was also measured using a conventional volumetric apparatus (Bel Japan, BELSORP 18)

at 25 °C. Prior to adsorption measurements, the calcined samples (ca. 0.1 g) were evacuated at 400 °C for 10 h.  $^{13}\text{C}$  CP/MAS NMR,  $^{27}\text{Al}$  MAS NMR and  $^{29}\text{Si}$  MAS NMR spectra were recorded using a 7 mm diameter zirconia rotor on Bruker Advance DRX-400 at 100.6 MHz, 104.3 MHz and 79.5 MHz, respectively. The rotor was spun at 6 kHz for  $^{13}\text{C}$  CP/MAS NMR, 9 kHz for  $^{27}\text{Al}$  MAS NMR and 4 kHz for  $^{29}\text{Si}$  MAS NMR. The spectra were accumulated with 6.0  $\mu\text{s}$  pulses, 25 s recycle delay and 1000 scans for  $^{13}\text{C}$  CP/MAS NMR, 2.3  $\mu\text{s}$ , 1 s and 4000 scans for  $^{27}\text{Al}$  MAS NMR and 5  $\mu\text{s}$ , 20 s and 2000 scans for  $^{29}\text{Si}$  MAS NMR. Glycine ( $\text{H}_2\text{NCH}_2\text{COOH}$ ),  $\text{Al}(\text{NO}_3)_3 \cdot 9\text{H}_2\text{O}$  and  $\text{Si}(\text{CH}_3)_4$  were used as chemical shift references for  $^{13}\text{C}$  CP/MAS NMR,  $^{27}\text{Al}$  MAS NMR and  $^{29}\text{Si}$  MAS NMR, respectively. Prior to  $^{27}\text{Al}$  MAS NMR measurement, the sample was moisture-equilibrated over a saturated solution of  $\text{NH}_4\text{Cl}$  for 24 h. The thermal analysis was carried out using a TG/DTA apparatus (SSC/5200 Seiko Instruments). The sample ca. 7 mg was heated in a flow of air ( $50 \text{ mL min}^{-1}$ ) at a heating rate of  $3 \text{ }^\circ\text{C min}^{-1}$  from room temperature to 800 °C.

### 3. Results and Discussion

At first, the interconversion of FAU-type zeolite was tried using several quaternary ammonium cations, which are employed as SDAs in the conventional hydrothermal synthesis of OFF-type zeolite. In the case of no addition of alkali metal cations, only BTMA cations yielded an OFF-type zeolite. However, the coexistence of CHA-type zeolite was observed (Table 5-1, sample no. 1). When a small amount of alkali metal hydroxide (LiOH or NaOH/ $\text{SiO}_2$  ratio of 0.05) was added to the mixture, an OFF-type zeolite was obtained only after 1 day of crystallization (sample no. 2, 3), indicating a

Table 5-1 Hydrothermal synthesis conditions and products obtained<sup>a</sup>

Sample no.	Synthesis conditions				Product (by-product)	
	Si/Al of FAU	MOH/SiO <sub>2</sub>	M <sup>+</sup>	Time/days	Phase	Bulk Si/Al
1	25	0		14	OFF (CHA)	
2	23	0.05	Na	1	OFF	
3	23	0.05	Li	1	OFF	
4	23	0.05	K	14	OFF	
5	23	0.05	Rb	14	OFF	
6	23	0.05	Na	14	OFF	7.6
7	12	0.05	Na	14	FAU	
8	16	0.05	Na	1	OFF (FAU)	
9	16	0.05	Na	14	OFF	
10	31	0.05	Na	1	OFF	8.0
11	45	0.05	Na	14	Am. <sup>b</sup>	
12 <sup>c</sup>	23	0.05	Na	14	Am. <sup>b</sup>	
13 <sup>d</sup>	23	0.05	Na	14	Am. <sup>b</sup>	

<sup>a</sup> BTMAOH/SiO<sub>2</sub> = 0.4, H<sub>2</sub>O/SiO<sub>2</sub> = 5.5, Temp.: 125 °C.

<sup>b</sup> Am.: Amorphous.

<sup>c</sup> SiO<sub>2</sub> and  $\gamma$ -Al<sub>2</sub>O<sub>3</sub> were used as Si and Al source, respectively.

<sup>d</sup> SiO<sub>2</sub> and Al(OH)<sub>3</sub> were used as Si and Al sources, respectively.

fast crystallization rate as compared to the conventional hydrothermal synthesis using amorphous starting materials. No other phases were observed during the course of crystallization even after 14 days (sample no. 6). Fig. 5-1 (b) and (c) show XRD patterns of the as-synthesized OFF-type zeolites. This indicates that under these hydrothermal conditions, the OFF-type zeolite is a stable phase. There is no detectable amount of ERI intergrowth in the product [28], suggesting strongly no or very little amount of ERI-type zeolite. When KOH was employed instead of NaOH or LiOH, the further crystallization time was needed (sample no. 4). On the other hand, in the case of RbOH, only a very small amount of OFF-type zeolite was obtained (sample no. 5). These results seem to suggest that smaller cations such as Na<sup>+</sup> and Li<sup>+</sup> act as structure-forming cation, whereas larger alkali metal cations such as K<sup>+</sup> and Rb<sup>+</sup> act as structure-breaking cation [29].

My previous results concerning the interzeolite conversion showed that the

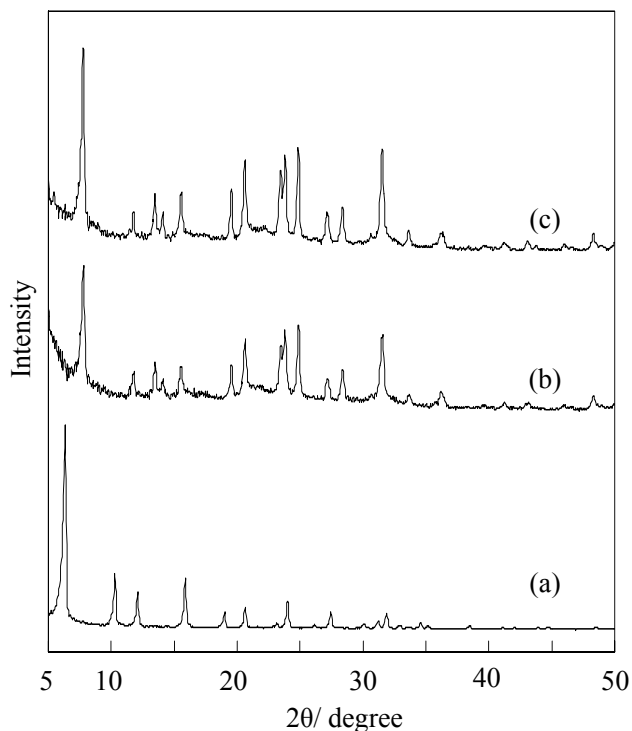


Fig. 5-1 XRD patterns of the OFF-type zeolites obtained from FAU type zeolite with Si/Al ratio of 23. (a) used sample of FAU type zeolite, and the products obtained during the hydrothermal treatment of FAU type zeolite for 1 day (b) and 14 days (c).

conversion strongly depended on the Si/Al ratio of the starting FAU-type zeolite [22,24–27]. In order to investigate the influence of Si/Al ratio of the starting FAU-type zeolite on OFF-type zeolite synthesis, FAU-type zeolites with various Si/Al ratios of 12–45 were prepared by the dealumination treatment and subjected to the hydrothermal treatment. The hydrothermal conditions are listed in Table 5-1. It is obvious that only FAU-type zeolites with Si/Al ratios of 23–31 could be converted into OFF-type zeolites in one day, indicating a very narrow synthesis region. Under this hydrothermal condition, FAU-type zeolite with Si/Al ratio of 12 was not decomposed (sample no. 7). In the case of FAU-type zeolite with a Si/Al ratio of 16, the prolonged crystallization time was required (sample nos. 8 and 9), while in the case of a Si/Al ratio of 45, only

amorphous phase was detected even after 14 days of crystallization (sample no. 11). For comparison, I attempted to synthesize the OFF-type zeolite from amorphous  $\text{SiO}_2/\gamma\text{-Al}_2\text{O}_3$  (sample no. 12) and amorphous  $\text{SiO}_2/\text{Al}(\text{OH})_3$  (sample no. 13). However, OFF-type zeolite was not obtained, demonstrating the advantage and uniqueness of the hydrothermal conversion of FAU-type zeolite.

Fig. 5-2 shows SEM images of OFF-type zeolites obtained from FAU-type zeolites with various Si/Al ratios. After through observation, I did not find any crystals of the starting FAU and impurities. Only crystals of OFF-type zeolite with spherical shape were observed. The average diameter of the crystals was ca. 100 nm. As there was no difference in the crystal morphology between sample no. 2 (1 day of crystallization time) and sample no. 6 (14 days), it was confirmed that OFF-type zeolite is a stable

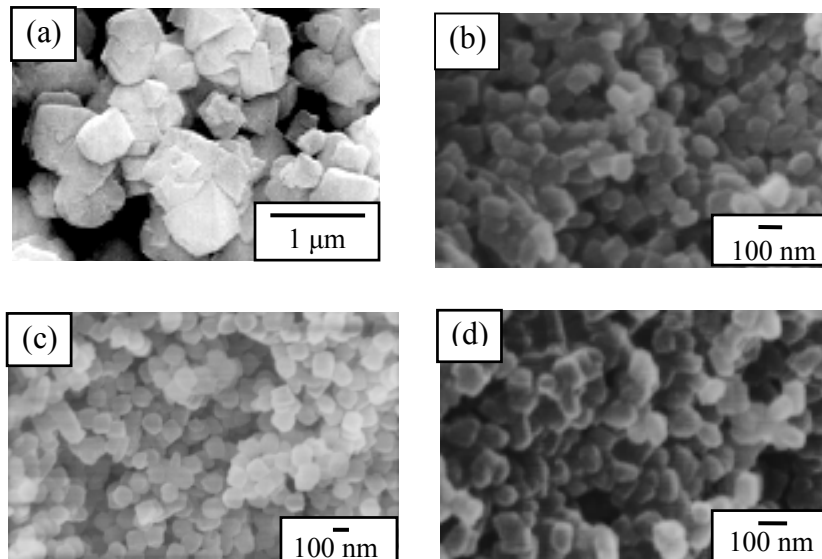


Fig. 5-2 SEM images of FAU-type zeolite and as-synthesized OFF-type zeolites. (a) starting FAU-type zeolite with Si/Al ratio of 23, OFF-type zeolites obtained during the hydrothermal treatment of FAU-type zeolite with Si/Al ratio of 23 for 1 day (b), for 14 days (c), and (d) OFF-type zeolite obtained during the hydrothermal treatment of FAU-type zeolite with Si/Al ratio of 31 for 14 days.

phase under the present hydrothermal condition. The bulk Si/Al ratio of OFF-type zeolite determined by XRF was 7.6–8.0, which is lower than that of the starting FAU-type zeolite. However, the values were considerably higher than those of zeolite T (Si/Al = 2.3–3.2) and ZSM-34 (Si/Al = 3.8–4), indicating the formation of high-silica OFF-type zeolite.

The characteristics of organic molecules occluded in the zeolitic pores of OFF-type zeolite were characterized by  $^{13}\text{C}$  CP/MAS NMR spectroscopy and thermal analysis. As can be seen in Fig. 5-3, the  $^{13}\text{C}$  CP/MAS NMR spectrum consists of three resonances centered at ca. 53, 72 and 130 ppm, which are assigned to the methyl carbon, methylene carbon and phenyl carbon of BTMA cation, respectively. The weak resonance was also observed at ca. 56 ppm, which corresponds to methyl carbon of tetramethylammonium cation. This implies that decomposition of small amount of BTMA cation occurred. Therefore, most of BTMA cation was the only organic species existing in OFF-type zeolite pores. From the TG/DTA curves, the amount of BTMA cation was calculated to be ca. 13 wt%.

Next, to clarify the structural features of the OFF-type zeolite synthesized by the present method, adsorption measurements with nitrogen and benzene molecules were carried out. As it has already been recognized that a relatively little amount of stacking faults can effectively block the 12MR windows in OFF structure, I can get information concerning the degree of stacking faults within the crystals based on nitrogen and benzene adsorption behaviors. Fig. 5-4 shows the nitrogen and benzene adsorption isotherms of the OFF-type zeolite calcined at 450 °C for 2 days. The nitrogen adsorption isotherm showed I type. The BET surface area and micropore volume calculated were  $670 \text{ m}^2\text{g}^{-1}$  and  $0.23 \text{ cm}^3\text{g}^{-1}$ , respectively. The benzene adsorption

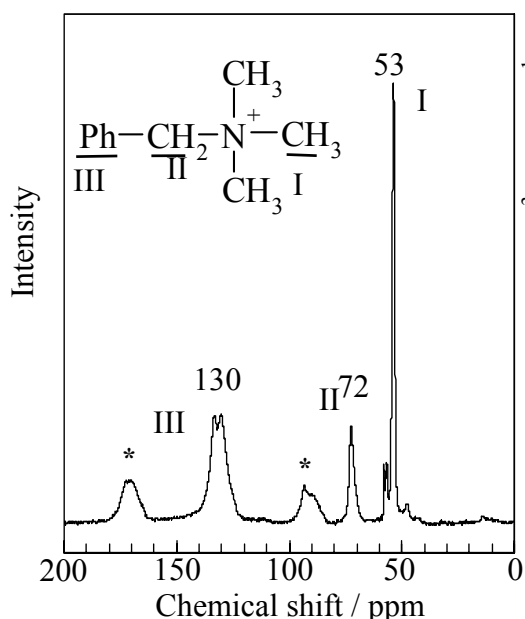


Fig. 5-3  $^{13}\text{C}$  CP/MAS NMR spectrum of OFF-type zeolite (sample no. 6). Asterisks denote spinning sidebands (SSB).

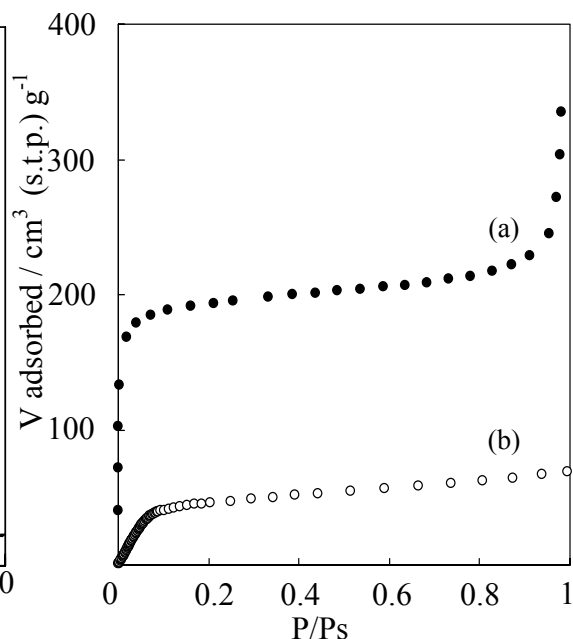


Fig. 5-4 (a) Nitrogen and (b) benzene adsorption isotherms of calcined OFF-type zeolite (sample no. 6).

isotherm also exhibited I type behavior. Since the molecular size of benzene is larger than 8MR windows, it can adsorb only in the pores with 12MR windows of OFF structure. The pore volume estimated from the amount of benzene adsorbed was  $0.16 \text{ cm}^3 \text{ g}^{-1}$ , if it is assumed that the density of benzene adsorbed in the pores is equal to that of liquid benzene ( $0.879 \text{ g/cm}^3$ ). This value is approximately 70% of total micropore volume calculated from nitrogen adsorption isotherm. Take into account that other offretites, Linde type T (ERI 30%) and TMA-offretite (ERI 10%), suggested low benzene adsorption  $0.00124$  and  $0.045 \text{ cm}^3 \text{ g}^{-1}$ , respectively [4,30], indicating strongly the existence of no or very little amount of stacking faults of ERI within the OFF-type zeolite crystals obtained.

The chemical states of aluminum and silicon in the obtained OFF-type zeolite were investigated by  $^{27}\text{Al}$  and  $^{29}\text{Si}$  MAS NMR. The  $^{27}\text{Al}$  MAS NMR spectrum of the as-synthesized OFF-type zeolite is shown in Fig. 5-5. It is clear that only one resonance

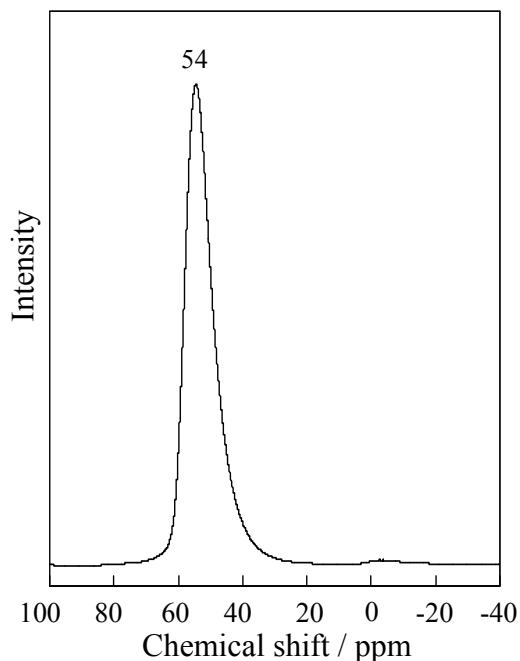


Fig. 5-5  $^{27}\text{Al}$  MAS NMR spectrum of as-synthesized OFF-type zeolite (sample no. 6).

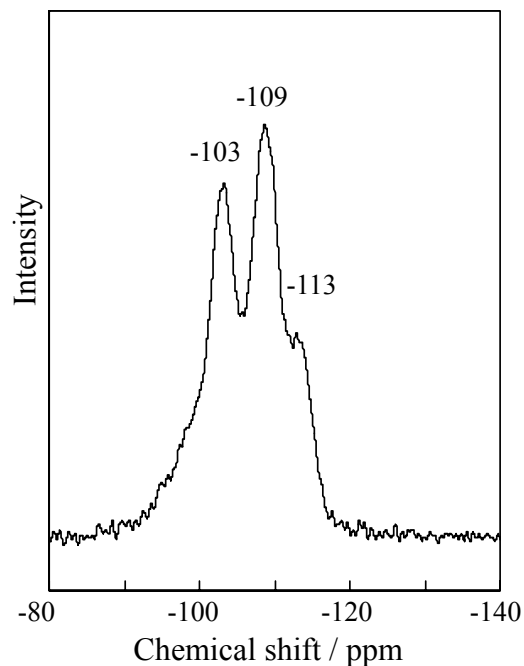


Fig. 5-6  $^{29}\text{Si}$  MAS NMR spectrum of as-synthesized OFF-type zeolite (sample no. 6).

centered at ca. 54 ppm was observed, while resonance corresponding to octahedrally coordinated aluminum species, namely extraframework aluminum species, around 0 ppm was not observed. This means that all of aluminum species present in OFF-type zeolite obtained from the hydrothermal conversion of FAU-type zeolite exist within the zeolitic framework. The  $^{29}\text{Si}$  MAS NMR spectrum of the as-synthesized OFF-type zeolite is also shown in Fig. 5-6. The spectrum consists of at least three resonances at ca. -103, -109 and -113 ppm. The OFF structure contains two crystallographically different tetrahedrally sites ( $T_1$  and  $T_2$ ). Therefore, the NMR resonance at -113 ppm is assigned to Si(0Al) configuration of the  $T_2$  site. According to the literature [31], the other NMR resonances could be interpreted as follows: -103 ppm (Si(1Al) $_{T_1}$  & Si(2Al) $_{T_2}$ ), -109 ppm (Si(0Al) $_{T_1}$  & Si(1Al) $_{T_2}$ ).

From above results, I estimated conversion process of FAU-CHA and FAU-OFF

interzeolite conversion in Fig. 5-7. Taking into account CHA- and OFF-type zeolites were not obtained from amorphous materials, nanoparts was produced by decomposition/dissolution of FAU-type zeolite. During the FAU–OFF interzeolite conversion process, decomposition of FAU-type zeolite proceeds more than the FAU–CHA interzeolite conversion process due to high alkalinity. As a consequence, different types of zeolites were obtained.

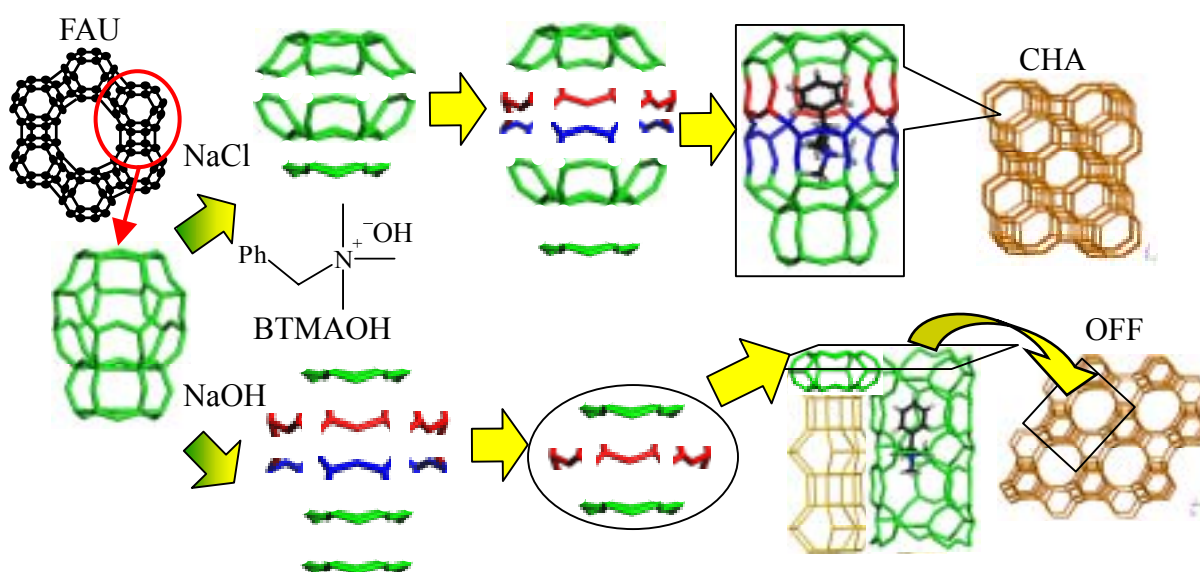


Fig. 5-7 Conversion processes of FAU–CHA and FAU–OFF interzeolite conversions.

#### 4. Conclusion

Hydrothermal conversion parameters influencing the conversion of FAU-type zeolite into OFF-type zeolite were investigated in detail. The hydrothermal conversion of FAU-type zeolite into OFF-type zeolite effectively proceeded in the presence of both BTMAOH and the structure-forming alkali metal cations such as  $\text{Li}^+$  and  $\text{Na}^+$ , and strongly depended on the Si/Al ratio of the starting FAU-type zeolite. Only the FAU-type zeolites with Si/Al of 23–31 were converted into OFF-type zeolites in one

day. As confirmed by  $^{13}\text{C}$  CP/MAS NMR spectrum, almost all of BTMA cations existed intact in zeolitic pores. In addition, benzene adsorption measurements showed that there is no or very little amount of stacking faults of ERI within the crystals, suggesting a high potential of the OFF-type zeolite for several catalytic reactions.

**References**

- [1] T. Maeson, *Stud. Surf. Sci. Catal.* 168 (2007) 1.
- [2] M. Stöcker, *Micropor. Mesopor. Mater.* 82 (2005) 257.
- [3] J.A. Rabo, M.W. Schoonover, *Appl. Catal. A* 222 (2001) 61.
- [4] D.W. Breck, N.A. Acara, U.S. Pat. 2,950,952 (1960).
- [5] E.N. Gives, C.J. Plank, E.J. Rosinski, U.S.Pat. 4,079,095 (1978).
- [6] N.Y. Chen, W.E. Garwood, J.L. Schlenker, G.T. Kokotailo, *J. Catal.* 86 (1984) 24.
- [7] M.L. Occelli, J.T. Hsu, L.G. Galya, *J. Mol. Catal.* 32 (1985) 377.
- [8] E.N. Gives, E.J. Rosinski, JP-53-58499 (1978).
- [9] A. Auroux, M.L. Occelli, *Stud. Surf. Sci. Catal.* 84A (1994) 693.
- [10] S. Yang, N.P. Evmiridis, *Micropor. Mater.* 6 (1996) 19.
- [11] J.C. Vartuli, G.J. Kennedy, B.A. Yoon, A. Malek, *Micropor. Mesopor. Mater.* 38 (2000) 247.
- [12] R. Aiello, R.M. Barrer, J.A. Davies, I.S. Kerr, *Trans. Faraday Soc.* 66 (1970) 1610.
- [13] C.S. Cundy, P.A. Cox, *Micropor. Mesopor. Mater.* 82 (2005) 1.
- [14] B. Subotić, D. Škrtić, I. Šmit, L. Sekovanić, *J. Cryst. Growth* 50 (1980) 498.
- [15] B. Subotić, L. Sekovanić, *J. Cryst. Growth* 75 (1986) 561.
- [16] B. Subotić, I. Šmit, O. Madžija, L. Sekovanić, *Zeolites* 2 (1982) 135.
- [17] S.I. Zones, *J. Chem. Soc. Faraday Trans.* 87 (1991) 3709.
- [18] S.I. Zones, L.T. Yuen, Y. Nakagawa, R.A. van Nordstrand, D.D. Toto, in: R. von Ballmoos, J.B. Higgins, M.M.J. Treacy (Eds.), *Proceedings of the 9<sup>th</sup> International Zeolite Conference*, Butterworth-Heinemann, Boston (1993) 163.
- [19] S.I. Zones, Y. Nakagawa, *Micropor. Mesopor. Mater.* 2 (1994) 557.

- [20] Y. Kubota, H. Maekawa, S. Miyata, T. Tatsumi, Y. Sugi, *Micropor. Mesopor. Mater.* 101 (2007) 115.
- [21] R.K. Ahedi, Y. Kubota, Y. Sugi, *J. Mater. Chem.* 11 (2001) 2922.
- [22] H. Jon, K. Nakahata, B. Lu, Y. Oumi, T. Sano, *Micropor. Mesopor. Mater.* 96 (2006) 72.
- [23] H. Jon, N. Ikawa, Y. Oumi, T. Sano, *Chem. Mater.* 20 (2008) 4135.
- [24] H. Jon, S. Takahashi, H. Sasaki, Y. Oumi, T. Sano, *Micropor. Mesopor. Mater.* 113 (2008) 56.
- [25] H. Sasaki, H. Jon, M. Itakura, T. Inoue, T. Ikeda, Y. Oumi, T. Sano, *J. Porous Mater.* 16 (2009) 465.
- [26] M. Itakura, T. Inoue, A. Takahashi, T. Fujitani, Y. Oumi, T. Sano, *Chem. Lett.* 39 (2008) 908.
- [27] T. Inoue, M. Itakura, H. Jon, A. Takahashi, T. Fujitani, Y. Oumi, T. Sano, *Micropor. Mesopor. Mater.* 122 (2009) 149.
- [28] M.M.J. Treacy, J.B. Higgins, *Collection of Simulated XRD Powder Patterns for Zeolites* (2007) 484.
- [29] Z. Gabelica, N. Blom, E.G. Derouane, *Appl. Catal.* 5 (1983) 227.
- [30] L.B. Sand, U.S. Pat. 4,093,699 (1978).
- [31] G. Engelhardt, D. Michel, *High Resolution Solid State NMR of Silicates and Zeolites* (1987).

## Chapter 6

### **Influence of starting zeolite on synthesis of RUT-type zeolite by interzeolite conversion method**

#### **1. Introduction**

Zeolite having solid acidity, high internal surface area, molecular sieving and ion-exchange ability is a class of microporous crystalline aluminosilicate and has been widely used in adsorption, catalysis and ion-exchange applications. If a new framework topology is accepted by the Structure Commission of the International Zeolite Association, it is given a unique framework code consisting of three capital letters. A RUT-type zeolite, designated as Nu-1 (nomenclature- unknown-1), was synthesized for the first time in 1977 by Whittam et al. in the presence of tetramethylammonium (TMA) cations that served as a structure-directing agent (SDA). The Nu-1 zeolite has a Si/Al ratio of 10–75, and its protonated form shows high activity and selectivity for xylene isomerization [1]. After this disclosure, many attempts have been made by researchers to extend this area of synthesis. Consequently, Nu-1 zeolites with boro-, gallo-, and ferro- frameworks were synthesized [2–5]. Moreover, Patarin et al. reported the synthesis of a pure aluminosilicate Nu-1 zeolite in fluoride media, and Marler et al. succeeded in the synthesis of an all-silica Nu-1 zeolite using pyrrolidine as the SDA in the presence of ammonium fluoride [6,7]. However, in general, the synthesis of RUT-type zeolites still requires a prolonged crystallization time.

Recently, I have investigated the potential of the interzeolite conversion method, which has attracted much attention as an alternative synthesis strategy for the hydrothermal conversion of one zeolite into another. Subotić et al. synthesized a P type zeolite (GIS) and sodalite (SOD) using an A type zeolite (LTA) as the starting material [8–10]. Zones et al. reported the conversion of various zeolites, for instance, a Y type zeolite (FAU) to SSZ-13; B-\*BEA to B-SSZ-24, B-SSZ-31, and B-SSZ-33; and Al-\*BEA to Al-SSZ-24 and Al-SSZ-31, in the presence of adamantammonium cations and its derivatives [11–13]. Kubota et al. also succeeded in the interconversion of Al-\*BEA and Ti-\*BEA into Al-SSZ-31 and Ti-SSZ-24, respectively [14,15]. Very recently, several interzeolite conversions of FAU- \*BEA, CHA, MTN, OFF, LEV, and RUT were succeeded using FAU-type zeolite as the starting zeolite in the presence of a variety of SDAs such as tetraethylammonium hydroxide (TEAOH), tetramethylammonium hydroxide (TMAOH), benzyltrimethylammonium hydroxide (BTMAOH), and choline hydroxide [16–21]. In the hydrothermal conversion of FAU-type zeolite, it was found that when SDA is also employed as an alkali source, the use of FAU-type zeolite as a starting material shows the enhanced crystallization rate zeolite as compared to amorphous silica/alumina, which are usually used as starting materials for the conventional zeolite synthesis. The hydrothermal conversion of FAU-type zeolites into \*BEA-type zeolites also revealed that the enhancement in the crystallization rate of \*BEA-type zeolites is due to the locally ordered aluminosilicate species (nanoparts) produced by the decomposition/dissolution of the FAU-type zeolites [22]. That is, the assembly of the nanoparts under a specific SDA gives rise to a fast crystallization rate and a high selectivity for a particular zeolite. In previous chapters, I presented the effect of SDA and synthesis condition in the interzeolite conversion

meiod, although these results led us to the hypothesis that the structure of the nanoparts produced can be altered by changing the framework structure of the starting zeolite. To test this hypothesis, in this work, I investigated the influence of the framework structure of starting zeolites on the synthesis of RUT-type zeolites by using the interzeolite conversion method. \*BEA-type zeolites as well as FAU-type zeolites were used as the starting zeolites because the Si/Al ratio of \*BEA-type zeolites can be easily controlled.

## **2. Experimental**

### **2.1 Synthesis**

The starting FAU- and \*BEA-type zeolites with various Si/Al ratios were prepared from NH<sub>4</sub>-Y zeolite (Si/Al = 2.8, Tosoh Co., Japan) and H-\*BEA zeolites (Si/Al = 15, Tosoh Co., Japan) by carrying out steaming and/or H<sub>2</sub>SO<sub>4</sub> treatments for dealumination. The hydrothermal conversion was performed as follows. The dealuminated zeolite was thoroughly mixed with an aqueous solution containing an SDA such as TMAOH, BTMAOH, or choline hydroxide, and then the mixture was placed into a 30 cm<sup>3</sup> Teflon-lined stainless steel autoclave. The hydrothermal conversion was carried out at 125–170 °C for 2 h–21 days in a convection oven. After crystallization, the solid product was collected by centrifugation and washed thoroughly with deionized water until a near neutral pH was achieved, and then dried overnight at 70 °C.

### **2.2 Characterization**

The powder X-ray diffraction (XRD) patterns of the solid products were collected on a Rigaku Mini Flex diffractometer with curved-graphite monochromatized Cu K $\alpha$

radiation operated at 30 kV and 15 mA. XRD measurement was repeated 5 times and the relative crystallinity was defined as follows:

$$\text{Relative crystallinity (\%)} = \frac{\text{Sum of intensities of peaks with reflections } (-111), (111), (-222), (022), (130), (203) \text{ and } (113) \text{ for the product obtained at different synthesis times}}{\text{Sum of intensities of peaks with reflections } (111), (111), (222), (022), (130), (203) \text{ and } (113) \text{ for the RUT type zeolite obtained at synthesis time of 4 d using FAU type zeolite with Si/Al ratio of 77}}$$

Si/Al ratios were determined by X-ray fluorescence (XRF, Philips PW 2400). In these experiments, 0.5 g of sample was fused with 5 g of dilithium tetraborate ( $\text{Li}_2\text{B}_4\text{O}_7$ ) at 1100 °C. The Si/Al ratio was calculated from the Si and Al concentrations determined by the corresponding calibration curves. The crystal morphologies were observed using scanning electron microscopy (SEM, JEOL JSM-6320FS).  $^{13}\text{C}$  CP/MAS NMR,  $^{27}\text{Al}$  MAS NMR, and  $^{29}\text{Si}$  MAS NMR spectra were recorded using a 7 mm diameter zirconia rotor on Bruker Avance DRX-400 operating at 100.6 MHz, 104.3 MHz, and 79.5 MHz, respectively. The rotor was spun at 4 kHz for  $^{13}\text{C}$  CP/MAS NMR, 6 kHz for  $^{27}\text{Al}$  MAS NMR, and 4 kHz for  $^{29}\text{Si}$  MAS NMR. The spectra were accumulated with 6.0  $\mu\text{s}$  pulses, 20 s recycle delay and 1000 scans for  $^{13}\text{C}$  CP/MAS NMR, 2.3  $\mu\text{s}$ , 1 s and 1000 scans for  $^{27}\text{Al}$  MAS NMR, and 5  $\mu\text{s}$ , 100 s and 500 scans for  $^{29}\text{Si}$  MAS NMR.  $\text{Al}(\text{NO}_3)_3 \cdot 9\text{H}_2\text{O}$  was used as a chemical shift reference for  $^{27}\text{Al}$  MAS NMR and  $\text{Si}(\text{CH}_3)_4$  was used as chemical shift references for  $^{13}\text{C}$  CP/MAS NMR and  $^{29}\text{Si}$  MAS NMR. Prior to  $^{27}\text{Al}$  MAS NMR measurement, the samples was moisture-equilibrated over a saturated solution of  $\text{NH}_4\text{Cl}$  for 24 h. Thermal analyses were carried out using a TG/DTA apparatus (SSC/5200 Seiko Instruments). A sample (ca. 7 mg) was heated in a flow of air (50 mL  $\text{min}^{-1}$ ) at a heating rate of 10 °C  $\text{min}^{-1}$  from room temperature to 800 °C.

### 3. Results and discussion

First, in order to investigate the potential of interzeolite conversion of \*BEA-type zeolites into RUT-type zeolites, I attempted the hydrothermal conversion of \*BEA-type zeolites using TMAOH, BTMAOH, and choline hydroxide, which were previously reported to be effective for interzeolite conversion of FAU-type zeolites [16–21]. The synthesis conditions and products obtained are listed in Table 6-1. For comparison, the results of the interzeolite conversion of FAU-type zeolites into RUT-type zeolites are also listed. When BTMAOH and choline hydroxide were employed as SDAs in the absence and presence of additives such as NaOH and NaCl, the hydrothermal conversion of \*BEA-type zeolites did not proceed at all, indicating that \*BEA-type zeolites are more stable than an FAU-type zeolites under the present hydrothermal conversion conditions. On the other hand, when TMAOH was employed as a SDA, decomposition and dissolution of the \*BEA-type zeolites were observed. When \*BEA-type zeolites with high Si/Al ratios were tested, the hydrothermal conversion of \*BEA-type zeolites into RUT-type zeolites occurred at 170 °C (Sample nos. 8–10). Therefore, the influence of the Si/Al ratio of \*BEA-type zeolites during the formation of RUT-type zeolites was investigated (Sample nos. 6–11). Figure 6-1 shows the XRD patterns of the products obtained. Crystallization of RUT-type zeolites was strongly dependent on the Si/Al ratio of the starting zeolite. Although \*BEA-type zeolites with Si/Al ratios of 21–41 were not dissolved/decomposed, pure RUT-type zeolites were obtained from \*BEA-type zeolites with Si/Al ratios of 77–105. However, in the case of \*BEA-type zeolites with a Si/Al ratio of 139, only an amorphous phase was detected.

Table 6-1 Interzeolite conversion of \*BEA and FAU type zeolites and products obtained.

Run no.	Starting gels				Synthesis conditions		Product	
	SDA (SDA/SiO <sub>2</sub> )	Additive (Additive/SiO <sub>2</sub> )	Si/Al ratio of *BEA	H <sub>2</sub> O/SiO <sub>2</sub>	Temp. /°C	Time /days	Phase <sup>b</sup>	Si/Al
1	BTMAOH (0.4)	NaOH (0.05)	21	5.5	125	7	*BEA	
2	BTMAOH (0.2)	NaCl (0.1)	77	5.5	120	21	*BEA	
3	Choline (0.5)	NaCl (0.2)	21	5	125	7	*BEA	
4	Choline (0.5)	NaCl (0.2)	77	5	125	7	*BEA	
5	TMAOH (0.2)		77	5	140	7	*BEA	
6	TMAOH (0.2)		21	5	170	7	*BEA	
7	TMAOH (0.2)		41	5	170	7	*BEA	
8	TMAOH (0.2)		52	5	170	7	RUT, BEA	
9	TMAOH (0.2)		77	5	170	7	RUT	77
10	TMAOH (0.2)		105	5	170	7	RUT	105
11	TMAOH (0.2)		139	5	170	7	Am.	
12 <sup>a</sup>	TMAOH (0.2)		17	5	140	7	RUT	17
13 <sup>a</sup>	TMAOH (0.2)		28	5	140	7	RUT	28
14 <sup>a</sup>	TMAOH (0.2)		15	5	170	7	RUT	15
15 <sup>a</sup>	TMAOH (0.2)		77	5	170	7	RUT, Am.	77
16 <sup>a</sup>	TMAOH (0.2)		77	5	170	14	RUT	77
17 <sup>a</sup>	TMAOH (0.2)		105	5	170	7	Am.	

<sup>a</sup> FAU type zeolite was used instead of \*BEA type zeolite as Si & Al sources.

<sup>b</sup> Am.: amorphous

These results demonstrated that the highly crystalline and pure RUT-type zeolites could be also obtained from \*BEA-type zeolites as well as FAU-type zeolites. However, a higher crystallization temperature and a large Si/Al ratio of the starting zeolites were required for interzeolite conversion of \*BEA-type zeolites as compared to FAU-type zeolites (Sample nos. 12–17). This is probably due to the difference in the stability of the zeolite framework under the present alkali conditions. That is, the framework structure of \*BEA-type zeolites is more stable than that of FAU-type zeolites. The effective Si/Al ratios of starting \*BEA and FAU-type zeolites for the synthesis of RUT-type zeolites at 170 °C for 7 days are summarized in Table 6-2. A clear difference in the effect of the Si/Al ratio was observed between the two starting zeolites.

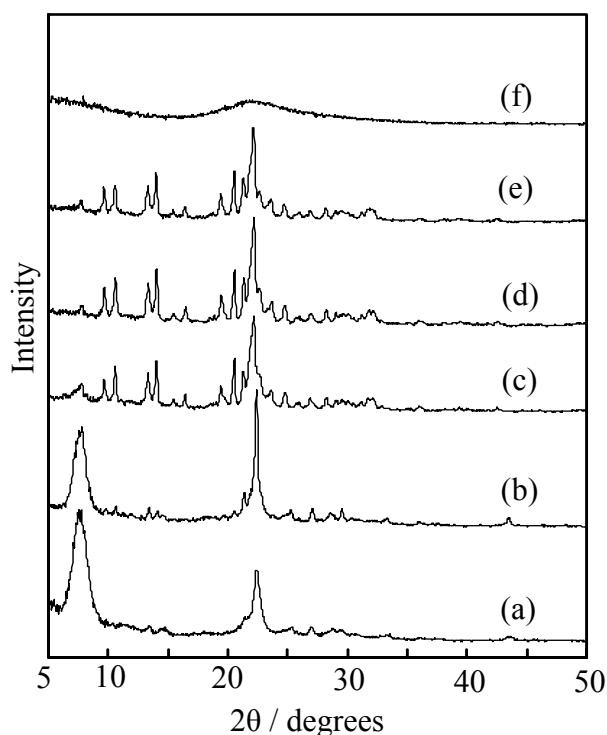


Fig. 6-1 XRD patterns of (a) the starting \*BEA-type zeolite and the products obtained from \*BEA-type zeolites with Si/Al ratios of (b) 21, (c) 52, (d) 77, (e) 105, and (f) 139.

Table 6-2 Influence of Si/Al ratio of starting \*BEA- and FAU-type zeolites on synthesis of RUT-type zeolite.

Si/Al ratio of starting zeolite	Product	
	From *BEA	From FAU
15	*BEA	RUT
21	*BEA	RUT
52	RUT, *BEA	RUT
77	RUT	RUT, Am.
105	RUT	Am.

Temp. = 170 °C, Synthesis time = 7 days

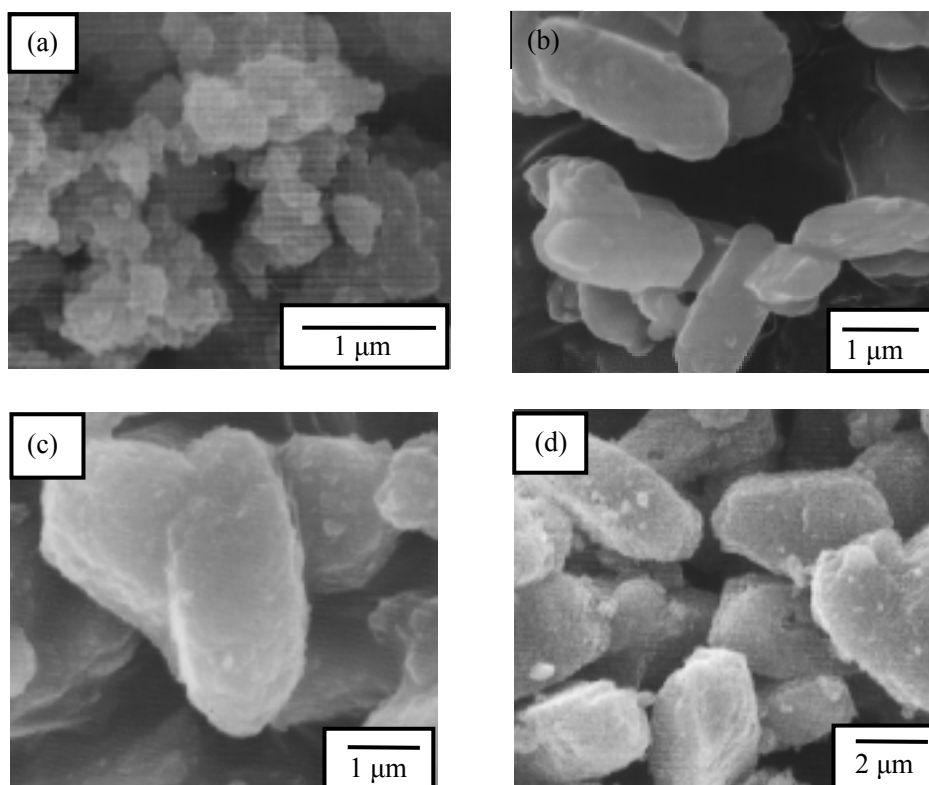


Fig. 6-2 SEM images of (a) the starting \*BEA-type zeolite and the RUT-type zeolites obtained from (b) FAU-type zeolite with Si/Al ratio of 77 and \*BEA-type zeolites with Si/Al ratios of (c) 77 and (d) 105.

Figure 6-2 shows SEM images of the starting \*BEA-type zeolite and the RUT-type zeolites obtained from \*BEA-type zeolites with Si/Al ratios of 77 and 105. For reference, the SEM image of a RUT-type zeolite obtained from a FAU-type zeolite is

also shown. After thorough observation, I could not find any crystals of the starting FAU-type zeolite; only crystals with football-like morphology were observed. There was no difference in the crystal morphology between both RUT-type zeolites obtained from \*BEA and FAU-type zeolites.

To investigate the characteristics of organic materials included in the zeolitic pores of RUT-type zeolite (Sample no. 9) obtained from the hydrothermal conversion of \*BEA-type zeolites,  $^{13}\text{C}$  CP/MAS NMR measurements and thermal analyses were conducted. Figure 6-3 depicts the  $^{13}\text{C}$  CP/MAS NMR spectrum of a RUT-type zeolite obtained from a \*BEA-type zeolite. The spectrum revealed the presence of one strong resonance centered at ca. 57 ppm, which is assigned to the methyl carbon of the  $\text{TMA}^+$  cation. A very weak resonance was also observed at 44 ppm, which is assigned to the methylene carbon of  $\text{N-CH}_2\text{-CH}_3$  moieties that are formed by the degradation of a small amount of TMAOH [23]. Although there was a small amount of degraded  $\text{TMA}^+$ , most of the  $\text{TMA}^+$  cations existed intact in the zeolitic pores. The TG/DTA curves of the RUT-type zeolite are presented in Fig. 6-4. In the DTA curve, I can categorize the thermal profile into five zones: (I) 25–200 °C, (II) 200–350 °C, (III) 350–500 °C, (IV) 500–700 °C, and (V) 700–800 °C. The first zone of the endothermic profile (25–200 °C) corresponds to desorption of adsorbed water. The second zone of the exothermic profile (200–350 °C) is attributed to the decomposition and oxidation of either TMAOH in the pores [24] or  $\text{TMA}^+$  cations interacting with silanol groups of crystal defects. The third zone centered at 450 °C is assigned to the decomposition and oxidation of  $\text{TMA}^+$  cations, which balance the negative charge of the framework generated by Al [24,25]. The fourth zone (500–700 °C) seems to correspond to the decomposition and oxidation of pyrolysis products in the former steps. The fifth zone

corresponds to dehydration that occurs through the condensation of silanol groups, which implies structure collapse [26]. On the basis of the profile described above, the weight loss between 200 and 700 °C that corresponds to the total decomposition of organic moieties is ca. 15 wt%, which is approximately equivalent to 5 TMA<sup>+</sup> cations/u.c. that are occluded in the zeolitic pores.

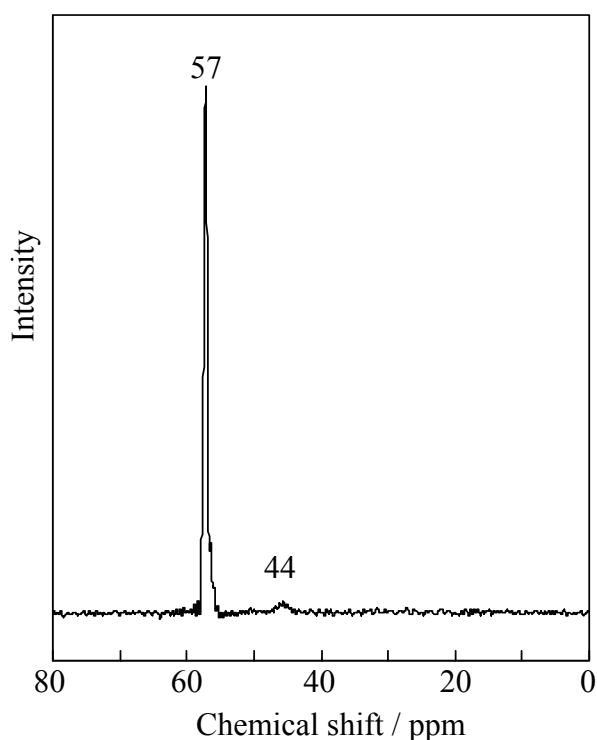


Fig. 6-3 <sup>13</sup>C CP/MAS NMR spectrum of RUT-type zeolite (Sample no. 9).

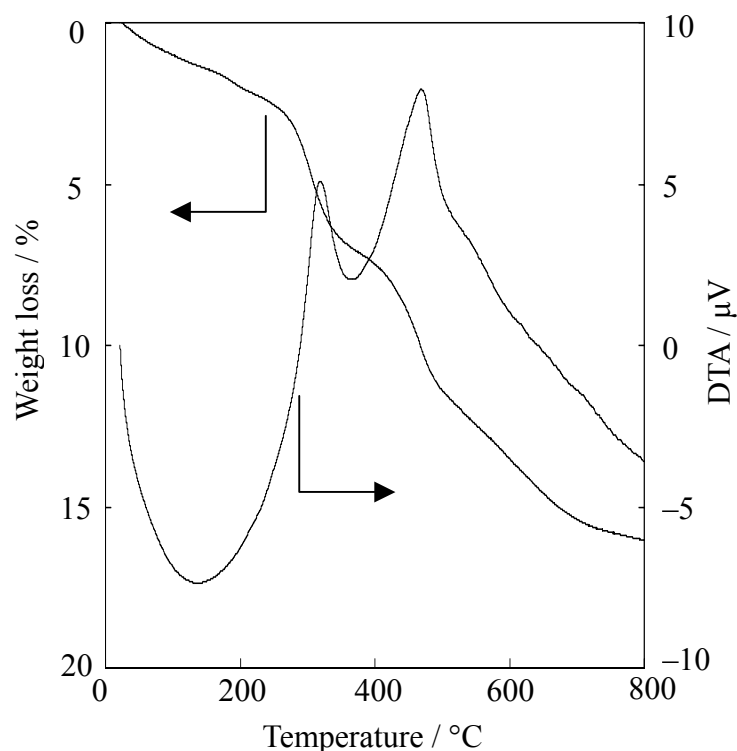


Fig. 6-4 TG/DTA curves of RUT-type zeolite (Sample no. 9).

The chemical states of the aluminum and silicon in the resulting RUT-type zeolites were investigated by <sup>27</sup>Al and <sup>29</sup>Si MAS NMR measurements. The <sup>27</sup>Al MAS NMR spectrum of the as-synthesized RUT-type zeolite (Sample no. 9) is shown in Fig. 6-5. Although RUT-type zeolite consists of five crystallographically different tetrahedral sites according to the crystallographic data in literature [27], only one resonance is present, and it is centered at ca. 50 ppm, which corresponds to a tetrahedrally coordinated species. Resonance corresponding to octahedrally coordinated aluminum

species, that is, an extra-framework aluminum species at around 0 ppm, was not observed. Furthermore, the bulk Si/Al ratios of RUT-type zeolites determined by XRF measurements were consistent with those of the starting zeolites (Table 1), indicating that \*BEA and FAU-type zeolites were completely converted into RUT-type zeolites during hydrothermal treatment in TMAOH media. Figure 6 shows the  $^{29}\text{Si}$  MAS NMR spectra of as-synthesized RUT-type zeolites obtained from \*BEA-type zeolites (Sample no. 9) and FAU-type zeolites (Sample no. 16). Two resonances were observed at ca.  $-113$  and  $-100$  ppm, which can be assigned to  $\text{Q}^4$  (0Al and/or 1Al) and  $\text{Q}^3$ , respectively. There was no difference between the RUT-type zeolites obtained from FAU- and \*BEA-type zeolites.

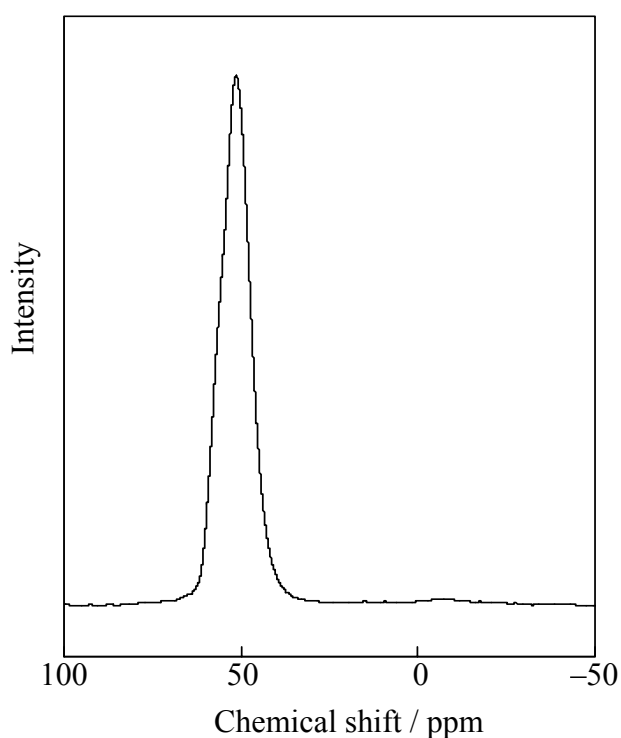


Fig. 6-5  $^{27}\text{Al}$  MAS NMR spectrum of RUT-type zeolite (Sample no. 9).

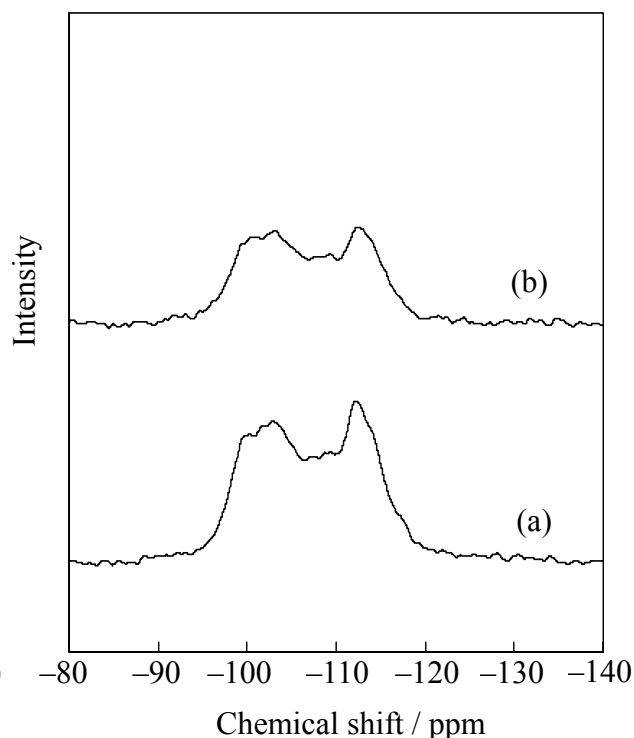


Fig. 6-6  $^{29}\text{Si}$  MAS NMR spectra of RUT-type zeolites obtained from (a) \*BEA-type zeolite (Sample no. 9) and (b) FAU-type zeolite (Sample no. 16).

Next, to clarify the influence of the framework structure of the starting zeolite on the crystallization rate, I studied the crystallization kinetics of RUT-type zeolites from

\*BEA- and FAU-type zeolites with different Si/Al ratios. The crystallization curves are presented in Fig. 6-7. For \*BEA-type zeolites, there was no difference in the crystallization rate toward RUT-type zeolites. On the other hand, for FAU-type zeolites, a large difference in the crystallization rate was observed; the FAU-type zeolite with a Si/Al ratio of 52 exhibited a faster crystallization rate as compared zeolites with a Si/Al ratio of 77. The crystallization rate of RUT-type zeolites from FAU-type zeolites with a Si/Al ratio of 52 is considerably faster than that from \*BEA-type zeolites with a Si/Al ratio of 52. However, in the case where the Si/Al ratio is 77, an opposite phenomenon was observed. These results strongly indicate that the chemical structure and concentration of locally ordered aluminosilicate species produced by the decomposition/dissolution of the starting zeolites can be altered by changing the framework structure of starting zeolite. Although the chemical structure of locally ordered aluminosilicate species is not clarified at the present time due to a limited data, I have now speculated the difference in crystallization behavior as follows. The stability

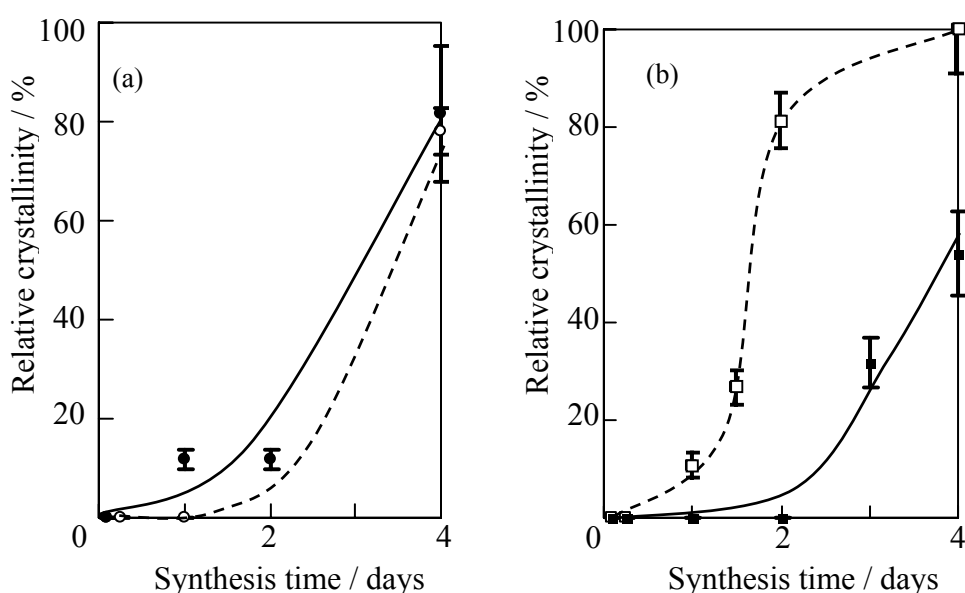


Fig. 6-7 Crystallization curves of RUT-type zeolites obtained from (a) \*BEA-type zeolites and (b) FAU-type zeolites. (○), (□): Si/Al ratio = 52, (●), (■): Si/Al ratio = 77.

of \*BEA-type zeolite is higher than that of FAU-type zeolite in spite of Si/Al ratio, suggesting an existence of locally ordered aluminosilicate species during the \*BEA–RUT interzeolite conversion process. On the other hand, the framework structure of FAU-type zeolite is decomposed into fragments without locally ordinary due to less stability.

#### **4. Conclusion**

Highly crystalline and pure RUT-type zeolites were obtained from the interzeolite conversion of FAU and \*BEA-type zeolites. Although the resulting RUT-type zeolites exhibited similar characteristics, there was a large difference in the effect of the Si/Al ratio in the starting zeolite on the synthesis of RUT-type zeolites. Moreover, the crystallization rate for the FAU–RUT interzeolite conversion strongly depended on the starting Si/Al ratio, whereas no dependence was observed for the \*BEA–RUT interzeolite conversion. This is due to differences in the chemical structure and concentration of locally ordered aluminosilicate species produced by the decomposition/dissolution of starting zeolites during the interzeolite conversion process.

## References

- [1] T.V. Whittam, B. Youll, US Patent 4 060 590, Imperial Chemical Industries Ltd., London, 1977.
- [2] M. Taramasso, G. Perego, B. Notari, in L.V.C. Rees (Ed.), Proceedings of the Fifth International Conference on Zeolites, Naples, Heyden, London, (1980) 40.
- [3] G. Bellussi, R. Millini, A. Carati, G. Maddinelli, A. Gervasini, Zeolites 10 (1990) 642.
- [4] R.K. Ahedi, S.S. Shevade, A.N. Kotasthane, Zeolites 18 (1997) 361.
- [5] A. Bhaumik, T. Tatsumi, Micropor. Mesopor. Mater. 34 (2000) 1.
- [6] J. Patarin, P. Caullet, B. Marler, A.C. Faust, J.L. Guth, Zeolites 14 (1994) 675.
- [7] B. Marler, U. Werthmann, H. Gies, Micropor. Mesopor. Mater. 43 (2001) 329.
- [8] B. Subotić, D. Škrčić, I. Šmit, L. Sekovanić, J. Cryst. Growth 50 (1980) 498.
- [9] B. Subotić, L. Sekovanić, J. Cryst. Growth 75 (1986) 561.
- [10] B. Subotić, I. Šmit, O. Madžija, L. Sekovanić, Zeolites 2 (1982) 135.
- [11] S.I. Zones, J. Chem. Soc. Faraday Trans. 87 (1991) 3709.
- [12] S.I. Zones, L.T. Yuen, Y. Nakagawa, R.A. van Nordstrand, D.D. Toto, in: R. von Ballmoos, J.B. Higgins, M.M.J. Treacy (Eds.), Proceedings of the 9<sup>th</sup> International Zeolite Conference, Butterworth-Heinemann, Boston (1993) 163.
- [13] S.I. Zones, Y. Nakagawa, Micropor. Mesopor. Mater. 2 (1994) 557.
- [14] Y. Kubota, H. Maekawa, S. Miyata, T. Tatsumi, Y. Sugi, Micropor. Mesopor. Mater. 101 (2007) 115.
- [15] R.K. Ahedi, Y. Kubota, Y. Sugi, J. Mater. Chem. 11 (2001) 2922.
- [16] H. Jon, S. Takahashi, H. Sasaki, Y. Oumi, T. Sano, Micropor. Mesopor. Mater. 113 (2008) 56.

- [17] H. Jon, K. Nakahata, B. Lu, Y. Oumi, T. Sano, *Micropor. Mesopor. Mater.* 96 (2006) 72.
- [18] M. Itakura, T. Inoue, A. Takahashi, T. Fujitani, Y. Oumi, T. Sano, *Chem. Lett.* 39 (2008) 908.
- [19] H. Sasaki, H. Jon, M. Itakura, T. Inoue, T. Ikeda, Y. Oumi, T. Sano, *J. Porous Mater.* 16 (2009) 465.
- [20] T. Inoue, M. Itakura, H. Jon, A. Takahashi, T. Fujitani, Y. Oumi, T. Sano, *Micropor. Mesopor. Mater.* 122 (2009) 149.
- [21] M. Itakura, Y. Oumi, M. Sadakane, T. Sano, *Mater. Res. Bull.* 45 (2010) 646.
- [22] H. Jon, N. Ikawa, Y. Oumi, T. Sano, *Chem. Mater.* 20 (2008) 4135.
- [23] C.J. Pouchert, J. Behnke, *The Aldrich Library of  $^{13}\text{C}$  and  $^1\text{H}$  FT NMR Spectra*, Aldrich Chemical Co. Inc., USA, 1993.
- [24] A. Abraham, S.-H. Lee, C.-H. Shin, S.B. Hong, R. Prins, J.A. van Bokhoven, *Phys. Chem. Chem. Phys.* 6 (2004) 3031.
- [25] E. Bourgeat-Lami, F. Di Renzo, F. Fajula, P.H. Mutin, T.D. Courieres, *J. Phys. Chem.* 96 (1992) 3807.
- [26] M.A. Camblor, A. Corma, S. Valencia, *J. Mater. Chem.* 8 (1998) 2137.
- [27] R.W. Broach, N.K. McGuire, C.C. Chao, R.M. Kirchner, *J. Phys. Chem. Solids* 56 (1995) 1363.

## Chapter 7

### Interzeolite conversion process of FAU-type zeolite

#### 1. Introduction

Zeolites are the crystalline aluminosilicates with microporous structure, which possesses unique properties such as high surface area, ion-exchange ability, and acidity. Thus, zeolites has used for solid catalysis, adsorbents, detergent, and etc. Most of zeolite syntheses were carried out using amorphous aluminosilicate gels as starting materials in the presence of inorganic and/or organic structure-directing agents (SDAs). However, crystallization process of zeolite is not clarified completely. Davis and Moor et al. proposed structure-directing mechanism in the tetrapropylammonium-mediated synthesis of MFI-type zeolite using NMR [1-3] and SAXS/WAXS [4-6] techniques. Mintova et al. investigated the formation of several zeolite crystals from aqueous solutions using TEM, DLS, and XRD and found direct conversion of amorphous gel particles, which were the first particles observed after the reaction start, to crystalline structures [7-9]. Matsukata et al. investigated the formation mechanism of \*BEA structure using high energy X-ray diffraction measurement [10,11]. Schüth et al. have pointed out the high potential of electrospray ionization mass spectroscopy (ESI-MS) technique for analysis of structures of oligomeric aluminosilicate species present in the liquid phase during crystallization [12-14]. As the ionization process under the ESI-MS conditions is free of fragmentation reaction, it is possible to analyze many different

aluminosilicate species simultaneously. Recently, they succeeded in measuring some kinds of chemical species observed during crystallization process of several zeolites [15,16].

In the zeolite synthesis process, the formation of a zeolite phase proceeds often through the gradual transformation in sequence: amorphous phase → less stable zeolite → most stable zeolite [17]. As this phenomenon can be considered to be an alternative synthesis strategy for the hydrothermal conversion of one zeolite into another, i.e., interzeolite conversion, this method has attracted much attention.

I have also investigated the potential of the interzeolite conversion method, and already succeeded in synthesizing several types of zeolites from FAU- and \*BEA-type zeolites [18,19]. In the conversion process, it is considered that the locally ordered aluminosilicate species (nanoparts) are produced by decomposition/dissolution of starting zeolite and then their assembly proceeds under a specific SDA, resulting in a fast crystallization rate and a high selectivity to a particular zeolite. However, I do not have enough data for understanding of nanoparts [20]. In this study, therefore, to get further information concerning nanoparts present during interzeolite conversion process, I investigated both FAU–RUT [21] and FAU–\*BEA [22] interzeolite conversion processes using several techniques such as XRD, NMR, and ESI-MS.

## **2. Experimental**

### **2.1 Interzeolite conversion**

The FAU-type zeolites with various Si/Al ratios that were used in this work were

prepared from NH<sub>4</sub>-Y zeolite (Si/Al = 2.8, Tosoh Co., Japan) through a dealumination treatment that involved a combination of steaming at 700 °C and H<sub>2</sub>SO<sub>4</sub> (0.42–0.86 M) treatment at 75 °C for 4 h. The XRD pattern of the dealuminated zeolite showed no peaks other than those corresponding to the FAU structure, and the intensities of the peaks observed were almost the same as those of the parent zeolite, which indicate no structural degradation. The particle size of the dealuminated FAU-type zeolite was 0.4–0.8 μm. The dealuminated zeolite was added into an aqueous solution containing SDA (tetramethylammonium hydroxide: TMAOH or tetraethylammonium hydroxide: TEAOH), and then the mixture was placed into a 30 cm<sup>3</sup> Teflon-lined stainless steel autoclave. The molar composition of starting gel was SiO<sub>2</sub>:0.02Al<sub>2</sub>O<sub>3</sub>:0.2SDA:5H<sub>2</sub>O. The hydrothermal conversion was conducted at 140 °C for 2 h–7 d in the convection oven. The solid and solution parts were collected by centrifugation, and the solid product was washed thoroughly with deionized water. For comparison, starting gels from amorphous silica powder produced by a wet process (SiO<sub>2</sub> = 88 wt%, Al<sub>2</sub>O<sub>3</sub> = 0.27 wt%, Nipsil, Nippon Silica Ind. Japan), and γ-Al<sub>2</sub>O<sub>3</sub> (JGC Catalysts and Chemicals Ltd. Japan) or Al(OH)<sub>3</sub> (Wako Pure Chemical Ind., Ltd. Japan) as other Si and Al sources, respectively, were also prepared.

## 2.2. Characterization

The powder X-ray diffraction (XRD) patterns of the solid products were obtained using a powder X-ray diffractometer (Rigaku, Mini Flex) with graphite monochromatized Cu Kα radiation at 30 kV and 15 mA. The crystal morphology was observed with a scanning electron microscope (SEM, Hitachi S-4800). <sup>13</sup>C CP/MAS

NMR,  $^{27}\text{Al}$  MAS NMR, and  $^{29}\text{Si}$  (CP/) MAS NMR spectra were recorded using a 7 mm diameter zirconia rotor on a Bruker Avance DRX-400 at 100.6 MHz, 104.3 MHz, and 79.5 MHz, respectively. The rotor was spun at 4 kHz for  $^{29}\text{Si}$  and  $^{13}\text{C}$  CP/MAS NMR, and at 6 kHz for  $^{27}\text{Al}$  MAS NMR. The spectra were accumulated with 6.0  $\mu\text{s}$  pulses, a 25 s recycle delay, and 1000 scans for  $^{13}\text{C}$  CP/MAS NMR, 2.3  $\mu\text{s}$ , 1 s, and 1000 scans for  $^{27}\text{Al}$  MAS NMR, and 5  $\mu\text{s}$ , 20 s and 2000 scans for  $^{29}\text{Si}$  MAS NMR.  $\text{Al}(\text{NO}_3)_3 \cdot 9\text{H}_2\text{O}$  was used as a chemical shift reference for  $^{27}\text{Al}$  MAS NMR, and  $\text{Si}(\text{CH}_3)_4$  was used as a chemical shift reference for  $^{13}\text{C}$  CP/MAS NMR and  $^{29}\text{Si}$  MAS NMR. Prior to  $^{27}\text{Al}$  MAS NMR measurement, the sample was moisture-equilibrated over a saturated solution of  $\text{NH}_4\text{Cl}$  for 24 h. ESI-MS measurement was performed using LCMS-2020 (Shimadzu Co.). The samples were measured with a applied voltage of  $-3.5$  kV, and desolvation temperature was  $200$  °C.

### 3. Results and discussion

Fig. 7-1 shows XRD patterns of \*BEA-type zeolites obtained from FAU-type zeolite and amorphous materials in the presence of TEOH and FAU–RUT interzeolite conversion. As can be seen in Fig. 7-1A, the peaks corresponding to the starting FAU-type zeolite completely disappeared at 2 h, and then pure and highly crystalline \*BEA-type zeolite was obtained after synthesis time of 2 d. On the other hand, prolonged synthesis time (7 d) was required in the case of amorphous materials (Fig. 7-1B). This indicates that the use of FAU-type zeolite enhances the crystallization rate of \*BEA-type zeolite, namely the advantage of interzeolite conversion method. Figs. 7-2 and 3 show SEM images of products obtained from FAU-type zeolite and

amorphous materials in the presence of TEAOH, respectively. As shown in Fig. 7-2 (a), FAU-type zeolite was decomposed only after 2 h of hydrothermal treatment and small particle, precursor of \*BEA-type zeolite, was observed after 12 h (Fig. 7-2 (c)). In the case of using amorphous materials, the precursor was observed after 2 d of hydrothermal treatment (see Fig. 7-3). As a matter of course synthesis of RUT-type

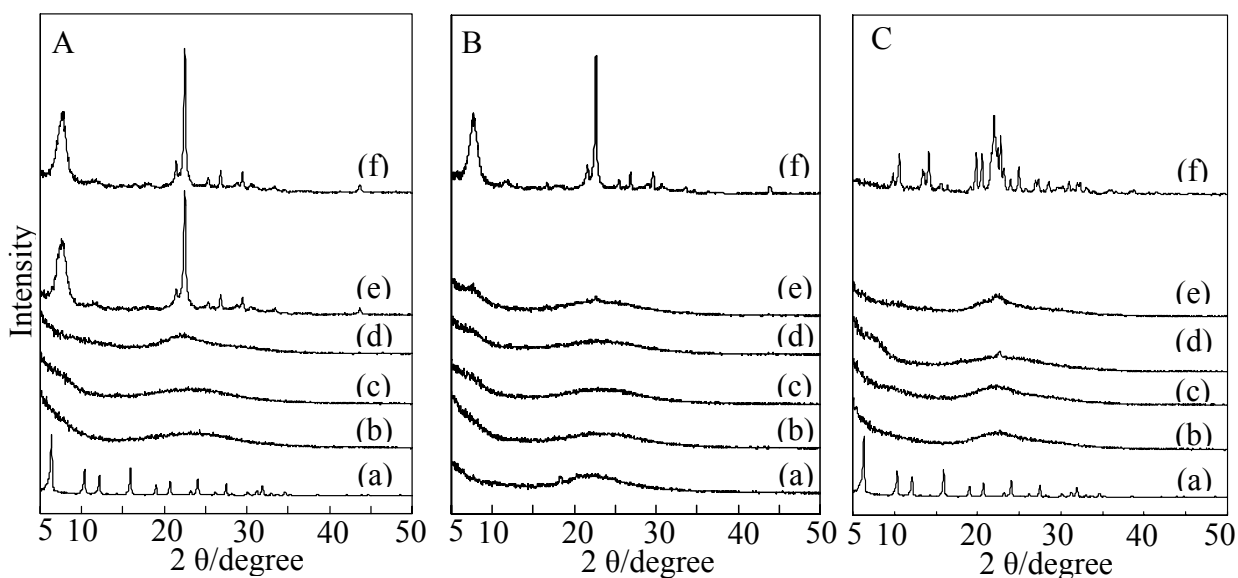


Fig. 7-1 XRD patterns of solid products obtained from (A) FAU and (B) amorphous in the presence of TEAOH and (C) TMAOH. Synthesis time: (a) 0 h, (b) 2 h, (c) 12 h, (d) 1 d, (e) 2 d, and (f) 7 d.

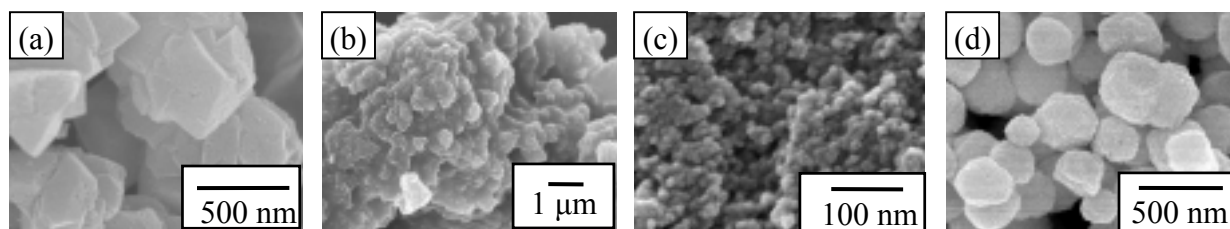


Fig. 7-2 SEM images of solid products obtained from FAU-type zeolite in the presence of TEAOH. Synthesis time: (a) 0 h, (b) 2 h, (c) 12 h, and (d) 7 days.

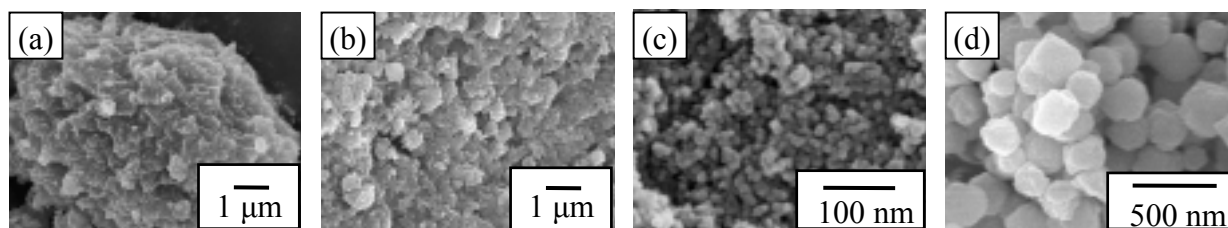


Fig. 7-3 SEM images of solid products obtained from amorphous materials in the presence of TEAOH. Synthesis time: (a) 0 h, (b) 12 h, (c) 2 d, and (d) 7 d.

zeolite using FAU-type zeolite was faster than that of amorphous materials [21], in Figs. 7-1A and C, crystallization rate of FAU–RUT interzeolite conversion was slower than FAU–\*BEA interzeolite conversion process). I considered that this difference was caused by not only SDA also structural similarities between the starting FAU and desired \*BEA- and RUT-type zeolites.

The fast crystallization of \*BEA-type zeolite from FAU-type zeolite was also confirmed by  $^{29}\text{Si}$  CP/MAS NMR (Figs. 7-4A and B). The intensities of the peaks at  $-100$  and  $-90$  ppm corresponding to  $Q^3$  and  $Q^2$  species in the case of the use of FAU-type zeolite were larger than in the case of amorphous materials at the initial stage of hydrothermal conversion. Moreover, as shown in Fig. 7-4C, FAU–RUT interzeolite conversion process in the presence of TMAOH also displayed the similar behavior. The intensities of peaks corresponding to  $Q^3$  and  $Q^2$  species were larger than peak of  $Q^4$  species. These results strongly suggest a difference in the chemical structure of nanoparts generated at the initial stage of hydrothermal conversion..

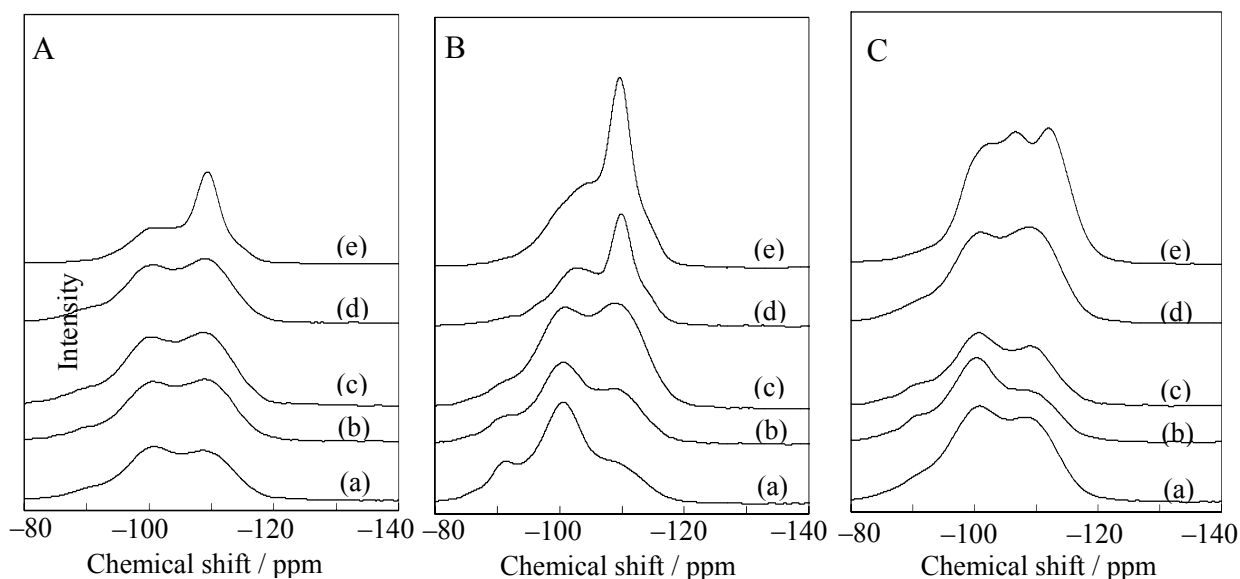


Fig. 7-4  $^{29}\text{Si}$  CP/MAS NMR spectra of solids obtained from (A) FAU and (B) amorphous materials (C) FAU–RUT interzeolite conversion process. Synthesis time: (a) 2 h, (b) 12 h, (c) 1 d, (d) 2 d, and (e) 7 d.

Fig. 7-5 shows the  $^{27}\text{Al}$  NMR spectra of aqueous parts obtained after synthesis time of 2 h. In the case of the synthesis of \*BEA-type zeolite from amorphous materials, there were no peaks. On the other hand, however, the peak assigned to tetrahedral coordinated aluminum species was observed at ca. 50 ppm for FAU-\*BEA interzeolite conversion. The peak was also observed in FAU-RUT interzeolite conversion in the presence of TMAOH.

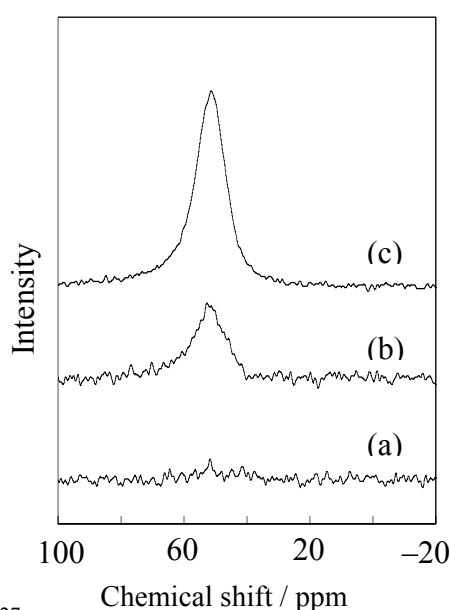


Fig. 7-5  $^{27}\text{Al}$  NMR spectra of aqueous solutions obtained after synthesis time of 2 h for (a) amorphous-\*BEA, (b) FAU-\*BEA, and (c) FAU-RUT interzeolite conversion.

In order to clarify the difference, the aqueous solutions obtained at the initial stage of hydrothermal conversion were analyzed by ESI-MS. ESI-MS spectra of FAU-\*BEA and FAU-RUT interzeolite conversion process was showed in Figs. 7-6, 7, and 8. In all negative-ion ESI-MS spectra, two types of chemical species with various masses, clustered with and without cations ( $\text{SDA}$  and  $\text{Na}^+$ ), were detected. The assignment of chemical species detected in ESI-MS spectrum was denoted to TX-YW. The “X” denotes T-atom number and the “Y” denotes number of condensation ( $2\text{SiOH} \rightarrow \text{Si-O-Si} + \text{H}_2\text{O}$ ). Furthermore, speculated structure of chemical species also showed

above the peaks. In the range of  $m/z = 50\text{--}350$ , similar chemical species were detected in both of ESI-MS spectra. However, in the range of  $350\text{--}950$ , most species observed in FAU-\*BEA interzeolite conversion were assigned to the higher masses species clusters without cations. On the other hand, in FAU-RUT interzeolite conversion, the species clustered with cations were observed. This result was consistent with the result of Al NMR, because SDA cation prefer to cluster with chemical species with Al atom. The chemical species of T6-4W, T8-3W, T8-5W, and T10-4W were detected only in the presence of TEOH. As shown in Fig. 7-7 and 8, I have now speculated that these species possess four-membered ring (4MR) chain structure. In the formation of \*BEA structure, Matsukata et al. extrapolated that pseudo-\*BEA structure formed by connecting 4MR structure (such as double three-membered ring and 4-2 secondary building unit) each other [11]. The 4MR structure was similar to species detected in ESI-MS spectrum. It is reasonable to consider that these 4MR structure species are also provided during the FAU-\*BEA interzeolite conversion process and contribute crystallization of \*BEA-type zeolite by connecting each other. Mass numbers of aluminosilicates in chemical species clustered with cations in liquid phase detected by ESI-MS after 2 h of hydrothermal conversion of amorphous materials and FAU-type zeolite are listed in Table 7-1. It became clear that chemical species detected are distributed diagonally. It implies that condensation reaction between aluminosilicate species takes place during interzeolite conversion process. The species with higher masses were detected in the ESI-MS spectrum of FAU-\*BEA interzeolite conversion as compared to the synthesis of \*BEA-type zeolite from amorphous materials. Detection of species with higher mass number as nanoparts for zeolite crystal growth supports enhancement of crystallization rate in interzeolite conversion method.

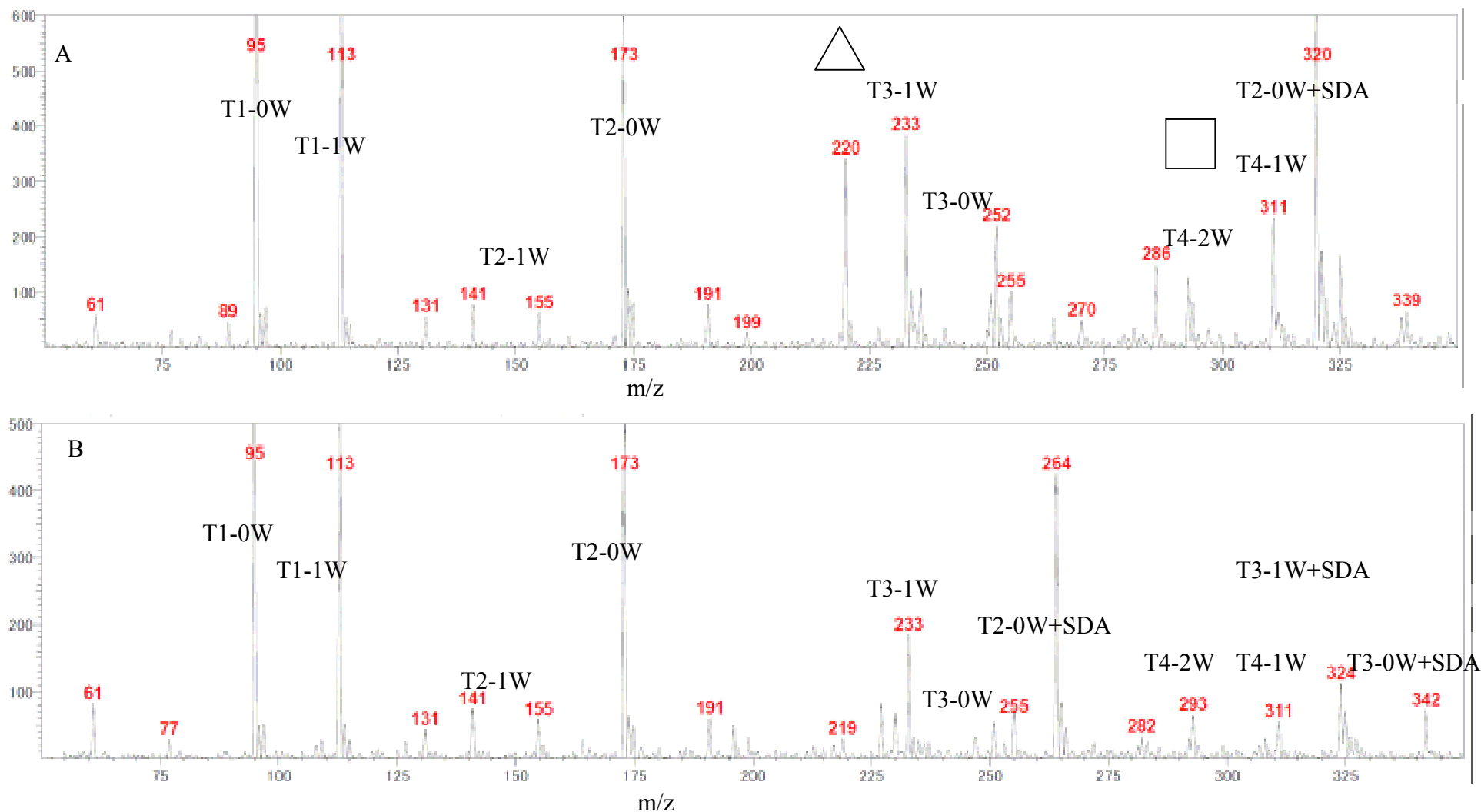


Fig. 7-6 ESI-MS spectra of  $m/z = 50-350$  during the (A) FAU-\*BEA and (B) FAU-RUT interzeolite conversion after 2 h of hydrothermal treatment.

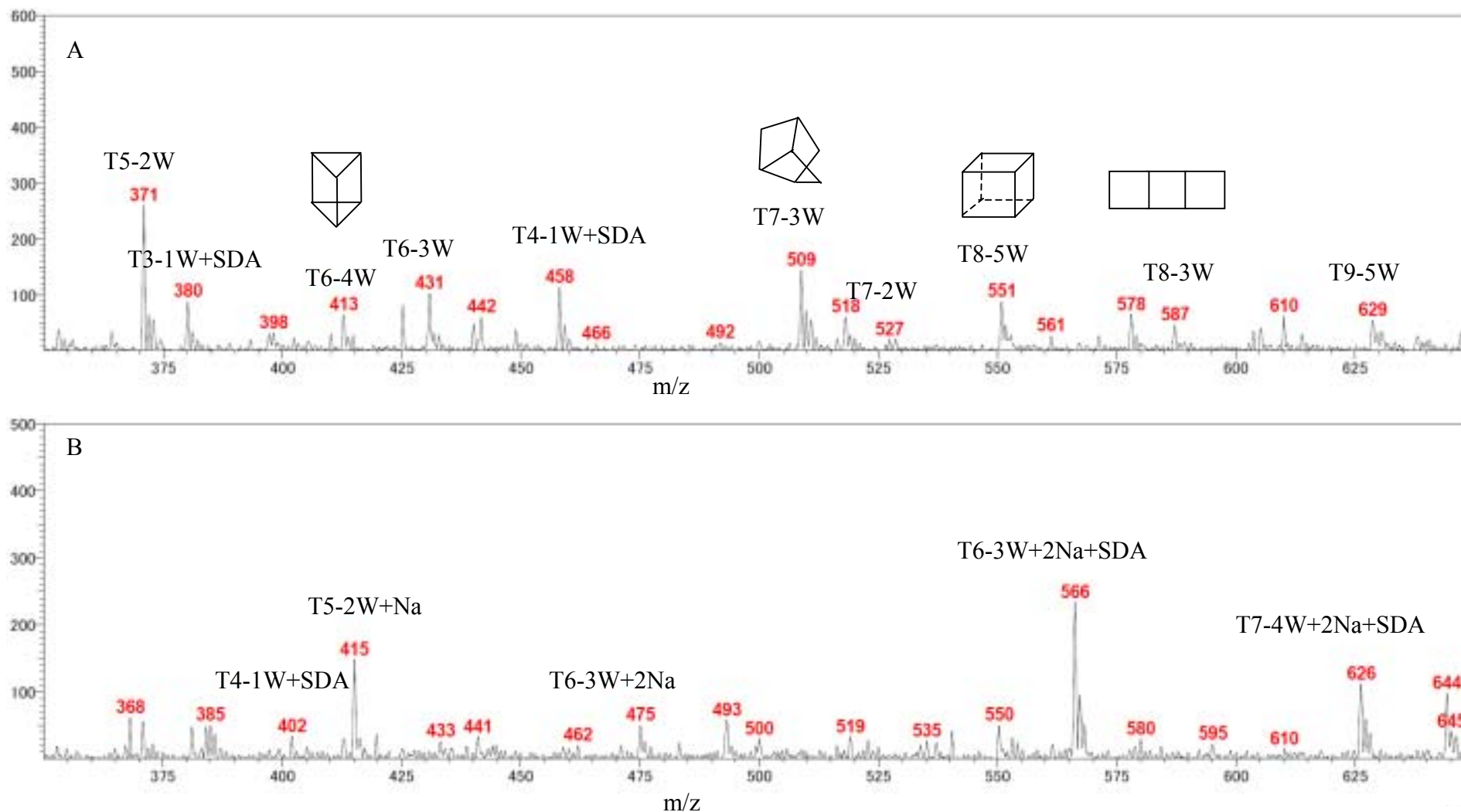


Fig. 7-7 ESI-MS spectra of  $m/z = 350\text{--}650$  during the (A) FAU-\*BEA and (B) FAU-RUT interzeolite conversion after 2 h of hydrothermal treatment.

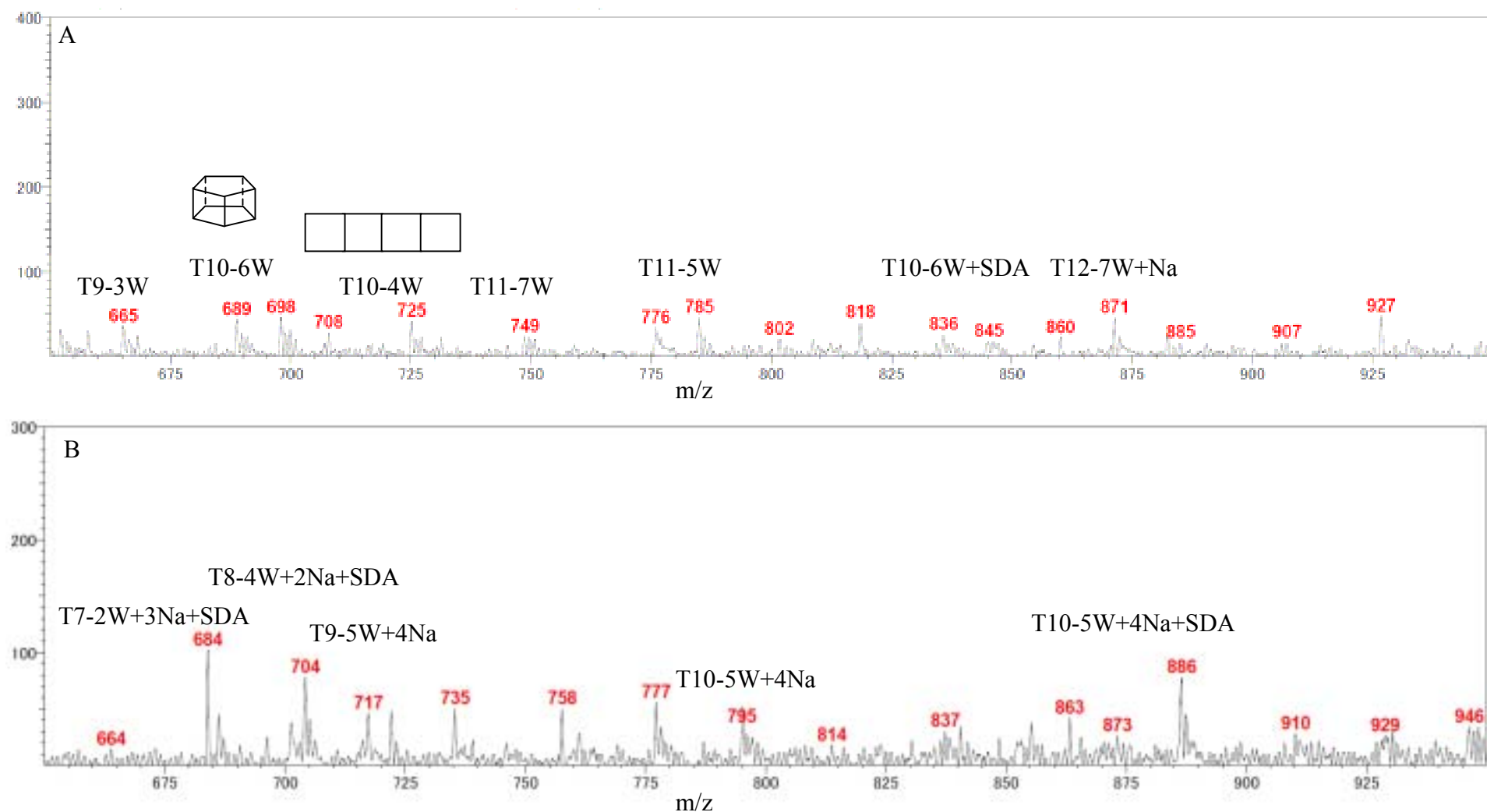


Fig. 7-8 ESI-MS spectra of  $m/z = 650-950$  during the (A) FAU-\*BEA and (B) FAU-RUT interzeolite conversion after 2 h of hydrothermal treatment.

Table 7-1 Mass numbers of aluminosilicate in chemical species clustered with cations in liquid phase detected by ESI-MS measurement after 2 h of hydrothermal conversion of amorphous materials (bold) and FAU-type zeolite (blue).

	-0W	-1W	-2W	-3W	-4W	-5W	-6W	-7W	-8W
T-1	<b>95</b>								
T-2	<b>173</b>								
T-3	<b>251</b>	<b>233</b>							
T-4		<b>311</b>	<b>293</b>						
T-5			<b>371</b>						
T-6				<b>431</b>					
T-7									
T-8						<b>551</b>			
T-9						<b>629</b>			
T-10							<b>689</b>		
T-11									
T-12								<b>827</b>	
T-13									

#### 4. Conclusions

Interzeolite conversion process of FAU-type zeolite was investigated using several measurement techniques. From XRD and SEM measurements, it was confirmed that the crystallization rate with FAU-type zeolite as the starting material was faster than that with amorphous aluminosilicate gel (the conventional synthesis). In the solid parts obtained from amorphous materials, the large amount of  $Q^2$  and  $Q^3$  species were observed. On the other hand, in the solution parts, there was a different in chemical species detected by ESI-MS between FAU-\*BEA and FAU-RUT interzeolite conversion process. The aluminosilicate species with 4MR structure was suggested

contribute formation of \*BEA structure. The clustered aluminosilicate species with higher masses were detected in the ESI-MS spectrum of FAU-\*BEA interzeolite conversion as compared to the synthesis of \*BEA-type zeolite from amorphous materials. From the detail analyses of both solid and solution parts during the conversion process, the existence of species with different chemical structures between the interzeolite conversion and conventional synthesis was suggested.

### **Acknowledgements**

I acknowledge Dr. H. Murata in Shimadzu Co. for ESI-MS measurements and valuable comments.

**References**

- [1] S. L. Burkett and M. E. Davis, *J. Phys. Chem.* 98 (1994) 4647.
- [2] S. L. Burkett and M. E. Davis, *Chem. Mater.* 7 (1995) 920.
- [3] S. L. Burkett and M. E. Davis, *Chem. Mater.* 7 (1995) 1453.
- [4] P.-P. E. A. Moor, T. P. M. Beelen, and R.A. van Santen, *J. Phys. Chem. B* 103 (1999) 1639.
- [5] P.-P. E. A. Moor, T. P. M. Beelen, and R.A. van Santen, *Chem. Mater.* 11 (1995) 36.
- [6] P.-P. E. A. Moor, T. P. M. Beelen, and R.A. van Santen, *J. Phys. Chem. B* 104 (2000) 7600.
- [7] S. Mintova, N. H. Olson, V. Valtchev, T. Bein, *Science* 283 (1999) 958.
- [8] S. Mintova, N. H. Olson, T. Bein, *Angew. Chem., Int. Ed.* 38 (1999) 3201.
- [9] S. Mintova, N. Petkov, K. Karaghiosoff, T. Bein, *Micropor. Mesopor. Mater.* 50 (2001) 121.
- [10] S. Inagaki, K. Nakatsuyama, Y. Saka, E. Kikuchi, S. Kohara, M. Matsukata, *Micropor. Mesopor. Mater.*, 108 (2007) 50.
- [11] S. Inagaki, K. Nakatsuyama, Y. Saka, E. Kikuchi, S. Kohara, M. Matsukata, *J. Phys. Chem. C*, 111 (2007) 10285.
- [12] P. Bussian, F. Sobott, B. Brutschy, W. Schrader, and F. Schüth, *Angew. Chem., Int. Ed.* 39 (2000) 3901.
- [13] S.A. Pelster, W. Schrader, and F. Schüth, *J. Am. Chem. Soc.* 128 (2006) 4310.
- [14] S.A. Pelster, W. Schrader, and F. Schüth, *Anal. Chem.* 79 (2007) 6005.
- [15] B.B. Schaack, W. Schrader, and F. Schüth, *Angew. Chem. Int. Ed.* 47 (2008) 9092.
- [16] B.B. Schaack, W. Schrader, A. Corma, and F. Schüth, *Chem. Mater.* 21 (2009) 4448.

- [17] C.S. Cundy, P.A. Cox, *Micropor. Mesopor. Mater.*, 82 (2005) 1.
- [18] H. Jon, H. Sasaki, T. Inoue, M. Itakura, S. Takahashi, Y. Oumi, T. Sano, *Stud. Surf. Sci. Catal.* 174 (2008) 229.
- [19] M. Itakura, K. Ota, S. Shibata, T. Inoue, Y. Ide, M. Sadakane, T. Sano, *J. Cryst. Growth* 314 (2011) 274.
- [20] H. Jon, N. Ikawa, Y. Oumi, T. Sano, *Chem. Mater.*, 20 (2008), 4135.
- [21] H. Jon, S. Takahashi, H. Sasaki, Y. Oumi, T. Sano, *Micropor. Mesopor. Mater.* 113 (2008) 56.
- [22] H. Jon, K. Nakahata, B. Lu, Y. Oumi, T. Sano, *Micropor. Mesopor. Mater.* 96 (2006) 72.

## Chapter 8

### Summary

Chapter 1, to make the purpose of my thesis clear, the historical and experimental overview of zeolite chemistry was described.

Next, in chapter 2, I reported that LEV-type zeolite can be the first time synthesized from the hydrothermal conversion of FAU-type zeolite. As LEV-type zeolite was not obtained from both amorphous  $\text{SiO}_2/\text{Al}_2\text{O}_3$  and amorphous  $\text{SiO}_2/\text{Al}(\text{OH})_3$ , the advantage and uniqueness of the hydrothermal conversion of FAU-type zeolite was proven. The obtained LEV-type zeolites were pure and highly crystalline, as confirmed by XRD patterns and SEM images. Based on the results of  $^{27}\text{Al}$  MAS NMR and FT-IR spectra, the obtained LEV-type zeolites have a significant acidic property, indicating that they are potential solid acid catalysts. The catalytic test showed that H-LEV-type zeolites are effective catalysts for ethanol to light olefins (ETO) reaction. From these findings, it was confirmed again that the hydrothermal conversion route is an alternative strategy for zeolite synthesis.

In chapter 3, I have investigated the influence of fluoride anions on the interzeolite conversion of FAU-type zeolite into LEV-type zeolite. When choline hydroxide was employed as a SDA, there was no difference between the characteristics and thermal stability of LEV-type zeolites synthesized in the presence and absence of fluoride anions,

which indicates that fluoride anions do not play pronounced role in the process. When 1-adamantanamine was employed instead of choline hydroxide, however, the fluoride anions exerted a pronounced influence. I succeeded in the synthesis of high silica LEV-type zeolites (Si/Al ratio = 13–29). In addition, the interzeolite conversion of FAU-type zeolite into LEV-type zeolite in the presence of fluoride anions was shown to occur in a short crystallization time (7–10 days), which is one of the advantages of zeolite synthesis that uses the interzeolite conversion method. A marked enhancement in the thermal stability of LEV-type zeolite synthesized in the presence of fluoride anions was also observed, which I attribute to fewer connectivity defects.

The largest differences in the FAU–LEV interzeolite conversion process were observed when choline hydroxide and 1-adamantanamine were used. In the case in which choline hydroxide is used, the decomposition/dissolution rate of FAU-type zeolite was relatively faster than the nucleation and crystal growth rates of LEV-type zeolites. In the case in which 1-adamantanamine was used in a fluoride medium, however, XRD diffraction patterns of the starting FAU-type zeolite were clearly observed during the FAU–LEV interzeolite conversion process. This takes place because of the difference between the mineralizing power of fluoride anions and hydroxide anions. That is, the rate of decomposition/dissolution of the starting FAU-type zeolite in the presence of fluoride anions is slower than that in the presence of hydroxide anions, and as a consequence, the nucleation and crystal growth of LEV-type zeolite proceeds simultaneously with the decomposition/dissolution of the starting FAU-type zeolite.

In chapter 4, high-silica CHA-type zeolite was synthesized by interzeolite conversion

method in the presence of BTMAOH. This is the first high-silica CHA-type zeolite synthesized with a SDA other than  $\text{TMAda}^+$  cation. The CHA-type zeolite was not obtained using amorphous materials. This seems to be due to an existence of locally ordered aluminosilicate species formed by decomposition or dissolution of zeolite. By adding seed crystals, CHA-type zeolites with a wide range of Si/Al ratios (13.4–21.5) were obtained with shorter crystallization time. We also achieved the first successful synthesis of high-silica CHA-type zeolite in the absence of  $\text{Na}^+$  cations by using a higher content of seed crystals, indicating that no  $\text{H}^+$  ion-exchange process is required for the use of a solid acid catalyst. The protonated CHA-type zeolite exhibited good performance in relation to the conversion of ethanol to light olefins. A maximum propylene yield of ca. 48 C-% was achieved at the Si/Al ratio of ca. 15. Furthermore, high acid stability towards several acids, such as acetic acid, HCl,  $\text{H}_2\text{SO}_4$ , and  $\text{HNO}_3$ , was confirmed. The acid stability of CHA-type zeolite was higher than that of SSZ-13. The CHA-type zeolite membrane prepared on the porous  $\alpha$ -alumina tube demonstrated the excellent pervaporation performance for dehydration of water/acetic acid (50/50 wt%) at 75 °C. The membrane showed a high separation factor,  $\alpha(\text{H}_2\text{O}/\text{CH}_3\text{COOH})$ , of ca. 2500 with a permeate flux of ca.  $8 \text{ kg m}^{-2} \text{ h}^{-1}$ . These indicate the potential for the effective future application of CHA-type zeolite membrane synthesized by interzeolite conversion methods

In chapter 5, hydrothermal conversion parameters influencing the conversion of FAU-type zeolite into OFF-type zeolite were investigated in detail. The hydrothermal conversion of FAU-type zeolite into OFF-type zeolite effectively proceeded in the presence of both BTMAOH and the structure-forming alkali metal cations such as  $\text{Li}^+$

and  $\text{Na}^+$ , and strongly depended on the Si/Al ratio of the starting FAU-type zeolite. Only the FAU-type zeolites with Si/Al of 23–31 were converted into OFF-type zeolites in one day. As confirmed by  $^{13}\text{C}$  CP/MAS NMR spectrum, almost all of BTMA cations existed intact in zeolitic pores. In addition, benzene adsorption measurements showed that there is no or very little amount of stacking faults of ERI within the crystals, suggesting a high potential of the OFF-type zeolite for several catalytic reactions.

In chapter 6, highly crystalline and pure RUT-type zeolites were obtained from the interzeolite conversion of FAU and \*BEA-type zeolites. Although the resulting RUT-type zeolites exhibited similar characteristics, there was a large difference in the effect of the Si/Al ratio in the starting zeolite on the synthesis of RUT-type zeolites. Moreover, the crystallization rate for the FAU–RUT interzeolite conversion strongly depended on the starting Si/Al ratio, whereas no dependence was observed for the \*BEA–RUT interzeolite conversion. This is due to differences in the chemical structure and concentration of locally ordered aluminosilicate species produced by the decomposition/dissolution of starting zeolites during the interzeolite conversion process.

In chapter 7, interzeolite conversion process of FAU-type zeolite was investigated using several measurement techniques. From XRD and SEM measurements, it was confirmed that the crystallization rate with FAU-type zeolite as the starting material was better than that with amorphous aluminosilicate gel (the conventional synthesis). During the interzeolite conversion process, solid parts possessed much  $Q^2$  and  $Q^3$  species than that of amorphous materials. In the solution parts, different chemical species were detected between the FAU–\*BEA and FAU–RUT interzeolite conversion process by

ESI-MS measurement. The aluminosilicate species with 4MR structure contributed formation of \*BEA structure. The clustered aluminosilicate species with higher masses were detected in the ESI-MS spectrum of FAU-\*BEA interzeolite conversion as compared to the synthesis of \*BEA-type zeolite from amorphous materials. From the detail analyses of both solid and solution parts during the conversion process, the existence of species with different chemical structures between the interzeolite conversion and conventional synthesis was suggested.

In this thesis, I clarified the influence of SDA, synthesis condition, and starting framework structure on the interzeolite conversion process. As a consequence, advantage of interzeolite conversion method was confirmed. Zeolites such as LEV-, CHA-, and OFF-type zeolites, whose frameworks structures are similar to the starting FAU-type zeolite, were effectively obtained by under mild synthesis condition. These zeolites were not obtained from amorphous aluminosilicate gels, suggesting strongly that nanoparts produced by dissolution/decomposition of FAU-type zeolite contribute formation of zeolite structures.

In future, the interzeolite conversion method will enable the design synthesis of zeolite and become new strategy for zeolite synthesis.

## List of publications

1. H. Jon, H. Sasaki, T. Inoue, M. Itakura, S. Takahashi, Y. Oumi, T. Sano, “Effects of structure-directing agents on hydrothermal conversion of FAU type zeolite”, *Stud. Surf. Sci. Catal.* 174 (2008) 229.
2. H. Sasaki, H. Jon, M. Itakura, T. Inoue, T. Ikeda, Y. Oumi, T. Sano, “Hydrothermal conversion of FAU zeolite into aluminous MTN zeolite”, *J. Porous Mater.* 16 (2009) 465.
3. T. Inoue, M. Itakura, H. Jon, A. Takahashi, T. Fujitani, Y. Oumi, T. Sano, “Synthesis of LEV zeolite by interzeolite conversion method and its catalytic performance in ethanol to olefins reaction”, *Micropor. Mesopor. Mater.* 122 (2009) 149.
4. M. Itakura, T. Inoue, A. Takahashi, T. Fujitani, Y. Oumi, T. Sano, “Synthesis of High-silica CHA Zeolite from FAU Zeolite In the Presence of Benzyltrimethylammonium Hydroxide”, *Chem. Lett.* 39 (2008) 908.
5. M. Itakura, Y. Oumi, M. Sadakane, T. Sano, “Synthesis of high-silica offretite by the interzeolite conversion method”, *Mater. Res. Bull.* 45 (2010) 646.
6. S. Shibata, M. Itakura, Y. Ide, M. Sadakane, T. Sano, “FAU LEV interzeolite conversion in fluoride media”, *Micropor. Mesopor. Mater.* 138 (2011) 32.
7. K. Honda, A. Yashiki, M. Itakura, Y. Ide, M. Sadakane, T. Sano, “Influence of seeding on FAU \*BEA interzeolite conversions” *Micropor. Mesopor. Mater.* 142 (2011) 161.
8. M. Itakura, K. Ota, S. Shibata, T. Inoue, Y. Ide, M. Sadakane, T. Sano, “Influence of starting zeolite on synthesis of RUT type zeolite by interzeolite conversion method”, *J. Cryst. Growth* 314 (2011) 274.
9. M. Itakura, I. Goto, A. Takahashi, T. Fujitani, Y. Ide, M. Sadakane, T. Sano, “Synthesis of high-silica CHA type zeolite by interzeolite conversion of FAU type zeolite in the presence of seed crystals”, *Micropor. Mesopor. Mater.* 144 (2011) 91.

10. M. Sadakane, Niklas Rinn, S. Moroi, H. Kitatomi, T. Ozeki, M. Kurasawa, M. Itakura, S. Hayakawa, K. Kato, M. Miyamoto, S. Ogo, Y. Ide, T. Sano, "Preparation and Structural Characterization of RuII-DMSO and RuIII-DMSO-substituted  $\alpha$ -Keggin-type Phosphotungstates,  $[\text{PW}_{11}\text{O}_{39}\text{Ru}^{\text{II}}\text{DMSO}]^5$  and  $[\text{PW}_{11}\text{O}_{39}\text{Ru}^{\text{III}}\text{DMSO}]^4$ , and Catalytic Activity for Water Oxidation", *Z. Anorg. Allg. Chem.* 637 (2011) 1467.
11. I. Goto, M. Itakura, S. Shibata, K. Honda, Y. Ide, M. Sadakane, T. Sano, "Transformation of LEV-type zeolite into less dense CHA-type zeolite", *Micropor. Mesopor. Mater.* 158 (2012) 117.
12. N. Yamanaka, M. Itakura, Y. Kiyozumi, Y. Ide, M. Sadakane, T. Sano, "Acid stability evaluation of CHA-type zeolites synthesized by interzeolite conversion of FAU-type zeolite and their membrane application for dehydration of acetic acid aqueous solution". *Micropor. Mesopor. Mater.*, 158 (2012) 141.
13. Y. Ide, N. Kagawa, M. Itakura, I. Imae, M. Sadakane, T. Sano, "Effective and Selective Bisphenol A Synthesis on a Layered Silicate with Spatially Arranged Sulfonic Acid", *ACS Appl. Mater. Interfaces* 4(4) (2012) 2186.
14. K. Honda, M. Itakura, Y. Matsuura, A. Onda, Y. Ide, M. Sadakane, T. Sano, "Role of structural similarity between starting zeolite and product zeolite in the interzeolite conversion process", *J. Nanosci. Nanotechnol.* Accepted.
15. M. Itakura, Y. Oumi, Y. Ide, M. Sadakane, T. Sano, "Interzeolite Conversion –Design and Synthesis of Zeolite–" *ZEORAITO* 27 (2010) 74 (in Japanese).

### **Presentations in international conference**

1. H. Jon, H. Sasaki, T. Inoue, M. Itakura, S. Takahashi, Y. Oumi, T. Sano, "Effects of structure-directing agents on hydrothermal conversion of FAU type zeolite", 4th International FEZA Conference, PI-A14, 2008, September in France (Paris).
2. M. Itakura, Y. Oumi, T. Sano, "Synthesis of high-silica zeolites by interzeolite

- conversion method using benzyltrimethylammonium hydroxide”, ZMPC2009 International Symposium on Zeolites and Microporous Crystals, RRR2-1, 2009, August in Tokyo.
3. K. Honda, A. Yashiki, M. Itakura, Y. Oumi, M. Sadakane, T. Sano, “Interzeolite conversion of FAU into \*BEA zeolite by seeding”, 16th International Zeolite Conference joint with the 7th International Mesostructured Materials Symposium, P-060, 2010, July in Italy (Sorrent).
  4. M. Itakura, K. Ota, S. Shibata, T. Inoue, Y. Ide, M. Sadakane, T. Sano, “Influence of starting zeolite on the interzeolite conversion”, 16th International Zeolite Conference joint with the 7th International Mesostructured Materials Symposium, P-059, 2010, July in Italy (Sorrent).
  5. A. Yashiki, A. Fujimoto, S. Shibata, K. Honda, M. Itakura, Y. Ide, M. Sadakane, T. Sano, “Hydrothermal conversion of FAU zeolite in the absence of organic structure-directing agents”, 5th International FEZA Conference, SC-P-012-Mon-012, 2011, July in Spain (Valencia).
  6. M. Itakura, Y. Ide, M. Sadakane, T. Sano, “Interzeolite conversion process of FAU type zeolite”, 5th International FEZA Conference, SC-P-009-Mon-009, 2011, July in Spain (Valencia).
  7. N. Kagawa, Y. Ide, M. Itakura, M. Sadakane, T. Sano, “Effectve and selective bisphenol A synthesis on a layered silica with spatially arranged arylsulfonic acid”, ZMPC2012 International Symposium on Zeolites and Microporous Crystals, P-047, 2012, July in Hiroshima.
  8. N. Yamanaka, M. Itakura, Y. Kiyozumi, Y. Ide, M. Sadakane, T. Sano, “Evaluation of acid stability of CHA zeolite synthesized by interzeolite conversion of FAU zeolite”, ZMPC2012 International Symposium on Zeolites and Microporous Crystals, P-031, 2012, July in Hiroshima.
  9. M. Itakura, I. Goto, S. Shibata, K. Honda, Y. Ide, M. Sadakane, T. Sano, “\*BEA-MFI and LEV-CHA interzeolite conversion in the absence of organic structure-directing agent and seed crystal”, ZMPC2012 International Symposium on

Zeolites and Microporous Crystals, P-018, 2012, July in Hiroshima.

10. Y. Kiyozumi, C. Abe, Y. Hasegawa, T. Nagase, T. Hanaoka, M. Itakura, Y. Ide, M. Sadakane, T. Sano, “Synthesis of high-silica CHA membrane by interzeolite conversion of FAU and its pervaporation performance”, ZMPC2012 International Symposium on Zeolites and Microporous Crystals, OB21, 2012, July in Hiroshima.

### **List of patents**

1. 清住嘉道, 長谷川泰久, 長瀬多加子, 山中直樹, 板倉正也, 井出裕介, 定金正洋, 佐野庸治, ゼオライト膜およびその製造方法, 特願 2012-052163.
2. 清住嘉道, 長谷川泰久, 長瀬多加子, 板倉正也, 佐野庸治, ゼオライト膜およびその製造方法, 特願 2011-251277.

## Acknowledgements

I would like to express my gratitude to all people who have helped me with the preparation of this doctoral thesis. Especially, I am deeply indebted to my supervisor Prof. Dr. Tsuneji Sano for his advice, support, and invaluable suggestions concerning science. Without his patient guidance, it is almost impossible to finish my study. I also gratefully acknowledge Prof. Masahiro Sadakane, Prof. Yasunori Oumi, and Prof. Yusuke Ide for teaching me laboratorial techniques and work as well as for valuable suggestions. I must also express special gratitude to Dr. Yoshimichi Kiyozumi, Dr. Tadahiro Fujitani, and Dr. Atsushi Takahashi (National Institute of Advanced Industrial Science and Technology) for providing input and some characterizations.

I am grateful to all of Sano Laboratory's members especially, Dr. H. Jon, Dr. S. Sumiya, Dr. N. Ikawa, Mr. T. Inoue, Mr. S. Shibata, Mr. K. Ota, Dr. K. Honda, Ms. A. Yashiki, Mr. I. Goto, Mr. Y. Furumoto, Ms. A. Fujimoto, Mr. N. Tsunoji, Mr. N. Yamanaka, Mr. Y. Umehara; and peers as well: Mr. H. Ueda, Mr. D. Goto, Mr. T. Miyano, Ms. C. Tsuyuki, and Ms. Y. Hisayuku for their help, cooperation and contributions to my study.

Hiroshima, March 2013

Masaya Itakura